

# Modeling Flows for Assessing Tidal Energy Generation Potential

Derek Scott Spurlock

Thesis submitted to the faculty of the Virginia Polytechnic Institute and State University in partial fulfillment of the requirements for the degree of

Master of Science

In

Civil Engineering

Panayiotis Diplas

William E. Cox

Marte Gutierrez

September 12, 2008

Blacksburg, Virginia

Keywords: Tidal Energy, Hydraulic Model, East River

# Modeling Flows for Assessing Tidal Energy Generation Potential

Derek Scott Spurlock

## Abstract

Tidal energy is a clean, sustainable, reliable, predictable source of energy. Recent developments in underwater turbines have made harvesting tidal energy feasible. Determining the power potential available in a given water body can be accomplished by using numerical hydraulic models to predict the flow velocity at a location of interest. The East River in Manhattan has been used here in an effort to develop a modeling methodology for assessing the power potential of a site. Two two-dimensional CFD models, FESWMS and TUFLOW, as well as one one-dimensional model, HEC-RAS, are used to analyze flows in the East River. Comparisons are made between the models and TUFLOW proves to best represent flows in the East River. HEC-RAS provides accurate results; however, the one-dimensional results lack the necessary detail of a two-dimensional model. FESWMS cannot produce results that mimic actual flow conditions in the East River. Using the TUFLOW model, power and energy estimates are made. These estimates show that a two-dimensional model, such as TUFLOW, can be a great tool for engineers and planners developing tidal energy projects. Using the results of this work, a methodology is developed to assess power potential at other sites using publicly available data.

## **Acknowledgements**

I would like to thank my heavenly Father for blessing me so richly and for giving me hope for the future. Thank you Jessica, you are a wonderful wife. Your love, encouragement, and support have carried me through this endeavor. To my parents, grandparents, and extended family, I thank you for the love, encouragement, and for giving me the tools to succeed in life. I would also like to thank Dr. Leftwich for encouraging me to pursue graduate studies. Dr. Diplas, thank you for all of your help, kindness, and patience throughout this endeavor. George Hagerman, thank you for all of your help and support.

## **Dedication**

I dedicate this work to friends lost during the tragedy on April 16, 2007.



## Contents

<b>List of Figures .....</b>	<b>ix</b>
<b>List of Tables.....</b>	<b>xi</b>
<b>List of Symbols .....</b>	<b>xii</b>
<b>1. Introduction .....</b>	<b>1</b>
<b>1.1. Purpose.....</b>	<b>1</b>
<b>1.2. Computer Specifications .....</b>	<b>1</b>
<b>2. Literature Review .....</b>	<b>3</b>
<b>2.1. Underwater Turbines and Tidal Energy .....</b>	<b>3</b>
<b>2.2. 1-D v. 2-D Models .....</b>	<b>4</b>
<b>2.3. The East River .....</b>	<b>6</b>
2.3.1. Study Site .....	7
<b>2.4. Description of Software Packages Used .....</b>	<b>9</b>
2.4.1. ArcView .....	10
2.4.2. Flow Models .....	10
<b>3. Model Development.....</b>	<b>16</b>
<b>3.1. Digital Terrain Model Creation.....</b>	<b>16</b>
3.1.1. Data Sources.....	16
3.1.2. Merging Land Elevation and Bathymetry Data .....	17
<b>3.2. Boundary Conditions .....</b>	<b>20</b>
<b>3.3. Calibration Data .....</b>	<b>21</b>
3.3.1. Calibration Data Source.....	21
3.3.2. Conversion of Depth Averaged Velocities to Turbine Average Velocities.....	22
<b>3.4. Conclusion.....</b>	<b>25</b>
<b>4. FESWMS Model .....</b>	<b>26</b>
<b>4.1. Finite Element Mesh Generation .....</b>	<b>26</b>
<b>4.2. Initial Runs.....</b>	<b>27</b>
<b>4.3. Sensitivity Analysis .....</b>	<b>27</b>
4.3.1. Eddy Viscosity .....	28
4.3.2. Manning's n .....	30
4.3.3. Time Step.....	33

4.3.4.	Mesh Resolution.....	35
4.3.5.	Sensitivity Analysis Conclusion .....	38
<b>4.4.</b>	<b>Attempt to Match Calibration Data .....</b>	<b>38</b>
<b>4.5.</b>	<b>Conclusion.....</b>	<b>40</b>
<b>5.</b>	<b>TUFLOW Model .....</b>	<b>41</b>
<b>5.1.</b>	<b>Model Setup .....</b>	<b>41</b>
<b>5.2.</b>	<b>Initial Runs.....</b>	<b>41</b>
<b>5.3.</b>	<b>Sensitivity Analysis .....</b>	<b>42</b>
5.3.1.	Grid Resolution .....	43
5.3.2.	Manning's n Value Analysis.....	44
5.3.3.	Eddy Viscosity Analysis.....	46
5.3.4.	Boundary Condition Analysis .....	47
5.3.5.	Time Step Analysis.....	48
5.3.6.	Sensitivity Analysis Conclusions .....	53
<b>5.4.</b>	<b>Attempt to Match Calibration Data .....</b>	<b>54</b>
<b>5.5.</b>	<b>Conclusion.....</b>	<b>55</b>
<b>6.</b>	<b>HEC-RAS Model .....</b>	<b>56</b>
<b>6.1.</b>	<b>Creating Model Geometry .....</b>	<b>56</b>
<b>6.2.</b>	<b>Boundary Conditions &amp; Initial Conditions.....</b>	<b>57</b>
<b>6.3.</b>	<b>Sensitivity Analysis .....</b>	<b>57</b>
6.3.1.	Manning's n .....	57
6.3.2.	Computational Time Step.....	60
6.3.3.	Channel Geometry Analysis .....	62
6.3.4.	Sensitivity Analysis Conclusion .....	66
<b>6.4.</b>	<b>Results .....</b>	<b>67</b>
<b>6.5.</b>	<b>Conclusion.....</b>	<b>67</b>
<b>7.</b>	<b>Comparison of Model Results in Relation to the Calibration Data .....</b>	<b>69</b>
<b>7.1.</b>	<b>Introduction .....</b>	<b>69</b>
7.1.1.	Determining the Error in Model Runs.....	69
7.1.2.	Correcting TUFLOW Results .....	70
<b>7.2.</b>	<b>Data Comparison .....</b>	<b>71</b>
7.2.1.	FESWMS Results .....	71

7.2.2.	TUFLOW Results .....	72
7.2.3.	HEC-RAS Results .....	74
7.3.	<b>Conclusion</b> .....	74
8.	<b>Comparison of 1-D and 2-D Model Results</b> .....	76
8.1.	<b>Introduction</b> .....	76
8.1.1.	Tidal Definitions.....	76
8.1.2.	HEC-RAS Model.....	76
8.1.3.	TUFLOW Model.....	77
8.2.	<b>Results</b> .....	77
8.2.1.	Time Series Data at the Calibration Point.....	77
8.2.2.	Cross Sectional Comparison of Spring Peak Velocities.....	79
8.3.	<b>Velocity Profile</b> .....	82
8.4.	<b>Conclusion</b> .....	84
9.	<b>Month Long Runs and Analysis</b> .....	86
9.1.	<b>Month Long Data Sets</b> .....	86
9.1.1.	Model Set Up .....	86
9.2.	<b>Results</b> .....	86
9.2.1.	Neap vs. Spring Tides .....	86
9.2.2.	Month Long Data.....	92
9.3.	<b>Conclusion</b> .....	94
10.	<b>Modeling Methodology</b> .....	96
10.1.	<b>Data</b> .....	96
10.2.	<b>Data Manipulation</b> .....	96
10.3.	<b>The Hydraulic Model</b> .....	97
11.	<b>Conclusions</b> .....	99
11.1.	<b>General Comments</b> .....	99
11.2.	<b>Model Development and Data</b> .....	99
11.3.	<b>Hydraulic Models</b> .....	100
11.4.	<b>Month Long Runs and Power Analysis</b> .....	100
11.5.	<b>Recommendations for Future Work</b> .....	100
11.6.	<b>Conclusion</b> .....	101
<b>Appendix A: Bibliography</b> .....		102

<b>Appendix B: Step by Step TUFLOW Model Creation.....</b>	<b>105</b>
--	------------

## List of Figures

Figure 1 The East River .....	8
Figure 2 East River Study Area .....	9
Figure 3 Finished Digital Terrain Model .....	20
Figure 4 Location of Calibration Data Point .....	22
Figure 5 Underwater Turbine .....	24
Figure 6 Vertical Velocity Profile .....	25
Figure 7 FESWMS Velocity vs. Eddy Viscosity .....	28
Figure 8 FESWMS WSE vs. Eddy Viscosity .....	29
Figure 9 FESWMS Flow vs. Eddy Viscosity .....	29
Figure 10 FESWMS Velocity vs. Time for Various Eddy Viscosities .....	30
Figure 11 FESWMS Velocity vs. Manning's n .....	31
Figure 12 FESWMS WSE vs. Manning's n .....	32
Figure 13 FESWMS Flow vs. Manning's n .....	32
Figure 14 FESWMS Velocity vs. Time for Various Manning's n Values .....	33
Figure 15 FESWMS Model Run Time vs. Time Step .....	34
Figure 16 FESWMS Flow Rate vs. Time Step .....	34
Figure 17 FESWMS Velocity vs. Time for Various Time Steps .....	35
Figure 18 FESWMS Velocity vs. Time for Various Mesh Resolutions .....	36
Figure 19 FESWMS Flow vs. Number of Elements in Mesh .....	37
Figure 20 FESWMS Run Time vs. Number of Elements in Mesh .....	37
Figure 21 FESWMS Model Results .....	40
Figure 22 TUFLOW 5-m Grid Showing the Part of Grid Turned Off .....	42
Figure 23 TUFLOW Velocity vs. Time for Various Grid Resolutions .....	44
Figure 24 TUFLOW Velocity vs. Time for Various Manning's n Values .....	45
Figure 25 TUFLOW Velocity vs. Manning's n .....	45
Figure 26 TUFLOW WSE vs. Manning's n .....	46
Figure 27 TUFLOW Flow vs. Manning's n .....	46
Figure 28 TUFLOW Velocity vs. Time for Various Boundary Conditions .....	48
Figure 29 TUFLOW Time Step Analysis Velocity vs. Time .....	49
Figure 30 TUFLOW Time Step Analysis Water Surface Elevation vs. Time .....	50
Figure 31 TUFLOW Time Step Analysis Velocity vs. Time Step .....	50
Figure 32 TUFLOW Time Step Analysis Water Surface Elevation vs. Time Step .....	51
Figure 33 TUFLOW Time Step Analysis Unit Flow Rate vs. Time Step .....	51
Figure 34 TUFLOW Time Step Analysis Model Run Time vs. Time Step .....	52
Figure 35 TUFLOW Time Step Analysis Velocity Oscillation vs. Time Step .....	52
Figure 36 TUFLOW Time Step Analysis Water Surface Oscillation vs. Time Step .....	53
Figure 37 TUFLOW Success .....	54
Figure 38 HEC-RAS Flow vs. Time for Various Manning's n Values .....	58
Figure 39 HEC-RAS Velocity vs. Time for Various Manning's n Values .....	59

Figure 40 HEC-RAS WSE vs. Time for Various Manning's n Values.....	59
Figure 41 HEC-RAS Flow vs. Time for Various Time Steps .....	60
Figure 42 HEC-RAS Velocity vs. Time for Various Time Steps .....	61
Figure 43 HEC-RAS WSE vs. Time for Various Time Steps.....	61
Figure 44 HEC-RAS Flow vs. Time for Single and Split (Multiple) Channels .....	63
Figure 45 HEC-RAS Velocity vs. Time for Single and Split (Multiple) Channels .....	63
Figure 46 HEC-RAS WSE vs. Time for Single and Split (Multiple) Channels .....	64
Figure 47 HEC-RAS Single Channel Model.....	65
Figure 48 HEC-RAS Split (Multiple) Channel Model .....	66
Figure 49 HEC-RAS Data Compared with Calibration Data.....	68
Figure 50 Smoothing of TUFLOW Data .....	71
Figure 51 Best Results from Each Model .....	75
Figure 52 1-D v. 2-D Velocity v. Time at Calibration Point.....	78
Figure 53 1-D v. 2-D WSE v. Time at Calibration Point.....	79
Figure 54 1-D v. 2-D Cross Section at Calibration Point .....	81
Figure 55 1-D v. 2-D Cross Section in the West Channel near Queensboro Bridge .....	82
Figure 56 HEC-RAS Velocity Profile .....	83
Figure 57 TUFLOW Velocity .....	84
Figure 58 Head vs. Time.....	87
Figure 59 Velocity vs. Time for Spring and Neap Tides.....	88
Figure 60 Power vs. Time for Spring and Neap Tides .....	89
Figure 61 Peak Power Output from a 5-m Diameter Turbine During the Extreme Neap Tide .....	90
Figure 62 Peak Power Output from a 5-m Diameter Turbine During the Extreme Spring Tide.....	91
Figure 63 Velocity vs. Head.....	92
Figure 64 Head vs. Time .....	93
Figure 65 Power vs. Time.....	94
Figure 66 Modeling Methodology Flow Chart.....	98

## List of Tables

Table 1 Vertical Datum Data.....	19
Table 2 Error from Select FESWMS Runs .....	72
Table 3 Error from Select TUFLOW Runs .....	73
Table 4 Error from Select HEC-RAS Runs .....	74

## List of Symbols

$A$ .....	Cross Sectional Area
$c$ .....	Power Loss Coefficient
$C$ .....	Chezy Coefficient
$c_{\mu 1}$ and $c_{\mu 2}$ .....	Dimensionless Coefficients
$F_x$ .....	Sum of External Force Components in x Direction
$F_y$ .....	Sum of External Force Components in y Direction
$g$ .....	gravity
$H$ .....	Water Depth
$i$ .....	Sample Index
$ J $ .....	Determinant of the Jacobian Matrix of Element Coordinate Transformations
$k$ .....	Von Karman's Constant
$k_s$ .....	Roughness Height
$n$ .....	Manning's Roughness Coefficient
$N$ .....	Number of Samples in a Set
$p_a$ .....	Atmospheric Pressure at the Water Surface
$Q$ .....	Flow Rate
$q_1$ and $q_2$ .....	Unit Flow Rates in the X and Y Directions, Respectively
$q_{in}$ .....	Lateral Inflow Per Unit Distance
$q_m$ .....	Inflow Rate Per Unit Area
$R$ .....	Hydraulic Radius
$S$ .....	Storage Term



$S_f$ .....	Friction Slope
$S_h$ .....	Energy Losses Due to a Swell Head Expressed as a Slope
$S_o$ .....	Channel Slope
$t$ .....	Time
$u$ .....	Depth Averaged Velocity in the X Direction
$u^*$ .....	Bed Shear Velocity
$v$ .....	Depth Averaged Velocity in the Y Direction
$V$ .....	Average Velocity
$V_{calibration}$ .....	Calibration Velocity
$V_{model}$ .....	Velocity Reported by Model
$V_{Turbine}$ .....	Velocities Averaged Across the Blade Swept Area from a Turbine
$x$ and $y$ .....	Horizontal Coordinates
$z$ .....	Vertical Coordinate Indicating Elevation or Distance Above the Channel Bed
$z_b$ .....	Channel Bed Elevation
$z_w$ .....	Water Surface Elevation
$\beta$ .....	Isotropic Momentum Flux Correction Coefficient
$\zeta$ .....	Water Surface Elevation
$\mu$ .....	Horizontal Diffusion of Momentum Coefficient
$\tau_{bx}$ and $\tau_{by}$ .....	Bed Shear Stress Acting in the X and Y Directions, Respectively
$\tau_{sx}$ and $\tau_{sy}$ .....	Surface Shear Stress Acting in the X and Y Directions, Respectively
$\tau_{xx}$ , $\tau_{xy}$ , $\tau_{yx}$ , and $\tau_{yy}$ .....	Shear Stresses Caused by Turbulence
$\nu_t$ .....	Eddy Viscosity

$\nu_{t0}$	.....	Base Eddy Viscosity
$\rho$	.....	Fluid Mass Density
$\Omega$	.....	Coriolis Parameter

# **1. Introduction**

As the world seeks new sources of renewable energy, tidal energy is one viable alternative. Tidal energy is a reliable, predictable, sustainable source of energy. Unlike solar and wind energy, tidal predictions are accurate and readily available for long time periods. Recent developments of underwater turbines (think windmill but under water) have made the idea of harvesting tidal energy feasible. In order to predict the amount of power available for a given site, the ability to model tidal flows is essential. The results from such models can provide a wealth of information to planners and engineers studying potential tidal power generation sites. In order to determine if a potential site is feasible for generating power, certain parameters, such as flow depths and velocities must be known. These parameters can be predicted by the use of hydraulic models. This work deals with modeling the East River in Manhattan using existing computational hydraulic models in order to assess power potential and to provide a methodology for assessing power potential at other sites.

## **1.1. Purpose**

The purpose of this work is to determine the steps necessary to develop a hydraulic model of the East River using publicly available data and existing modeling software. This will result in a methodology for modeling in the East and other rivers, and provide results for further analysis of tidal power and energy potential in the East River. Publically available data is used since surveys can be costly and time consuming. Publically available data can yield adequate estimates of power potential, and if sufficient potential is found, a full scale survey and analysis can be undertaken, if necessary. Since power generation is a function of velocity cubed, identifying velocity magnitudes in the East River is key. Both two-dimensional and one-dimensional (referred to as 1-D and 2-D) models will be evaluated for this purpose. This type of modeling also has the potential to predict any adverse impacts to nearby structures and ecology as a result of turbine installation and can be used to find ways to minimize such effects.

## **1.2. Computer Specifications**

It is important to consider the computer specifications when reviewing this work. Models are run on a personal notebook computer with Windows XP Media Center Edition. This computer has an Intel Core 2 Duo mobile processor, model T7200, with a clock speed of 2.0-GHz. This computer also has 2.00-GB of RAM, a dedicated graphics processor, and a 7,200-RPM Serial-ATA hard drive.

### **1.3. Summary**

Before beginning work on modeling the East River, a literature review is performed on tidal energy and underwater turbines. The literature review also contains a comparison of 1 and 2-D flow models, a description of the East River, and descriptions of the various software packages used. Then, the necessary data, such as geometry, boundary conditions, and calibration data, are obtained and manipulated into a format that is usable in the models. Once all of the data is prepared, model runs are made. Two 2-D models, FESWMS and TUFLOW, and the 1-D model, HEC-RAS are used to model the East River. For each model, sensitivity analyses are performed and additional model runs are made in an attempt to match the calibration data. It is found that both TUFLOW and HEC-RAS can match actual conditions in the East River; however, FESWMS is unable to produce satisfactory results. Although the 1-D HEC-RAS results match the calibration data, the greater detailed results from the 2-D model TUFLOW are much more beneficial for analyzing power potential. Further model runs are made with TUFLOW to analyze power potential and energy production in the East River for extreme tidal ranges.

## **2. Literature Review**

A review of current literature on topics relevant to this study is performed and summarized in this section. These topics include underwater turbines and tidal energy, hydraulic modeling, and the East River. Underwater turbines are driven by the flow of water. The power generated by an underwater turbine is a function of the flow velocity passing through the turbine cubed. In order to accurately estimate the flow velocity, hydraulic models are employed. Both 1 and 2-D hydraulic models are used in this study to find out if a 1-D model will be sufficient to predict power generation, or if the additional information from a 2-D model is necessary. A section comparing 1 and 2-D hydraulic models is contained below. Models of the East River, near Manhattan, are developed in order assess power generation potential, and develop a method for modeling other rivers in the future. A description of the various models and software packages used in this study is included at the end of this section.

### **2.1. Underwater Turbines and Tidal Energy**

Due to the threat of global warming and depleting fossil fuel reserves, the world is seeking environmentally friendly and renewable sources of energy. One such source of energy is tidal energy, in which underwater turbines are placed on the bed of water bodies that are influenced by ocean tides. These underwater turbines operate much like windmills underwater. As the tides rise and fall, the flow of water causes the turbine blades to rotate a shaft. The entire turbine assembly can rotate so that the blades are always perpendicular to the flow velocity. The shaft turns an electric generator, producing electricity. Tidal energy is an attractive renewable energy source because it is more predictable and reliable than other forms of energy such a solar or wind energy. Solar energy and wind energy rely on the weather, which is rather unpredictable. The tides which drive such currents are highly predictable, being a consequence of the gravitational effects of the planetary motion of the earth, the moon and the sun (Bahaj and Myers 2004). Energy from marine currents offers the promise of regular and predictable electricity at higher power density or flux ( $\text{kW/m}^2$ ) than many other renewables (Myers and Bahaj 2005). Tidal energy also has other advantages over other land based renewable energies. Land-based renewable energy technologies are already facing constraints owing to conflicts over land use, so an important factor is that the seas offer large open spaces where future new energy technologies could be deployed on a grand scale, perhaps with considerably less impact on either the environment or other human activities

(Fraenkel 2002). Although the energy in marine currents is generally diffuse, it is concentrated at a number of sites where sea flows are channeled through constraining topographies such as islands and straits (Bahaj and Myers 2004).

The power generated by an underwater turbine is a function of the flow velocity passing through the turbine cubed. The power,  $P$ , in a marine current has a similar dependence as a wind turbine and is governed by the following equation:

$$P = \frac{1}{2} \rho A V^3 \quad (1)$$

where  $\rho$  is the fluid density,  $A$  is the cross-sectional area of the turbine and  $V$  is the fluid velocity (Bahaj and Myers 2004). Only part of the energy from the flow of water can be converted to mechanical power by the turbine. There are also power losses associated with the various mechanisms with the turbine. To account for this, the above equation is multiplied by a coefficient,  $c$ .

$$P = \frac{1}{2} c \rho A V^3 \quad (2)$$

Typical values for  $c$  are estimated to be 0.25-0.5.

## **2.2. 1-D v. 2-D Models**

As stated above, power generated by an underwater turbine is a function of flow velocity cubed. In order to accurately estimate power generation, accurate flow velocities are needed. Hydraulic models are used in this study to estimate flow velocities. Since both 1-D and 2-D hydraulic models are used in this study, it is necessary to consider the advantages and disadvantages of each. While 2-D models yield more accurate, detailed results, 1-D models are generally more economical to purchase and operate. The following section reviews several comparisons of 1-D and 2-D hydraulic models.

The paper *1-D or 2-D Models for River Hydraulic Studies?* (Walton et al. 1997), compares the results of 1-D and 2-D hydraulic models. Two sites are modeled, the Sauk River in Washington and the Cispus River, also in Washington. The Sauk River contains a secondary channel, in which erosion is endangering a highway crossing. To evaluate various 'hard' engineering alternatives, the two-

dimensional, finite-element, hydrodynamic model, RMA-2 (run under FastTABS), was used to model the 100-year flow in the bridge reach (Walton et al. 1997). HEC-2, a 1-D model, was also used to model the site. The results from the two models compare well for river stage; however, the 1-D model is unable to reproduce the velocity distribution in the secondary channel. A flood on the Cispus River caused excessive scour, resulting in a bridge failure. The two-dimensional finite-element model, FESWMS, was applied in the modeling system SMS to evaluate the hydraulic and scour performance of a proposed replacement bridge, and to estimate riprap sizes to protect the banks from further erosion and migration (Walton et al. 1997). The 1-D model, HEC-RAS was also used. The two model results compare well in both stage and velocities; however, the 2-D model shows some velocities parallel to cross-sections. In both studies, the 2-D models shows superelevation in the water surface. Walton et al. conclude that 1-D models are adequate for narrow, uniform streams and provide adequate results most of the time. 2-D models are useful for wide shallow rivers, or if the system is too complex for a 1-D model. 2-D models are able to predict eddies and lateral flows that result from complex river geometries. Both two-dimensional models proved to be extremely difficult to run for sites with high Froude numbers (approaching 0.8) and complex geometries with locally very steep gradients (Walton et al. 1997).

*Practical Comparison of One-Dimensional and Two-Dimensional Hydraulic Analyses for Bridge Scour* (Ports et al. 1993), compares the results of WSPRO, a 1-D model, and the 2-D model FESWMS. The study analyzes the effects of the installation of a new bridge and approaches across the Ohio River between Kentucky and Indiana. The site contains a 4-mi wide floodplain, a sharp bend, and a contraction. The new river crossing will have multiple openings. The model results, including depth, velocity, and direction of flow, are used to calculate scour for the bridge. The 2-D model provides estimates of flow distribution and flow direction through the bridge and around piers. Such parameters have to be assumed from a 1-D model. In summary, the two-dimensional hydraulic analysis provides significantly improved estimates of velocity magnitude, direction of flow, and flow distribution for complex flow conditions around bends, through contractions, and through multiple openings (Ports et al. 1993).

Hydraulic models are used in the study and modeling of instream habitats. Papers have been written comparing the differences between 1-D and 2-D hydraulic models for such studies. One such study compares the 1-D hydraulic model within the PHABSIM modeling system to the 2-D RMA-2 hydraulic model on the Logan River in Utah (Tarbet and Hardy 1996)). These results [of the

study on the Logan River] would support the concept that the differences between applications of 1-dimensional and 2-dimensional hydraulic modeling of habitat based on suitability curves are relatively insensitive between the two approaches [1-D versus 2-D] given adequate coverage of cross sections (Tarbet and Hardy 1996). Another study on the Elbow River in Calgary, Alberta, Canada (Waddle et al. 2000) compared the 1-D hydraulic model within PHABSIM to the 2-D hydraulic model CDG-2D. The river reach contained large boulders, an island, and a bend. The authors of this study concluded:

Even with the data limitations encountered, we conclude that where the flow is essentially one-dimensional, both two-dimensional and the existing one-dimensional procedures can give comparable predictions. Where the flow exhibits significant lateral mass transfers, which vary with discharge, only the two-dimensional model can give an accurate prediction. (Waddle et al. 2000)

From the above paragraphs, one can conclude that in cases where the flow is complex, such as around islands and bends and where lateral flows are significant, a 2-D hydraulic model yields better results. When flows are through relatively simple, straight reaches, a 1-D model will generally suffice.

### **2.3. The East River**

Verdant Power, the company sponsoring this work, is in the process of developing underwater turbine technology. They plan on installing an array of underwater turbines in the East River near Roosevelt Island in New York City. The East River is a narrow tidally dominated system connecting Long Island Sound with the upper part of New York Harbor (Blumberg and Pritchard 1997). The East River is not actually a river, but a tidal strait that extends about 26-km from Willets Point in Long Island Sound to The Battery in New York Harbor (see Figure 1). Hell Gate (Dutch—"Helle Gat"—literally translated, "hole through hell"), a natural rock sill divides the East River almost exactly in half (Swanson et al. 1982). The lower section is narrower and deeper; the upper section is wider and shallower but contains deep areas of about 30-m around Willets Point (Blumberg and Pritchard 1997). The East River ranges in width from about 180-m to 1,200-m. The channel in the East River has been considerably deepened but the metropolitan area has also encroached beyond the pre-colonial channel banks (Swanson et al. 1982). The mean tidal range is considerable, approximately 4.3-ft (1.3-m) at the Battery, 5.1-ft (1.5-m) at Hell Gate east of the project area, and increasing to



7.2-ft (2.2-m) at Willets Point, the entrance to the Long Island Sound (Chang et al. 2007). The tide at Throgs Neck [across the river from Willets Point] has a range that is approximately 1-m greater than that at The Battery, and it lags that of The Battery by about 3-hr (Swanson et al. 1982). USACE reported velocities ranging from 2.0 to 7.9-ft/s [0.61 to 2.41-m/s] in the Lower East River (USACE 1998) and average maximum velocities of 4.7 and 2.9-ft/s [1.43 and 0.88-m/s] at the Brooklyn Bridge and Hunts Point, respectively (Chang et al. 2007). The lower East River primarily has a hard, rock bottom consisting of gravel, cobble, rocks, and boulders covered with a shallow layer of sediment (Chang et al. 2007).

### 2.3.1. Study Site

The study site to be modeled is in the immediate vicinity of Roosevelt Island, just south of Hell Gate (see Figure 2). The modeled reach extends from Horns Hook near East 90<sup>th</sup> St. in the north to East 41<sup>st</sup> St. Pier in the south. Both Horns Hook and East 41<sup>st</sup> St. Pier are former tidal gage stations. The reach is about 4-km long. Channel width at the northern end of the reach is about 400-m and approximately 800-m at the southern end of the reach. Roosevelt Island splits the channel and is about 3.1-km long and 230-m wide. At the midpoint of the reach, the west channel is roughly 230-m wide and the east channel is about 210-m wide. The average depth throughout the East River is roughly 10-m; however depths near the northern end of the modeled reach and in the west channel are as much as 30-m.

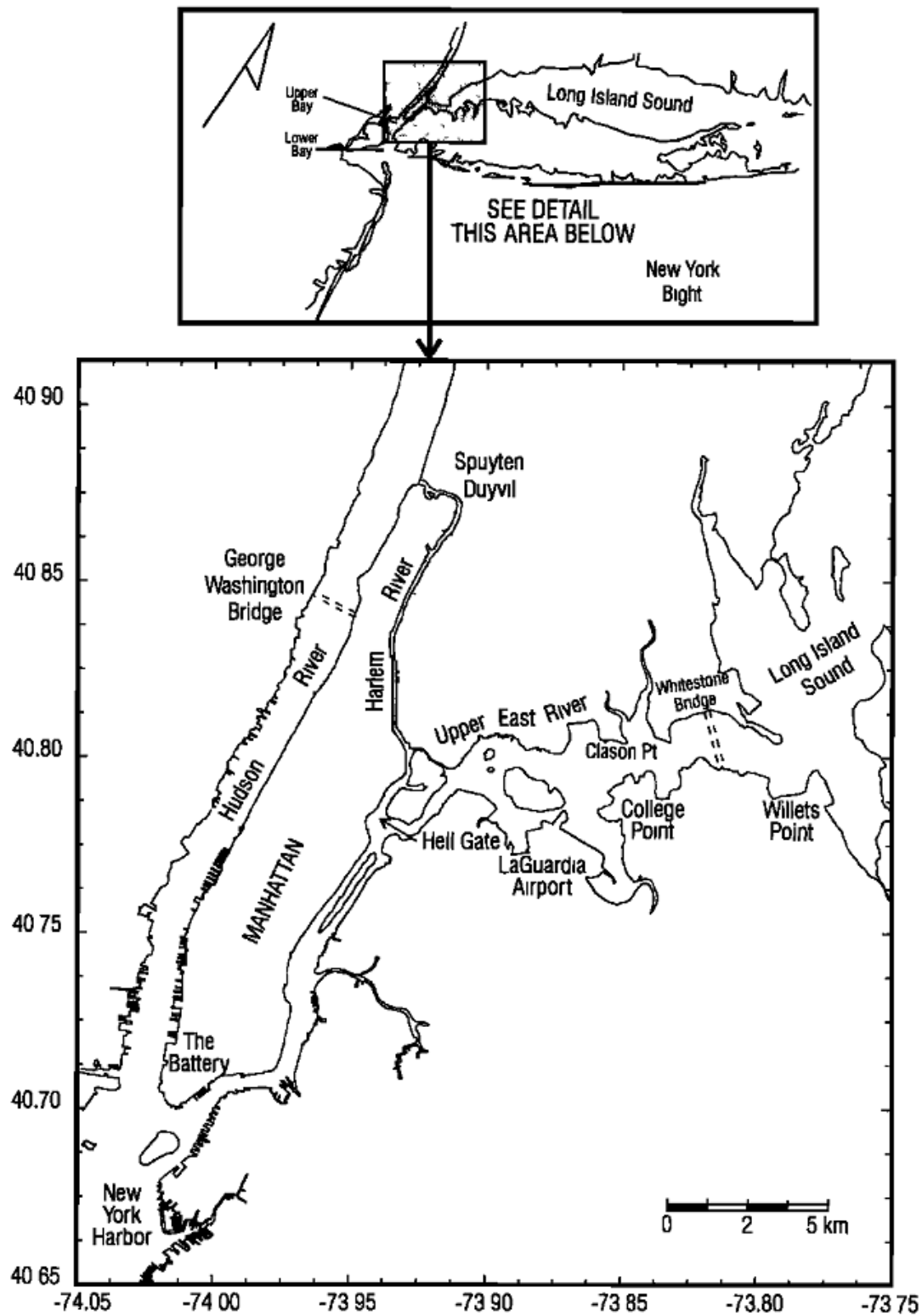


Figure 1 The East River (Blumberg and Pritchard 1997)



Figure 2 East River Study Area (image from Google Earth 2008)

## 2.4. Description of Software Packages Used

A description of the various software packages used in the development of the hydraulic models is contained in this section. ESRI's ArcView is a geographic information system used to develop a digital terrain model of the East River, which can then be loaded into the hydraulic modeling software. SMS is a pre- and post-processing software package that works in conjunction with various hydraulic models. FESWMS and TUFLOW are the 2-D hydraulic models used in this study. HEC-RAS is the 1-D hydraulic model employed in this work.

#### 2.4.1. ArcView

ArcView is part of ESRI's ArcGIS software package. ArcView Student Edition, version 9, is used to prepare the geometric data for the models. ArcView is full-featured geographic information system (GIS) software for visualizing, managing, creating, and analyzing geographic data (ESRI's Website 2007a). ArcView has many tools that allow the modifying, merging, and conversion of various data sources used to model the East River

#### 2.4.2. Flow Models

Both 2-D and 1-D flow models are used in this study. The 2-D flow models used in this study are FESWMS and TUFLOW, both of which are used within the SMS interface. The 1-D flow model HEC-RAS is also used. The FESWMS model within the SMS interface is chosen because of successful uses in the past and widespread usage, while the TUFLOW model is chosen because of its robust stability and ease of use. HEC-RAS is chosen based upon its widespread use and reliability. HEC-GeoRAS is a tool used to prepare the geometric data for input into HEC-RAS.

##### 2.4.2.1. SMS

SMS (Surface-water Modeling System) is a pre and post-processor with a graphical user interface for various hydraulic models. The program was developed by EMS-I (Environmental Modeling Systems, Inc.). SMS includes tools for the creation of finite element mesh, finite difference grids, triangulated irregular networks, and other geometric representations. SMS prepares the various data, such as geometry and boundary conditions, so that they can be input into the chosen hydraulic model. Once the hydraulic model is run, SMS displays the results as videos, various types of maps, charts, and tables. Version 9.2 is used.

##### 2.4.2.2. FESWMS

The Depth-averaged Flow and Sediment Transport Model (*FST2DH*) is a computer program that simulates movement of water and noncohesive sediment in rivers, estuaries, and coastal waters (Froehlich 2003). *FST2DH* is part of the Finite Element Surface-water Modeling System (FESWMS) developed by the Federal Highway Administration. This program uses the Galerkin finite element

method to solve the 2-D depth averaged continuity and momentum equations. This model was developed largely to deal with the complex flows that occur at highway river crossings. Release 3.3.2 is used.

The equations used in FESWMS are presented below. Equation 3 represents continuity and equations 4 and 5 represent momentum conservation in the x and y directions, respectively.

$$\frac{\partial z_w}{\partial t} + \frac{\partial q_1}{\partial x} + \frac{\partial q_2}{\partial y} = q_m \quad (3)$$

$$\frac{\partial q_1}{\partial t} + \frac{\partial}{\partial x} \left( \beta \frac{q_1^2}{H} + \frac{1}{2} g H^2 \right) + \frac{\partial}{\partial y} \left( \beta \frac{q_1 q_2}{H} \right) + g H \frac{\partial z_b}{\partial x} + \frac{H}{\rho} \frac{\partial p_a}{\partial x} - \Omega q_2 + \frac{1}{\rho} \left[ \tau_{bx} - \tau_{sx} - \frac{\partial (H \tau_{xx})}{\partial x} - \frac{\partial (H \tau_{xy})}{\partial y} \right] = 0 \quad (4)$$

$$\frac{\partial q_2}{\partial t} + \frac{\partial}{\partial x} \left( \beta \frac{q_1 q_2}{H} \right) + \frac{\partial}{\partial y} \left( \beta \frac{q_2^2}{H} + \frac{1}{2} g H^2 \right) + g H \frac{\partial z_b}{\partial y} + \frac{H}{\rho} \frac{\partial p_a}{\partial y} - \Omega q_1 + \frac{1}{\rho} \left[ \tau_{by} - \tau_{sy} - \frac{\partial (H \tau_{yx})}{\partial x} - \frac{\partial (H \tau_{yy})}{\partial y} \right] = 0 \quad (5)$$

where:

$g$  = Gravity

$z_w$  = Water Surface Elevation

$H$  = Water Depth

$\beta$  = Isotropic Momentum Flux Correction Coefficient

$p_a$  = Atmospheric Pressure at the Water Surface

$\tau_{bx}$  and  $\tau_{by}$  = Bed Shear Stress Acting in the X and Y Directions, Respectively

$q_1$  and  $q_2$  = Unit Flow Rates in the X and Y Directions, Respectively

$\tau_{sx}$  and  $\tau_{sy}$  = Surface Shear Stress Acting in the X and Y Directions, Respectively

$q_m$  = Inflow Rate Per Unit Area

$\tau_{xx}$ ,  $\tau_{xy}$ ,  $\tau_{yx}$ , and  $\tau_{yy}$  = Shear Stresses Caused by Turbulence

$t$  = Time

$\rho$  = Fluid Mass Density

$x$  and  $y$  = Horizontal Coordinates

$\Omega$  = Coriolis Parameter

$z_b$  = Channel Bed Elevation

Eddy viscosities are computed by equation 6. This equation allows three different methods of computing  $\nu_t$  by setting two of the constants,  $\nu_{t0}$ ,  $c_{\mu 1}$ , or  $c_{\mu 2}$  to zero and applying a positive non-zero value to the other. For example, applying a values of  $\nu_{t0} > 0$ ,  $c_{\mu 1} = 0$ , and  $c_{\mu 2} = 0$  leads to a constant  $\nu_t$  throughout the model. Applying  $\nu_{t0} = 0$ ,  $c_{\mu 1} = 0$ , and  $c_{\mu 2} > 0$  results in using the Smagorinsky

formulation for eddy viscosity. Combinations of these methods may also be used. Values of  $v_t$  are directly proportional to the shear stresses caused by turbulence,  $\tau_{xx}$ ,  $\tau_{xy}$ ,  $\tau_{yx}$ , and  $\tau_{yy}$ .

$$v_t = v_{t0} + c_{\mu1} u_* H + c_{\mu2} |J| \sqrt{\left(\frac{\partial u}{\partial x}\right)^2 + \left(\frac{\partial v}{\partial y}\right)^2 + \frac{1}{2} \left(\frac{\partial u}{\partial y} + \frac{\partial v}{\partial x}\right)^2} \quad (6)$$

where:

$c_{\mu1}$  and  $c_{\mu2}$  = Dimensionless Coefficients

$u_*$  = Bed Shear Velocity

$|J|$  = Determinant of the Jacobian Matrix of Element Coordinate Transformations

$v$  = Depth Averaged Velocity in the Y Direction

$u$  = Depth Averaged Velocity in the X Direction

$v_t$  = Eddy Viscosity

$v_{t0}$  = Base Eddy Viscosity

#### 2.4.2.3. TUFLOW

TUFLOW (Two-dimensional Unsteady FLOW) is another hydraulic model used in this analysis. TUFLOW is a computer program for simulating depth-averaged, two and one-dimensional free-surface flows such as those that occur from floods and tides (TUFLOW's user's manual 2005). TUFLOW's 2-D solution is based on the Stelling finite difference, alternating direction implicit (ADI) scheme that solves the full 2-D free surface shallow water flow equations (TUFLOW's website 2007b). The solution algorithm is documented in *Dynamically Linked Two-Dimensional / One-Dimensional Hydrodynamic Modeling Program for Rivers, Estuaries and Coastal Waters* (Syme 1991). This model is also capable of 1-D solutions, and linking 1 and 2 D models sections; however, only the 2-D portion is used. TUFLOW is specifically orientated towards establishing flow patterns in coastal waters, estuaries, rivers, floodplains and urban areas where the flow patterns are essentially 2-D in nature and cannot or would be awkward to represent using a 1-D network model (TUFLOW's user's manual 2005). The model was originally developed by WBM Oceanics Australia and The University of Queensland. The June 2006 software build is used in this study.

The 2-D free surface shallow water equations as presented by Syme are:

$$\frac{\partial \zeta}{\partial t} + \frac{\partial(zu)}{\partial x} + \frac{\partial(zv)}{\partial y} = 0 \quad (7)$$

$$\frac{\partial u}{\partial t} + u \frac{\partial u}{\partial x} + v \frac{\partial u}{\partial y} - \Omega v + g \frac{\partial \zeta}{\partial x} + gu \frac{\sqrt{u^2+v^2}}{c^2 H} - \mu \left( \frac{\partial^2 u}{\partial x^2} + \frac{\partial^2 u}{\partial y^2} \right) = F_x \quad (8)$$

$$\frac{\partial v}{\partial t} + u \frac{\partial v}{\partial x} + v \frac{\partial v}{\partial y} + \Omega u + g \frac{\partial \zeta}{\partial y} + gv \frac{\sqrt{u^2+v^2}}{c^2 H} - \mu \left( \frac{\partial^2 v}{\partial x^2} + \frac{\partial^2 v}{\partial y^2} \right) = F_y \quad (9)$$

where:

C = Chezy Coefficient

z = Vertical Coordinate Indicating Elevation or Distance Above the Channel Bed (the former in this case)

$F_x$  = Sum of External Force Components in x Direction

$\zeta$  = Water Surface Elevation

$F_y$  = Sum of External Force Components in y Direction

$\mu$  = Horizontal Diffusion of Momentum Coefficient

Equation 7 represents mass continuity and equations 8 and 9 represent momentum conservation in the x and y directions, respectively.

Eddy viscosity can be adjusted two different ways in TUFLOW. The first is to set a constant eddy viscosity throughout the model. The second is to let the model compute the eddy viscosity using the Smagorinsky formulation (equation 10).

$$v_t = \alpha \Delta x \Delta y \sqrt{\left( \frac{\partial u}{\partial x} \right)^2 + \left( \frac{\partial v}{\partial y} \right)^2 + \frac{1}{2} \left( \frac{\partial u}{\partial y} + \frac{\partial v}{\partial x} \right)^2} \quad (10)$$

#### 2.4.2.4. HEC-RAS

The U.S. Army Corps of Engineers' River Analysis System (HEC-RAS) is software that allows you to perform one-dimensional steady and unsteady flow river hydraulics calculations (Brunner 2002). For steady, gradually varied flow computations, HEC-RAS uses an iterative procedure to solve the 1-D energy equation. In situations where the flow is rapidly varied (non-uniform), HEC-RAS uses the momentum equation. For unsteady flow, the 1-D continuity equation (equation 11) and momentum equation (equation 12) are solved using the four-point implicit finite difference scheme. Version 3.1.3 released in 2005 is used.

$$\frac{\partial A}{\partial t} + \frac{\partial S}{\partial t} + \frac{\partial Q}{\partial x} - q_{in} = 0 \quad (11)$$

$$\frac{\partial Q}{\partial t} + \frac{\partial(VQ)}{\partial x} + gA \left( \frac{\partial z_w}{\partial x} + S_f + S_h \right) = 0 \quad (12)$$

where:

A = Cross Sectional Area

$S_f$  = Friction Slope

Q = Flow Rate

$S_h$  = Energy Losses Due to a Swell Head  
Expressed as a Slope

$q_{in}$  = Lateral Inflow Per Unit Distance

V = Average Velocity

S = Storage Term

HEC-GeoRAS is another software package used in conjunction with HEC-RAS. HEC-GeoRAS is [a] set of ArcGIS tools specifically designed to process geospatial data for use with the Hydrologic Engineering Center's River Analysis System (HEC-RAS) (Ackerman 2005). HEC-GeoRAS allows a user to create an input file for HEC-RAS containing geographic data. This is done by tracing the relevant features on a digital elevation model (DEM) or triangulated irregular network (TIN) in ArcView. HEC-GeoRAS reads the data from the DEM or TIN to create cross-sections, reach lengths, and other pertinent data. The file can then be easily imported into HEC-RAS. Version 4.1.1 released in 2006 is used.

## 2.5. Conclusion



From the above literature review, one can conclude that the East River has much potential for tidal power generation. Potential sites are typically near islands and straits where tidal flows are concentrated with accelerated velocities. The East River fits this description and has a rather large tidal range, resulting in peak velocities near 2.5-m/s. The fact that the location is within one of the most densely populated cities in the world illustrates that underwater turbines have the advantage of not requiring valuable land. The reach of the East River to be modeled is relatively straight; however, the presence of Roosevelt Island may complicate flows. It is assumed that a 2-D hydraulic model is necessary to model the flow patterns around the island; however, the effectiveness of a 1-D model is also studied. Two 2-D hydraulic models are used. FESWMS is a finite element model that has been used successfully in past studies. The finite difference model TUFLOW is used because it is touted as a robust, stable model that is user friendly. The free 1-D HEC-RAS model is also used.

### **3. Model Development**

The main goal of this modeling effort is to accurately estimate the velocities in the East River in order to assess the East's power potential and aid in future modeling efforts related to underwater turbines. As stated above, the amount of power an underwater turbine can generate is a function of the velocity flowing through it cubed. Three hydraulic models are used in this study. The 1-D model HEC-RAS and two 2-D models, FESWMS and TUFLOW, are used to model velocity in the East River.

In order to develop a successful hydraulic model of the East River, three types of data are needed: geometric data, boundary conditions, and calibration data. A digital terrain model (DTM) is used to represent the river's geometry. Boundary conditions are needed at both ends of the channel. Calibration data is needed to guide the choice of various model parameters so that model output mimics actual flows.

#### **3.1. Digital Terrain Model Creation**

This section details the creation of the DTM used to model the East River. Data is obtained from publically available sources on the internet. Some difficulties with datum conversions are encountered in merging the DTMs that comprise the final DTM used in the models. Solutions to these problems are detailed below.

##### **3.1.1. Data Sources**

Two sources of geometric data are used in this study. One data source represents the geometry that is under the surface of the water (bathymetry) and another represents the geometry that is not always below the surface of the water (referred to as land elevation or topography). This is necessary because the East River is driven by tides and the water surface elevation fluctuates over a large range; therefore, both geometric data sources are used in an attempt to better represent the East River.

## Bathymetry

The bathymetry data used in the development of the East River model is from the National Geophysical Data Center's website ([http://map.ngdc.noaa.gov/website/mgg/nos\\_hydro/viewer.htm](http://map.ngdc.noaa.gov/website/mgg/nos_hydro/viewer.htm)). The survey that collected the bathymetry was performed in July and August of 2004 by NOAA (National Oceanic and Atmospheric Administration). The horizontal datum used for this survey is the North American Datum of 1983 (NAD 83), projected using UTM zone 18 (from report accompanying data, registry number H11353). The vertical datum used is Mean Lower Low Water (MLLW). The survey was performed using a vertical beam echosounder and a shallow water multibeam system. The data has a resolution of 2-m.

## Land Elevation Data

The land elevation data is obtained from the USGS Seamless website (<http://seamless.usgs.gov/>). The data is part of the National Elevation Dataset 1/3 Arc Second. The data has a resolution of 1/3 of an arc second (about 30-m). The horizontal datum is referenced to NAD 83 UTM zone 18 and the vertical datum is the North American Vertical Datum of 1988 (NAVD 88).

### 3.1.2. Merging Land Elevation and Bathymetry Data

These two data sets are merged together using ESRI ArcView; however, a few problems are encountered. First, the bathymetry data has to be converted into a format ArcView can open. Then, a conversion between the vertical references used in the data sets is needed.

#### 3.1.2.1. Data Conflicts and File Conversions

### Bathymetry Data

The bathymetry is downloaded as a space delimited text file. ArcView cannot read this file, so the data is copied and pasted into Microsoft Excel and then saved as a comma separated value file (.csv). This has to be done in three steps due to the limit of 1,048,576 rows in Excel. An additional row is added to the top of the first Excel file to label the columns X, Y, and Z. The data from each

.csv file is copied and pasted into a single text file, which is then saved as a .csv file. One problem is found with the data. The data is listed as YXZ format (meaning the first column has Y coordinates, the second X coordinates, etc.); however, the data is actually XYZ format (this is easily proven once the data is plotted and compared with other maps).

Once the .csv file is created, the data can be loaded into ArcView. This is done by right-clicking on the .csv file in the Table of Contents (TOC) and clicking Display XY Data. A dialogue box then opens asking which columns are the X and Y values and if the data has a projection.

After the bathymetry data is displayed, it is then converted to a raster to be merged with the land elevation data, which is already in raster form. A cell size of 2-m was used since the bathymetry data is of a 2-m resolution.

#### 3.1.2.2. Vertical Datum Confusion and Conversion

As stated above, the bathymetry data is referenced to MLLW and the land elevation data is reference NAVD 88. Since the boundary condition data is reference to MLLW, the land elevation data is converted to MLLW; however, a simple conversion does not exist. In order to develop a conversion between MLLW and NAVD 88, data from tidal gages in the East River is used.

Three tidal gages with vertical datum data exist in the East River near the site to be modeled. These are Horns Hook, Queensboro Bridge, and Williamsburg Bridge. The Queensboro Bridge and Williamsburg Bridge gages have the difference between NAVD 88 and MLLW for both the present and superseded epoch listed. The Horns Hook gage only had the difference between the National Geodetic Vertical Datum of 1929 (NGVD 29) and MLLW for the superseded epoch listed. These values are given in the table below. VERTCON, a free internet program ([http://www.ngs.noaa.gov/cgi-bin/VERTCON/vert\\_con.prl](http://www.ngs.noaa.gov/cgi-bin/VERTCON/vert_con.prl)) is used to convert the Horns Hook datum from NGVD 29 to NAVD 88. Since the differences between the present and superseded epoch are known for two gages, 0.060-m in both cases, it is assumed that the value would shift the same for the Horns Hook gage. The final value for the Horns Hook gage for the present epoch is 0.811-m. Since all values are relatively close, they were averaged together and a conversion of 0.80-m was used (0.80-m NAVD 88 corresponds to 0.00-m MLLW).

**Table 1 Vertical Datum Data**

Difference Between Datum and MLLW (meters)			
Gage	Datum	Present Epoch	Superseded Epoch
Horns Hook	NGVD 29	-	0.540
Queensboro Bridge	NAVD 88	0.794	0.854
Williamsburg Bridge	NAVD 88	0.793	0.853

In ArcView, this conversion factor is subtracted from all data points in the land elevation raster dataset. This yields a land elevation dataset with a vertical reference to MLLW.

### 3.1.2.3. Merging Data

Once the two bathymetry data and land elevation data share a common vertical reference, they can be merged into a single data set which SMS can read. This is done using various tools within ArcView.

Since both datasets are in raster form, the Mosaic to New Raster tool is used in ArcView to merge the datasets. This simply combines the two rasters. If the rasters overlap, several options are available. In this instance, data from the bathymetry raster replaces data on the land elevation raster where available (the land elevation raster has a constant value of 0 for the section of land covered by the river).

SMS cannot open the raster file created by ArcView; therefore, the file has be converted into a format SMS can read. This is done in a “makeshift” fashion due to limitations in the version of ArcView being used. The raster created above is converted to a point shapefile. Since floating point rasters cannot be converted to shapefiles, the raster is multiplied by 1,000 and converted into an integer raster (integer rasters consist only of whole numbers, multiplying by 1,000 preserved the accuracy of the raster dataset). The raster is then converted to a point shapefile. This creates a shapefile with points at the center of each raster square. The values from each square in the raster grid are assigned to each new point. These values are placed in a column in the new shapefile’s attribute table. A new field is added in the attribute table of the shapefile, into which the values of the converted are divided by 1,000, thus restoring the original elevation values. Additional fields are added to the attribute table to calculate the X and Y location of each point. Extra points beyond the boundaries of the study area are removed from the dataset to save computational time and computer memory. Also, elevation values of 0 are deleted from the dataset (0 values represented

the flat plane of the water surface, it seems better to interpolate these values since they are not actually 0).

The attribute table of the above point shapefile is opened in Microsoft Excel, rearranged such that only the X, Y, and elevation fields remain, and saved as a new .csv file to be opened in SMS as a scatter set (see Figure 3).

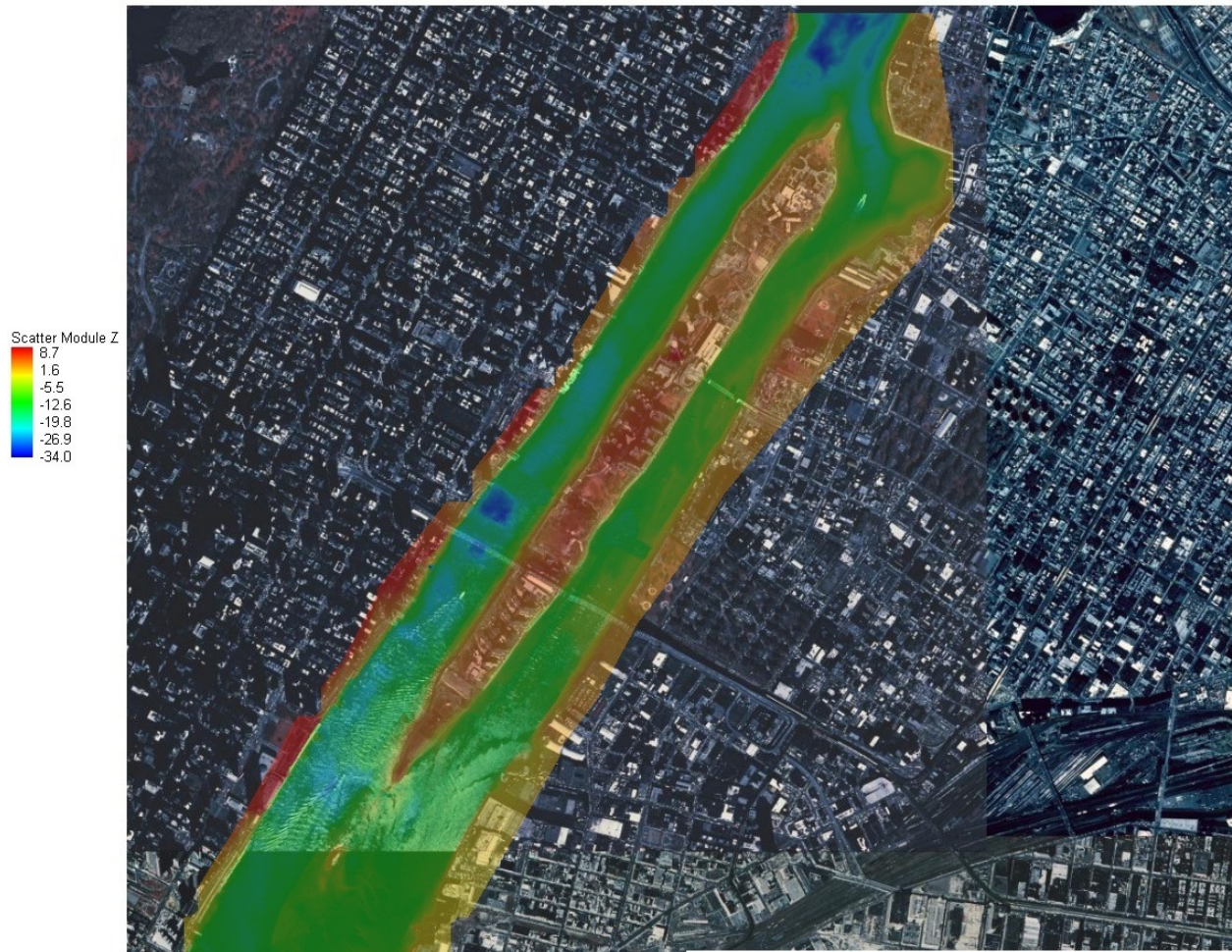


**Figure 3 Finished Digital Terrain Model**

### **3.2. Boundary Conditions**

In hydraulic models, boundary conditions tell the model what is happening at the open ends of the model (where the modeled water body is disconnected from the rest of the water body). Boundary

conditions consist of water surface elevations, velocities, flow rates, or combinations of these. The model uses boundary conditions to calculate what is happening within the modeled reach.

In this study, the modeled reach extends from Horns Hook near East 90<sup>th</sup> St. in the north to East 41<sup>st</sup> St. Pier in the south (see Figure 2). These two locations are former tidal gage stations. These stations are no longer monitored; however, software packages are available to generate predicted water surface elevations based upon historic data. The software package Tides and Currents version 3.3 developed by Nobeltec Corporation is used to generate boundary conditions for all the model runs completed in this study. Boundary conditions consist of water surface elevations at 6-min intervals at both the Horns Hook and East 41<sup>st</sup> St. Pier sites.

It should be noted that the goal of this project is to use publically available data to generate the model; however, Tides and Currents is a commercial program. Free alternatives exist, but were not used in this study. Two free potential alternatives to the commercial software exist:

1. tidal predictions on NOAA's website ([http://co-ops.nos.noaa.gov/tide\\_pred.html](http://co-ops.nos.noaa.gov/tide_pred.html)) and
2. a freeware program called WXTide32 (available at <http://www.wxtide32.com/download.html>).

### **3.3. Calibration Data**

Calibration data is needed to guide the choice of various model parameters in order to optimize the output generated by the models so that it matches real world situations. Model parameters such as Manning's roughness coefficient and eddy viscosity can be varied in order to force model results to match calibration data. If model results cannot mimic real world data, then they are of little use.

#### **3.3.1. Calibration Data Source**

Calibration data is provided by Verdant Power. This data consists of a velocity time series measured with an acoustic doppler current profiler (ADCP) placed on the river bottom. The raw ADCP data is not available, but velocities averaged across a circle representing the blade swept area from a turbine ( $V_{\text{Turbine}}$ ) are. Calibration data is obtained for a single point in the east channel (see Figure 4). This data is  $V_{\text{Turbine}}$  versus time. Velocities are reported with an angle for direction. It is assumed that angles greater than 200° correspond to flow in a south direction (negative velocities



in SMS) and angles less than  $70^\circ$  correspond to flow in a north direction (positive velocities in SMS). Since the calibration velocities are reported as turbine averaged and model velocities are reported as depth averaged ( $V_{AVG}$ ), a correction has to be calculated

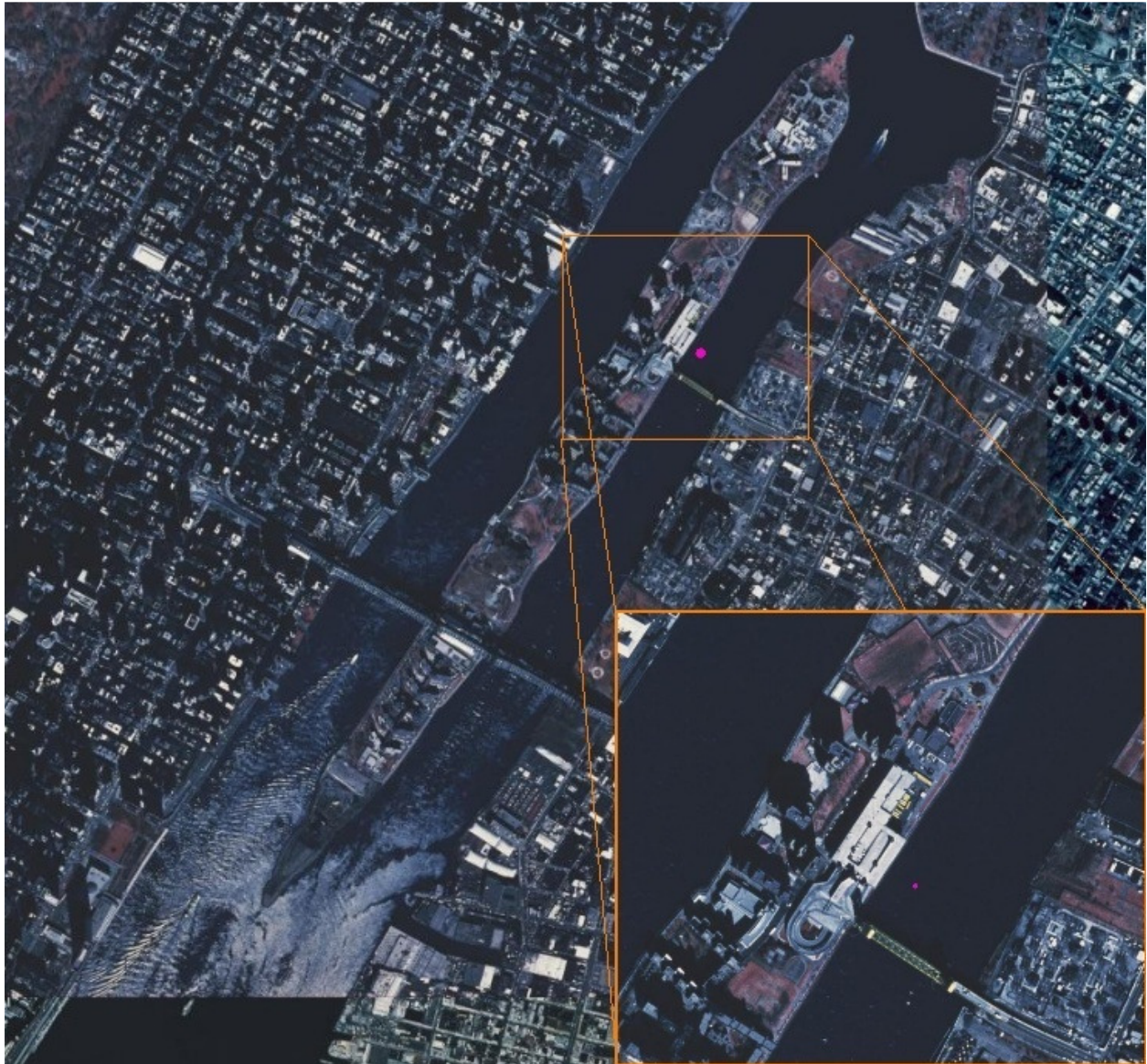


**Figure 4 Location of Calibration Data Point**

### 3.3.2. Conversion of Depth Averaged Velocities to Turbine Average Velocities

A comparison of depth averaged and turbine averaged velocities is made in the section. In order to compare these, a vertical velocity profile has to be assumed. Estimating the vertical velocity profile



in the East River presents a few slight problems. The concept of channel slope, which is included in most velocity profile equations, does not seem to make sense in a scenario where the flow reverses (this would result in a negative slope). Also, a roughness value is not known, which is also included in many velocity profile equations. Since average velocity occurs at 63.2% of the total flow depth (from Finnemore and Franzini 2001), one unknown in a velocity profile equation can be determined. The vertical velocity profile equation used is taken from the FESWMS's user's manual:

$$u(z) = \frac{u_*}{k} \ln \left( \frac{z}{k_s} \right) \quad (13)$$

where:

k = Von Karman's Constant

k<sub>s</sub> = Roughness Height

Another equation from *Error Propagation for Velocity and Shear Stress Prediction using 2d Models for Environmental Management* (Pasternack et al. 2006) is chose to calculate bed shear velocity since it does not include a term for slope.

$$u_* = V \sqrt{C_d} \quad (14)$$

where:

$$C_d = 9.81 \frac{n^2}{H^{1/3}} \quad (15)$$

where n = Manning's Roughness Coefficient.

The n value used in the above equation corresponds to the n value used in the model run. This leaves roughness height, k<sub>s</sub>, as the only unknown. Again, the fact that  $u = V$  when  $z = (1 - 0.632)H$  is used to solve for k<sub>s</sub>. Solving yeilds k<sub>s</sub> equal to 2.026 X 10<sup>-3</sup>-m. The resulting velocity profile is in Figure 6.

Now that a velocity profile is known, an equation for averaging velocity over the turbine swept area is needed. The estimated average velocity across the turbine swept area (see Figure 5) is simply a weighted average of the velocities across the turbine calculated from the above velocity profile. It is assumed that velocity does not vary laterally across the face of the turbine (the velocity is only a function of depth in the immediate area of the turbine). The following equation is used:

$$V_{turbine} = \frac{1}{Turbine\ Area} \int_{2.07}^{7.07} \int_{-\sqrt{-z^2+9.14z-14.6349}}^{\sqrt{-z^2+9.14z-14.6349}} u(z) dx dz \quad (16)$$

Where  $x = \sqrt{-z^2 + 9.14z - 14.6349}$  and  $x = -\sqrt{-z^2 + 9.14z - 14.6349}$ , the upper and lower limits on the first intergral, represent the upper and lower halves of the circle created by the turbine rotors (see Figure 5).

For a particular dataset ran in FESWMS ( $n=0.025$ ,  $Vo=5$ , 10,756 elements, data from 100 time steps, see Chapter 4 for further details FESWMS), this equation resulted in a velocity across the turbine that was on average 103.4% more than the depth averaged velocity. This small difference is deemed insignificant, and no further attempts are made to correct the change in depth averaged velocity and turbine averaged velocity.

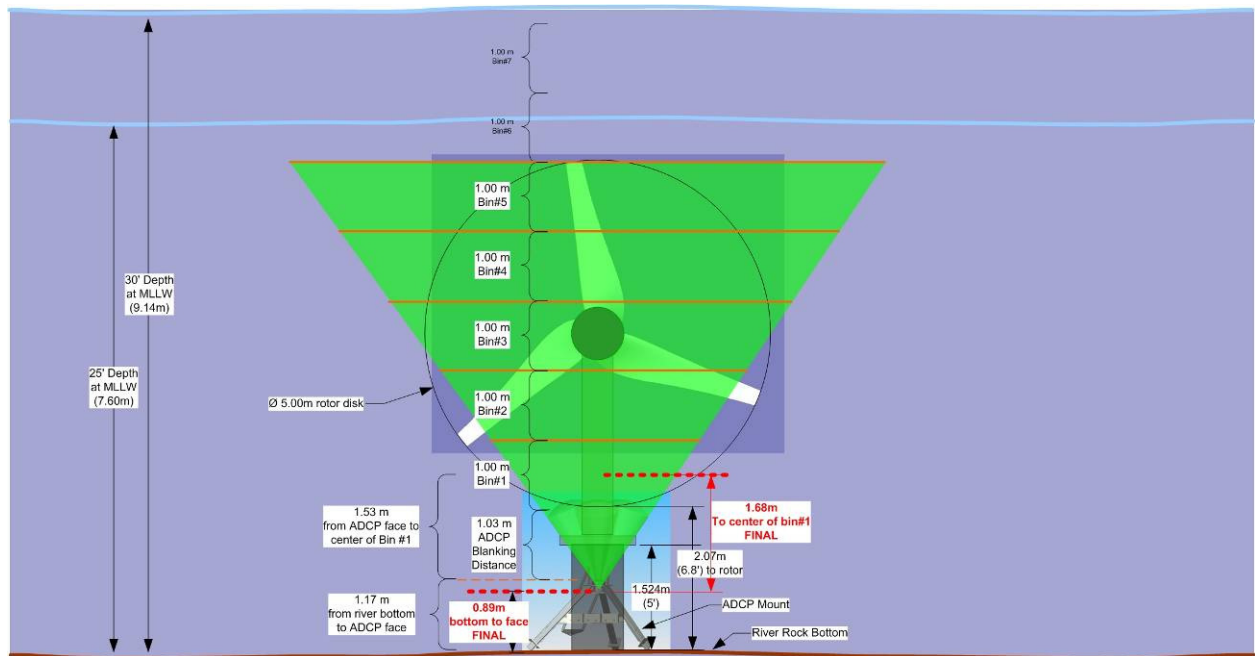


**Figure 5 Underwater Turbine**

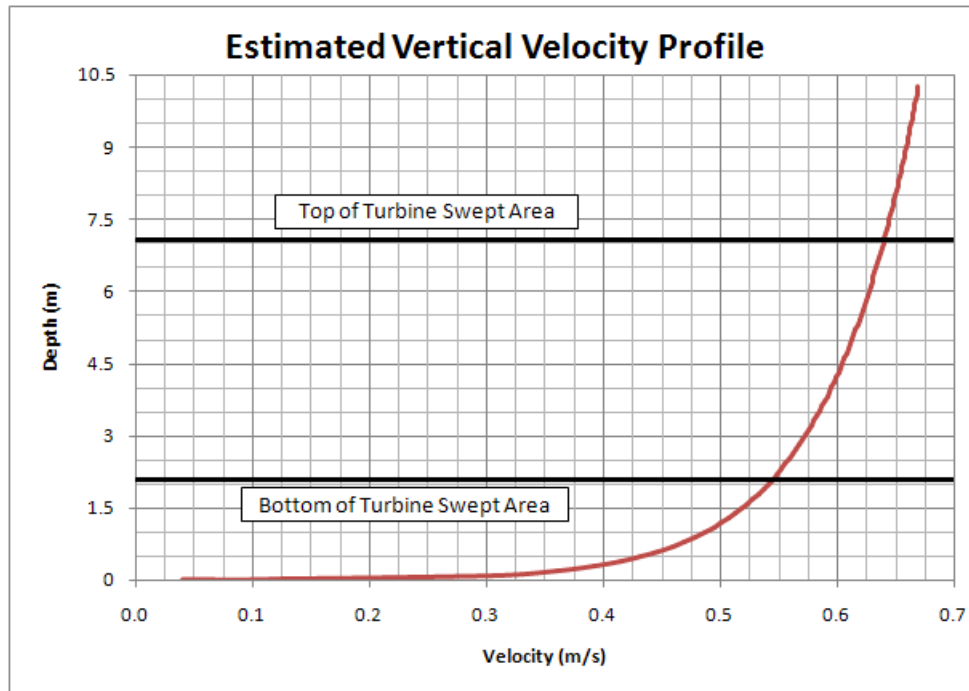


**Figure 6 Vertical Velocity Profile**

### **3.4. Conclusion**

The three main sources of data used in modeling the East River are geometric data, boundary condition data, and calibration data. The geometric data that represents the East River is composed of a combination of bathymetry data and land elevation data. Much work is done to merge these two datasets into a single dataset that can be opened in SMS. Boundary condition data used to drive the model are provided by a software package. The calibration data used to validate the model is composed of a velocity vs. time dataset for a single point in the modeled reach. These velocities are turbine averaged; however, it is shown that these do not vary significantly from depth averaged velocities. These three sets of data are the primary components that are used to create the hydraulic models in FESWMS, TUFLOW and HEC-RAS.

## **4. FESWMS Model**

The first attempt to model the East River is done with the FESWMS model. FESWMS is a 2-D finite element hydraulic model used within SMS (see section 2.4.2.2 for a more detailed description of the FESWMS model). In order to create the hydraulic model, a finite element mesh needs to be created. Then, the boundary condition data is entered and initial runs with the model are made. A sensitivity analysis is performed to see what affect changing various model parameters has upon output. Using the results from the initial runs and sensitivity analysis, an attempt is made to match the calibration data; however, attempts are unsuccessful.

### **4.1. Finite Element Mesh Generation**

The finite element mesh consists of connected nodes. Values for velocity, depth, etc. are calculated at these nodes. Each node also has an elevation value assigned, which comes from the DTM described in section 3.1. A boundary is drawn in SMS that represents the boundary of the modeled section of the East River. First, lines are drawn perpendicularly across the river at the north and south ends of the reach at the gage locations (Horns Hook gage in the north and East 41<sup>st</sup> St. Pier in the south,). The banks of the river are then traced using aerial photographs. These lines create the boundary for the finite-element mesh used in the model.

The boundary around the modeled reach is then divided into five subareas: the northern part of the channel before the island, the east channel around the island, the west channel around the island, the southern part after the island, and Hallets Cove off of the northern end of the east channel.

SMS can generate the finite element mesh with limited user input. These five subareas are each individually modified to allow SMS to create the finite-element mesh within each subarea. Four of the subareas (all except Hallets Cove) are comprised of quadrilateral elements. Hallets Cove is comprised of triangular elements. Attempts are made to create narrower elements along shorelines to minimize the effects of wetting and drying of elements. Also, once the mesh is created, it is edited to eliminate or reduce the number of bad elements. Some examples of bad elements are quadrilaterals with very large and small interior angles and adjacent elements that have a relatively large difference in surface area.

Once the finite element mesh is created and adequately edited, initial runs are made.

## **4.2. Initial Runs**

Initial runs are made to ensure that the finite element mesh is adequate and that the input parameters are in an acceptable range. The boundary conditions are loaded, which consist of water surface elevation vs. time data for both ends of the modeled reach. Model parameters in FESWMS are left at their default values.

Initial attempts to run the model show that it will not converge from a cold start (a cold start is when the model is run without well defined initial conditions). In order to overcome this, a steady-state solution is found to use as initial conditions for the unsteady runs. The boundary conditions from the first time step are applied to the steady-state model and a solution is found using the steering module.

The steering module is a program within SMS that is used to aid in model convergence. The steering module allows the use of exaggerated parameters that allow the model to easily converge. These exaggerated parameters are things such as an extremely high water surface, very low flow rates, very high eddy viscosities, and simplified geometry. One or any combination of these exaggerated parameters may be used. The model is ran with these exaggerated parameters and an intermediate solution is found (this is the solution based upon the exaggerated parameters, not the actual solution). This intermediate solution is then loaded into a new iteration as the initial conditions for the next run and a new intermediate solution is found. With each new iteration, the exaggerated parameters approach the actual parameters until the actual parameters are reached with a convergent final solution (assuming a solution can be found, otherwise the process will terminate).

The steady-state solution from the steering module is then used as the initial conditions for the dynamic (unsteady) runs.

Using this process, initial unsteady runs can be performed.

## **4.3. Sensitivity Analysis**

Once several initial modeling attempts are made, a sensitivity analysis is performed to see what effect various model parameters have on the model output. Parameters tested include eddy viscosity, Manning's  $n$ , time step, and mesh resolution. The resulting changes in model output

(velocity, water surface elevation, flow rate) are measured at the point where calibration data is provided (see Figure 4).

#### 4.3.1. Eddy Viscosity

An analysis is performed to see what effect changing the eddy viscosity will have on model results. A constant value is assigned for the eddy viscosity throughout the entire model domain. Values range from 5 to 50- $\text{m}^2/\text{s}$ . A period of 60-hr is modeled in 6-min time steps. A finite element mesh was created with 3,284 elements and 12,144 nodes. All other parameters are left at their default value ( $n=0.025$ ).

Varying the eddy viscosity has a profound impact on velocity, flow rate, and model stability and a small impact on depth. Decreasing the eddy viscosity has the following effects: increase in velocity magnitude, small decrease in water surface elevation, increase in unit flow rate, and when eddy viscosity values are below 10- $\text{m}^2/\text{s}$ , the model crashes before all time steps are complete. The FESWMS user manual states that an eddy viscosity of 1- $\text{m}^2/\text{s}$  is within reason for large to medium rivers; however, values less than 10- $\text{m}^2/\text{s}$  cause instabilities in the model.

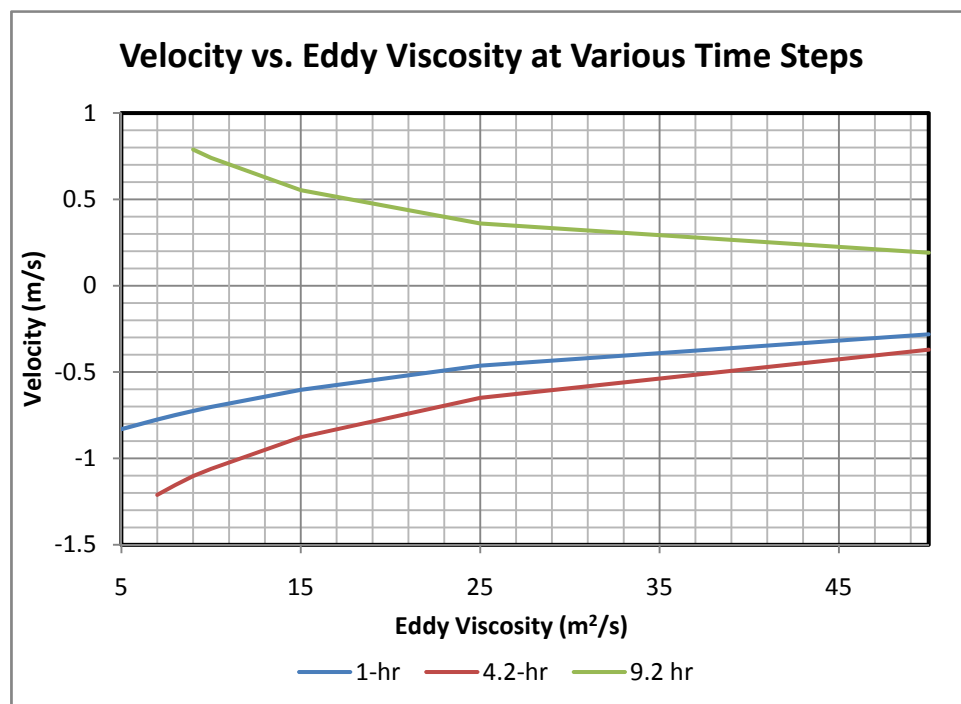


Figure 7 FESWMS Velocity vs. Eddy Viscosity

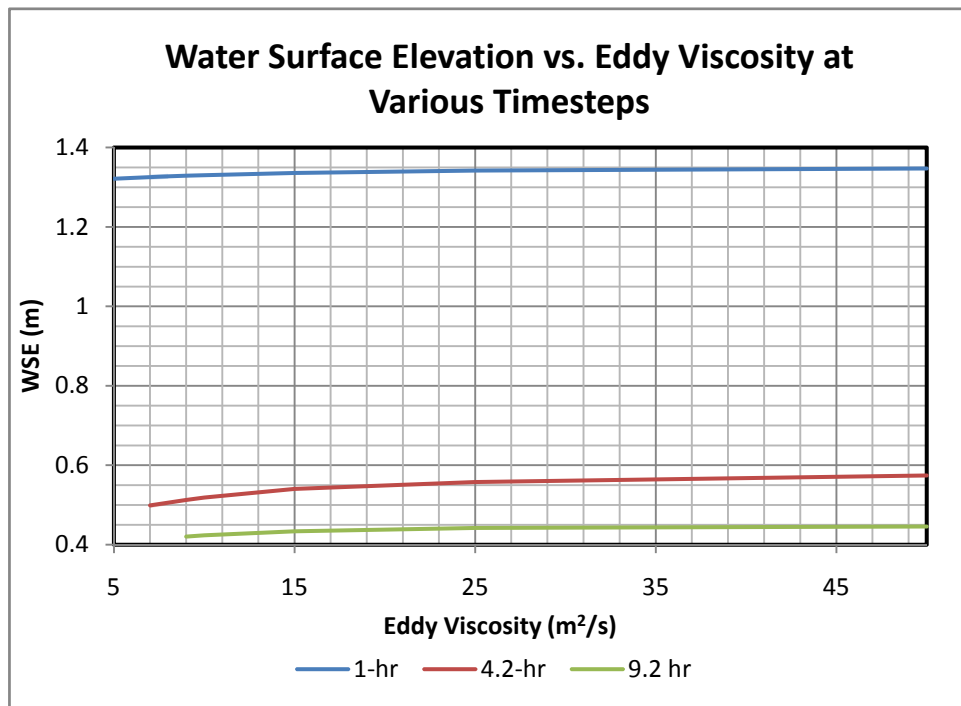


Figure 8 FESWMS WSE vs. Eddy Viscosity

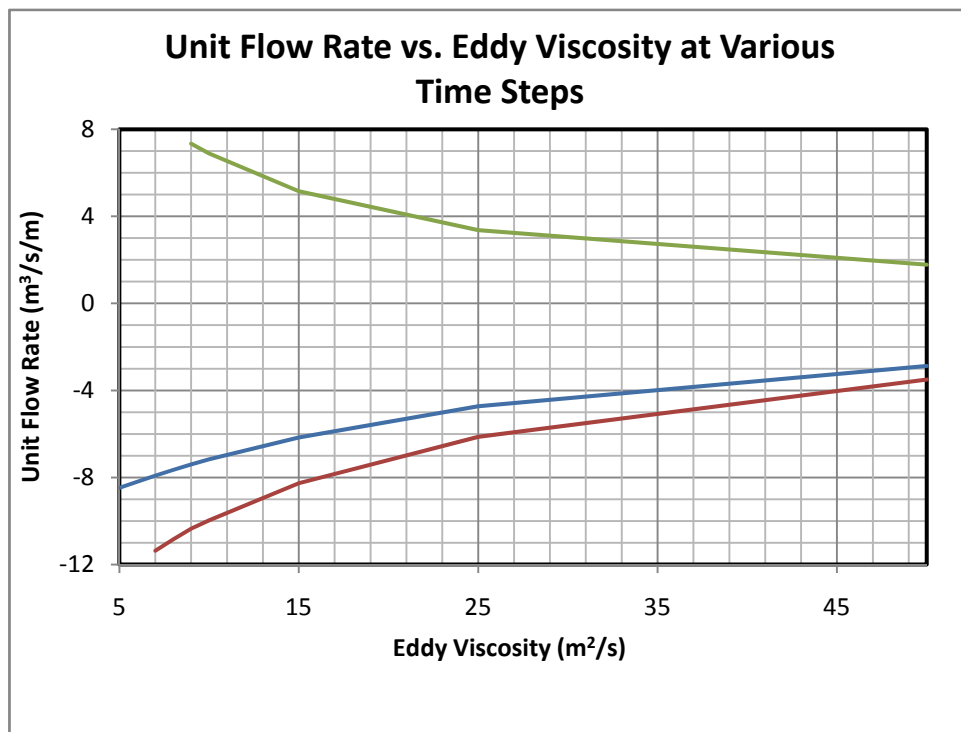
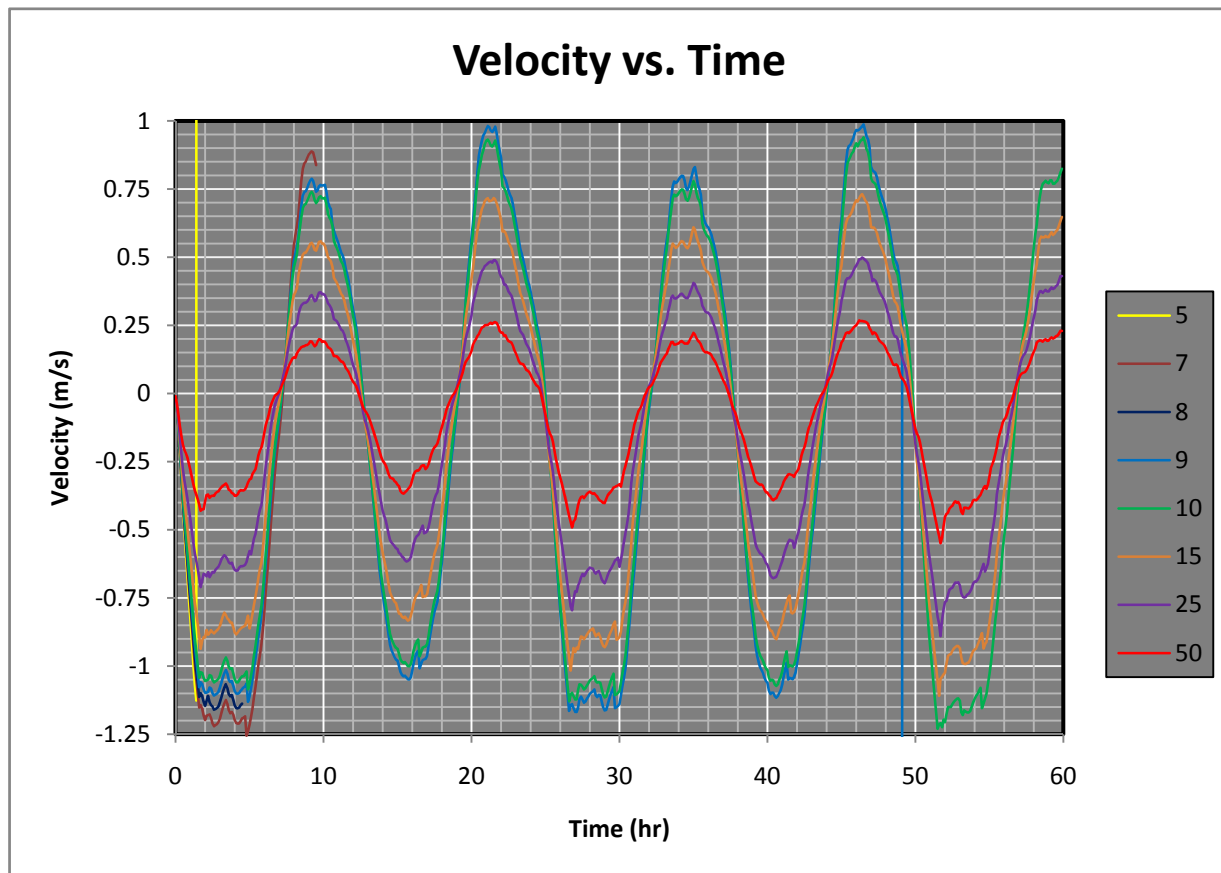


Figure 9 FESWMS Flow vs. Eddy Viscosity



**Figure 10 FESWMS Velocity vs. Time for Various Eddy Viscosities**

#### 4.3.2. Manning's n

The same model described in section 4.3.1 is used to measure model sensitivity to Manning's  $n$ . A constant eddy viscosity of  $15\text{-m}^2/\text{s}$  is used throughout the model runs. Initially, an eddy viscosity of  $10\text{-m}^2/\text{s}$  was used, but was increased to  $15\text{-m}^2/\text{s}$  due to stability issues.  $n$  values ranged from 0.012 to 0.030.

Decreasing Manning's  $n$  increases velocity and flow rate, and slightly decreases the water surface elevation (figures Figure 11, Figure 12, and Figure 13). It is interesting to note that according to Manning's equation (17(17)), velocity is inversely proportional to Manning's  $n$ . A look at Figure 11 shows that velocity increases about 1.2 times when  $n$  decreases by half. One would expect a more significant impact when  $n$  is halved.



$$V = \frac{1}{n} R^{2/3} S_o^{1/2} \quad (17)$$

where:

R = Hydraulic Radius

$S_o$  = Channel Slope

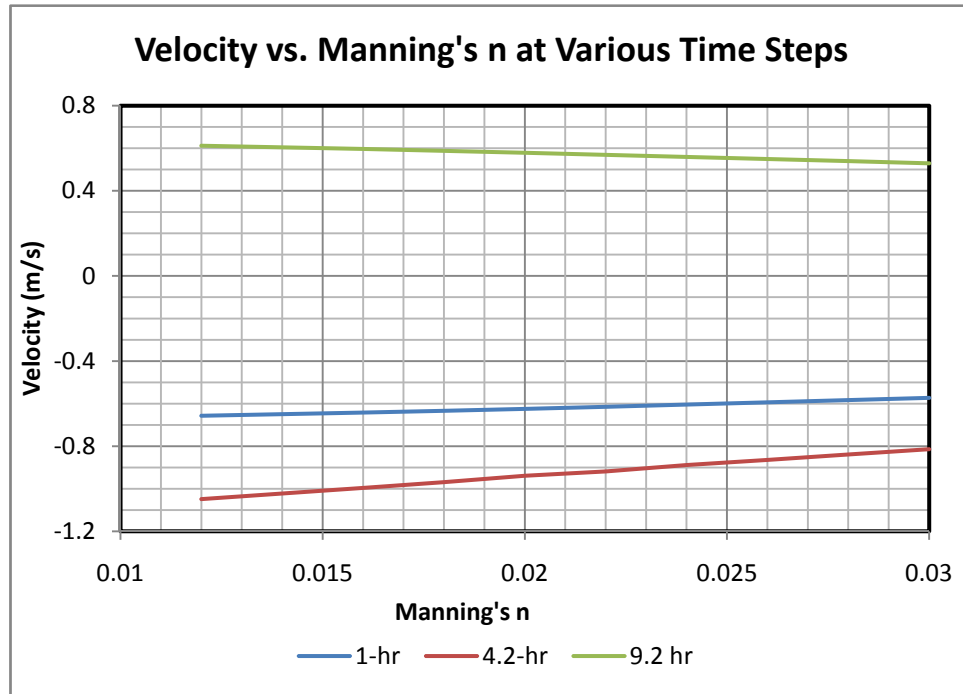


Figure 11 FESWMS Velocity vs. Manning's n

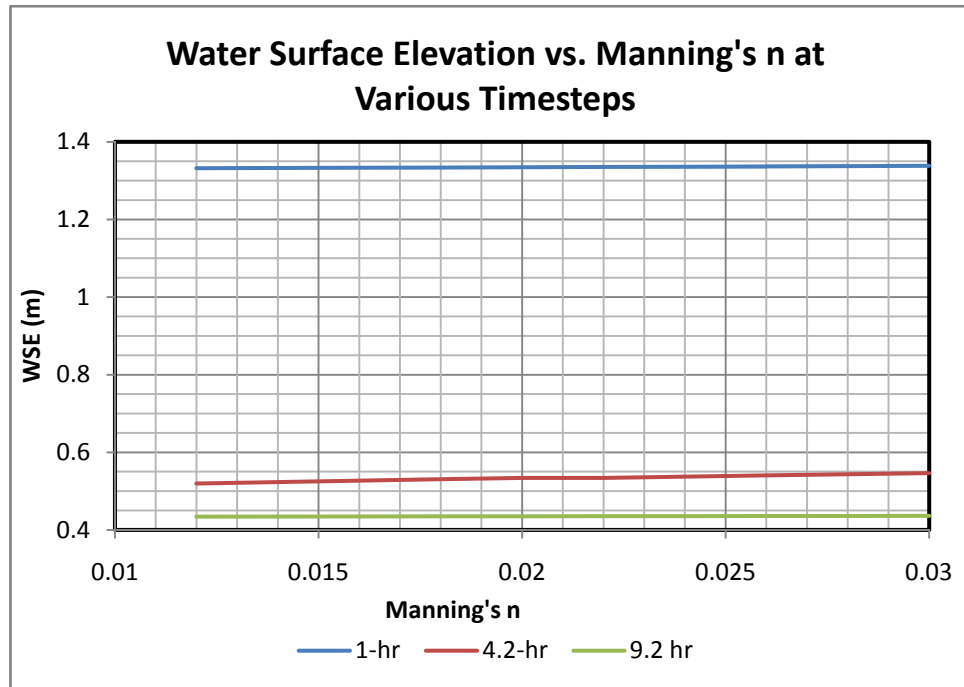


Figure 12 FESWMS WSE vs. Manning's n

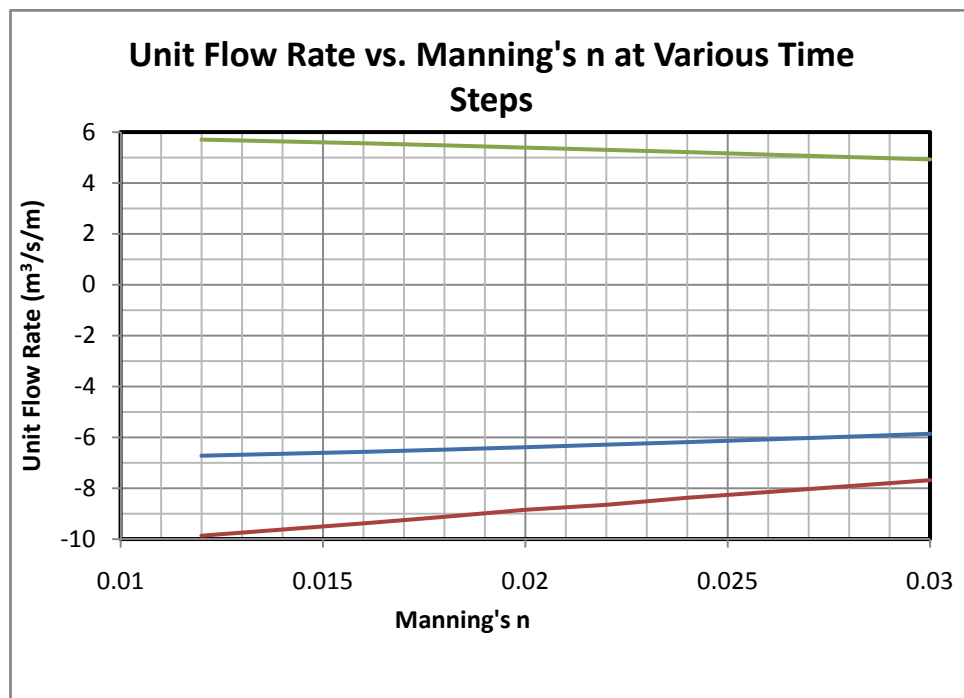


Figure 13 FESWMS Flow vs. Manning's n

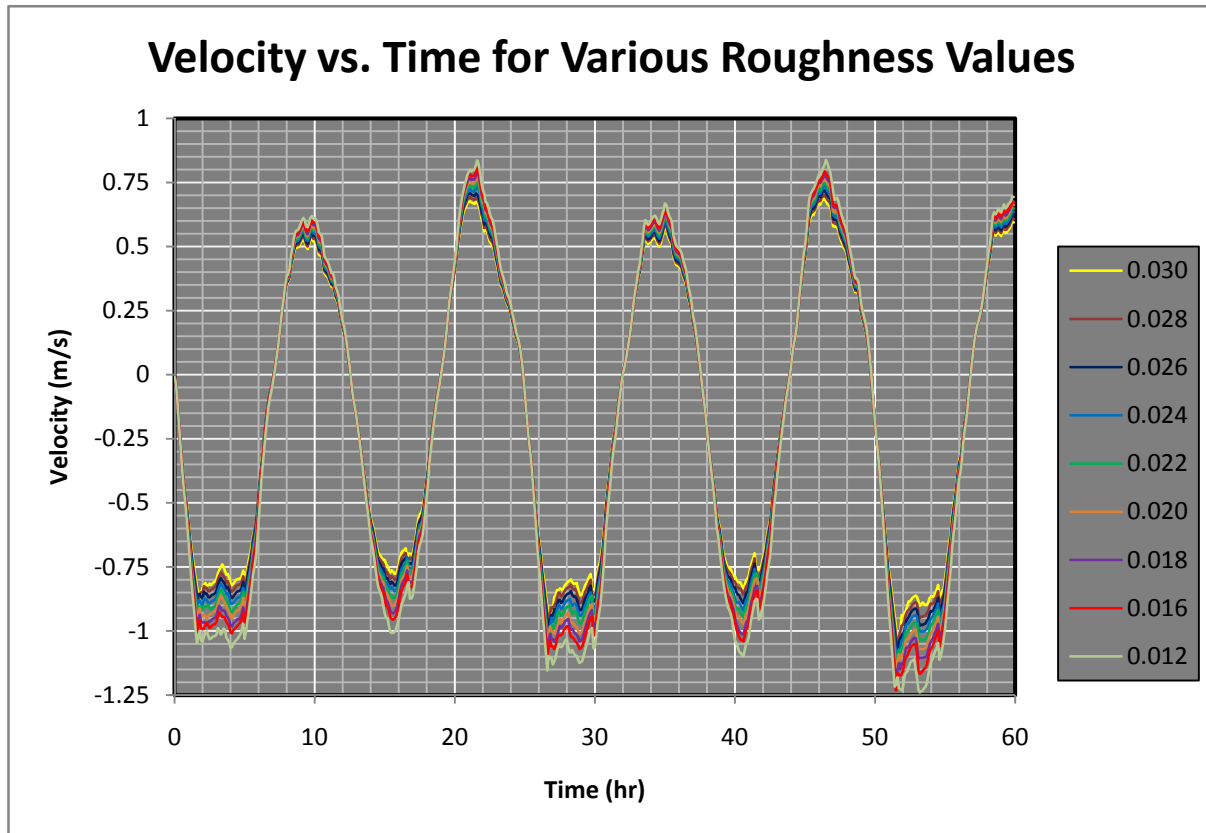


Figure 14 FESWMS Velocity vs. Time for Various Manning's n Values

#### 4.3.3. Time Step

The default computational time step used in FESWMS is 6-min. A brief analysis is done to see what effect varying the time step will have on model output and stability. Time steps of 3-min, 6-min, 9-min and 12-min are used. A Manning's n of 0.025 and eddy viscosity of 15-m<sup>2</sup>/s are used. Decreasing the time step increases model run time (see Figure 15). Time step has little impact upon reported velocity and water surface elevations. The maximum difference in reported velocity magnitudes for time steps of 3-min and 12-min is 0.14-m/s, the minimum is 0.00036-m/s, and the average is 0.043-m/s. Reported water surface elevations vary on average 3-cm with a maximum difference of 7-cm and a minimum difference of 1-mm between the 3-min and 12-min time step results. Unit flow rates change little with times step. For the 3-min time step, the model crashed before the entire 60-hr run was completed.

An attempt is also made to create a stable model with an eddy viscosity of  $5\text{-m}^2/\text{s}$  by changing the time step. Time steps of 1.5-min to 12-min are used without success.

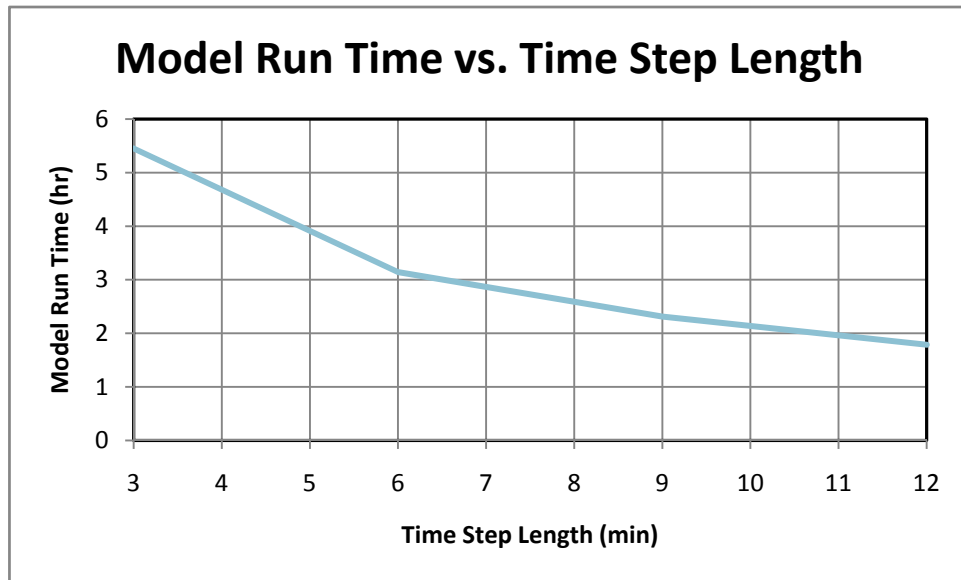


Figure 15 FESWMS Model Run Time vs. Time Step

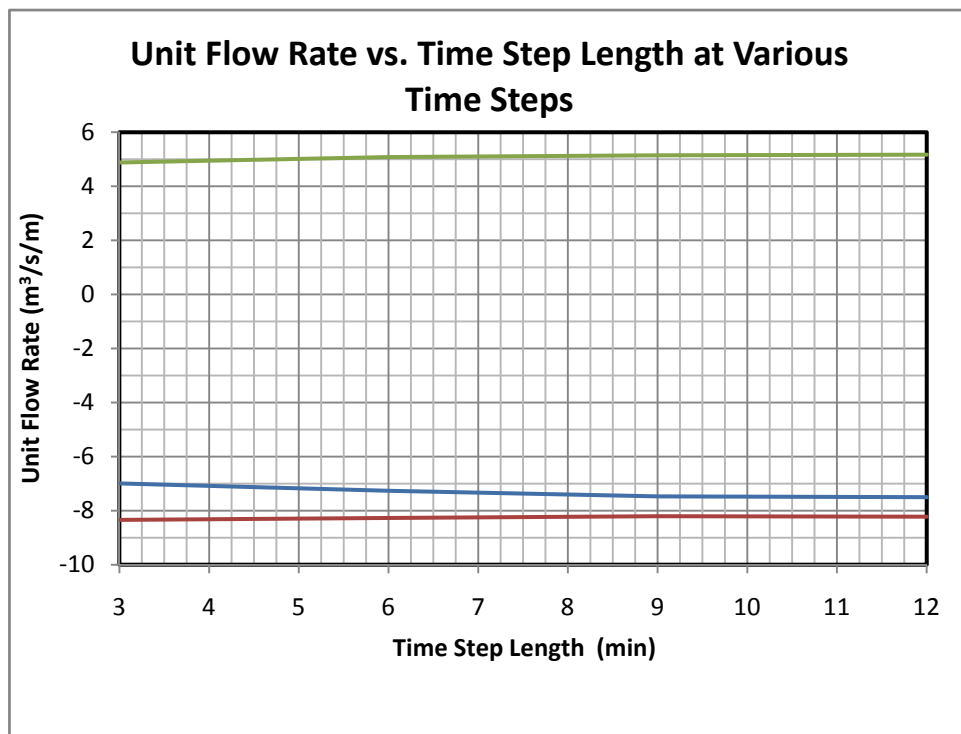
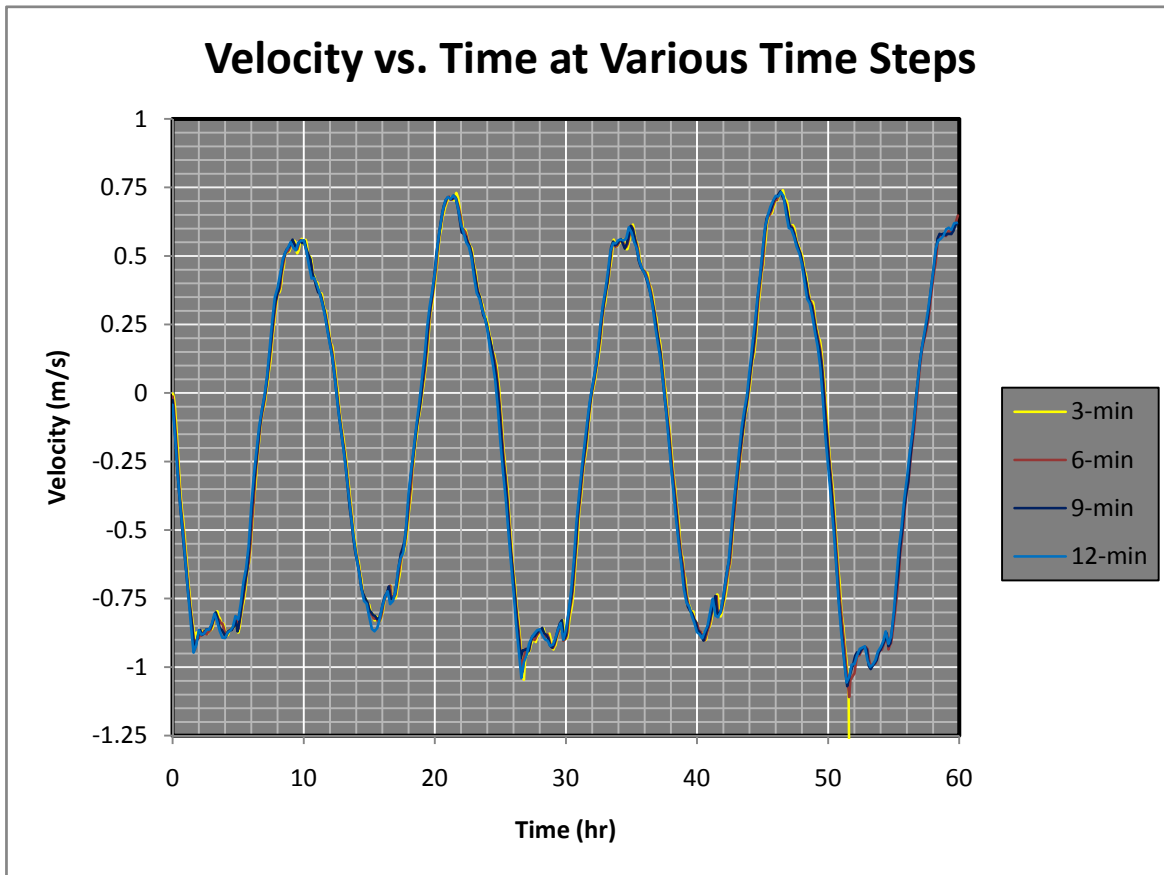


Figure 16 FESWMS Flow Rate vs. Time Step



**Figure 17 FESWMS Velocity vs. Time for Various Time Steps**

#### 4.3.4. Mesh Resolution

The effect of changing the size of the finite element mesh is also analyzed. Three mesh resolutions are used: 3,284, 13,136, and 52,544 element meshes. The corresponding numbers of nodes are 12,144, 47,670, and 188,868. The 3,284 element mesh is the same used in the above sensitivity analysis. The time step is 6-min, Manning's  $n$  is 0.025, and eddy viscosity of  $15\text{-m}^2/\text{s}$  for all runs. A time period of 24-hr is used.

The 13,136, and 52,544 element meshes are created from the 3,284 element mesh by using the refine tool in the SMS interface. This splits quadrilateral element into four new quadrilateral elements and triangular elements into three new triangular elements. The 3,284 element mesh is refined into the 13,136 element mesh which is then refined again into the 52,544 element mesh.

This was done in an attempt to minimize differences in the meshes that might have resulted from creating entirely new meshes.

Both the 3,284 and 13,136 element mesh models run the entire 24-hr period; however, the 52,544 element mesh model crashed 2.4-hr into the run. This seems to indicate that refining the mesh does not increase stability. This could be due to wetting and drying issues. Smaller elements cause more frequent changes in element wetting and drying from one time step to the next. Increasing the number of elements has the following effects: peak velocities increase, mostly in the south direction; unit flow rate increases during peaks; water surface elevations change little; and model run time increases significantly.

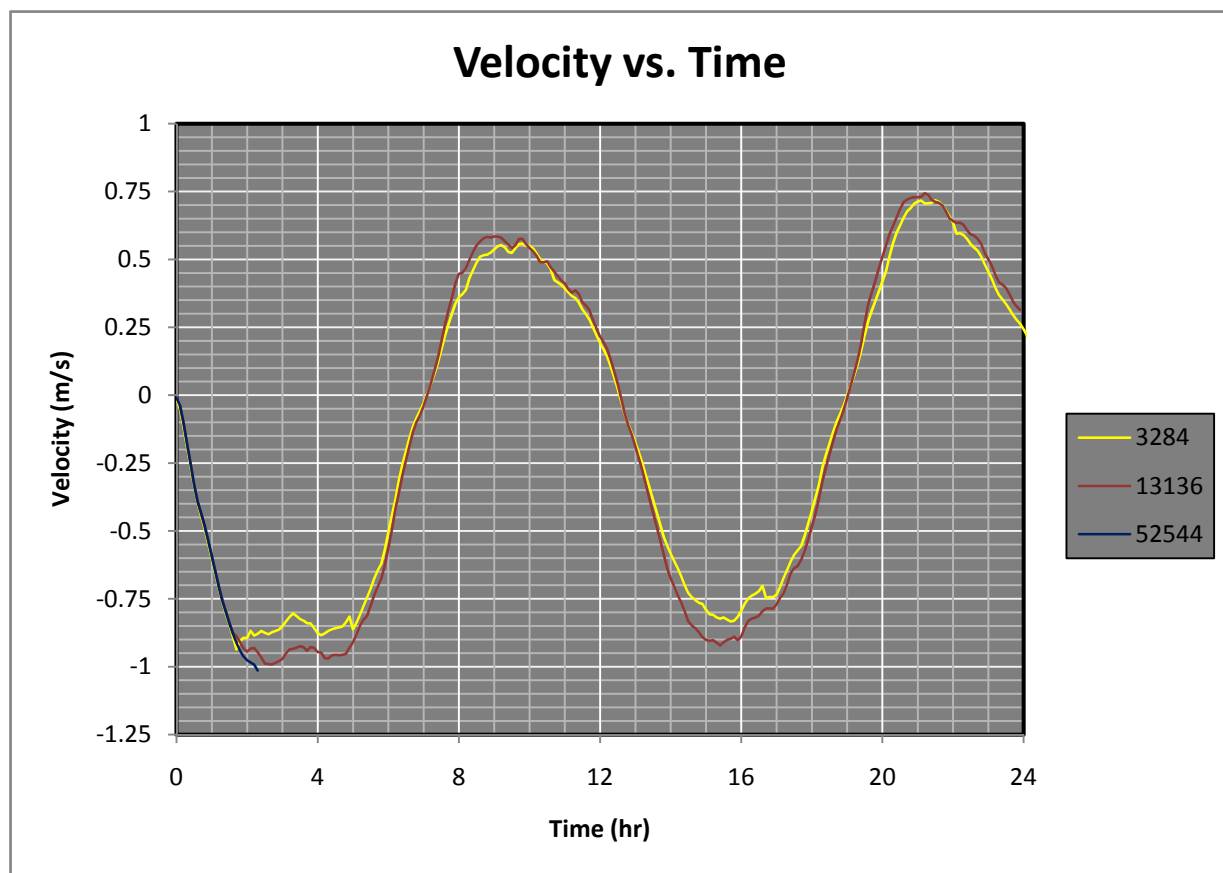


Figure 18 FESWMS Velocity vs. Time for Various Mesh Resolutions

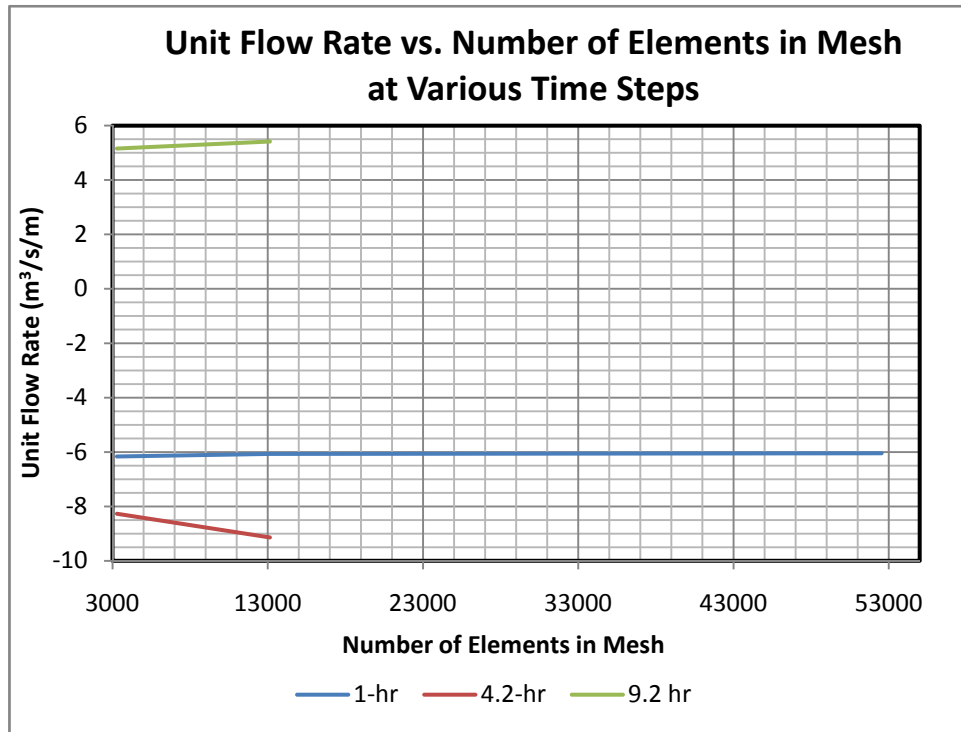


Figure 19 FESWMS Flow vs. Number of Elements in Mesh

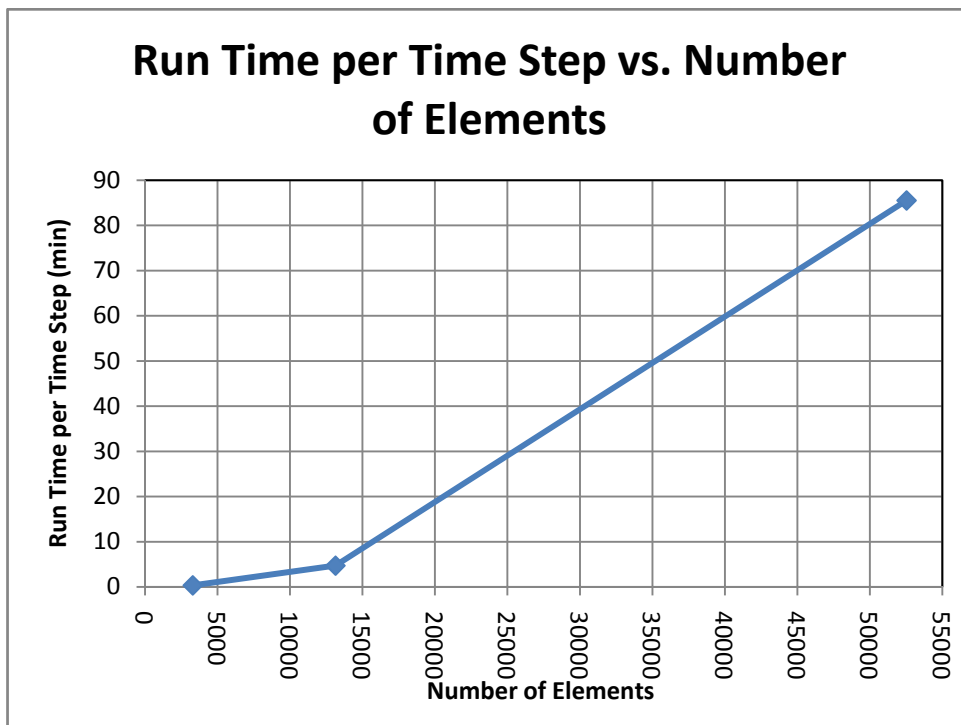


Figure 20 FESWMS Run Time vs. Number of Elements in Mesh

#### 4.3.5. Sensitivity Analysis Conclusion

Results from the sensitivity analysis indicate some issues with the model. First, realistic eddy viscosity cause the model to crash. The FESWMS user manual states that an eddy viscosity of  $1\text{-m}^2/\text{s}$  is within reason for large to medium rivers. Stability issues are encountered for eddy viscosity values less than  $10\text{-m}^2/\text{s}$ , an order of magnitude greater than the suggested value. These unreasonably high eddy viscosities are likely the reason that no FESWMS model runs approach the calibration data (see below). There is also reason to be concerned with the Manning's  $n$  analysis. Manning's equation shows that velocity is inversely proportional to  $n$ ; however, decreasing  $n$  by half did not result in doubling the velocity (velocity only increased by a factor of about 1.2). The model seemed to be rather insensitive to time step. Decreasing the time step did not aid stability. Increasing the number of elements in the mesh also did not seem to aid stability. This could be due to the increased frequency of wetting and drying due to finer mesh. Based upon this sensitivity analysis, creating an unsteady flow model of East River with FESWMS will be very difficult.

#### 4.4. Attempt to Match Calibration Data

In an attempt to match the calibration data, the following parameters are modified: the finite element mesh, Manning's  $n$ , eddy viscosity, number of iterations, and relaxation factor. Mesh resolutions used include 1,349, 5,660, 10,756, and 21,584 elements. In the vicinity where the calibration data is collected, these mesh resolutions correspond to approximate element sizes of 20-m by 60-m, 10-m by 30-m, 7-m by 20-m, and 5-m by 15-m, respectively. In general, increasing the number of elements has the following effects: increased model stability; allowed lower eddy viscosities and, to a lesser extent, allowed lower Manning's roughness values; decrease in reported velocities; and significantly increasing model run time. Some of these facts contradict findings in the above sensitivity analysis, which indicate that increasing the number of elements in the mesh has no conclusive affect on stability and increases peak velocities. This may also indicate the increasing the mesh resolution may aid stability up to a certain point. Values of eddy viscosity used range from  $3.3\text{-m}^2/\text{s}$  to  $15\text{-m}^2/\text{s}$ . Manning's  $n$  ranges from 0.013 (flow over concrete) to 0.080 (flow through dense weeds) (values taken from Mays 2001). The results of varying eddy viscosity and Manning's  $n$  correspond with the findings reported in the sensitivity analysis. The number of iterations and the relaxation factor are changed to aid model convergence, but seem to have little effect on the accuracy of the model.



One model run did provide results that are relatively close to the calibration data; however, it still did not provide satisfactory results. The parameters used in this model are an  $n$  value of 0.013, an eddy viscosity of  $10\text{-m}^2/\text{s}$ , and a mesh size of 5,660 elements. The negative velocities match the calibration data quite well; however, the positive velocities are only half of the calibration velocities. An  $n$  value of 0.013 seems very small for a natural channel ( $n=0.013$  corresponds to flow over smooth concrete, see Mays 2001). See section 7.2.1 for additional analysis on how well trial models runs match the calibration data.

There also seems to be some stability issues with FESWMS. Many of the model runs crash before the entire time period desired to be modeled (about 60-hr) finishes. Also there is great difficulty in modeling simpler channel geometries. Attempts are made to model trapezoidal channels; however, achieving a stable solution is very difficult. Also, an attempt is made to model a small section of the east channel of the East River, using HEC-RAS cross section results to drive the model (see sections 2.4.2.4 and 6 for more details on HEC-RAS). This is also unsuccessful. The fact that the East River model would run (albeit with unsuccessful results), but simpler channel geometries would not even yield results is very discouraging.

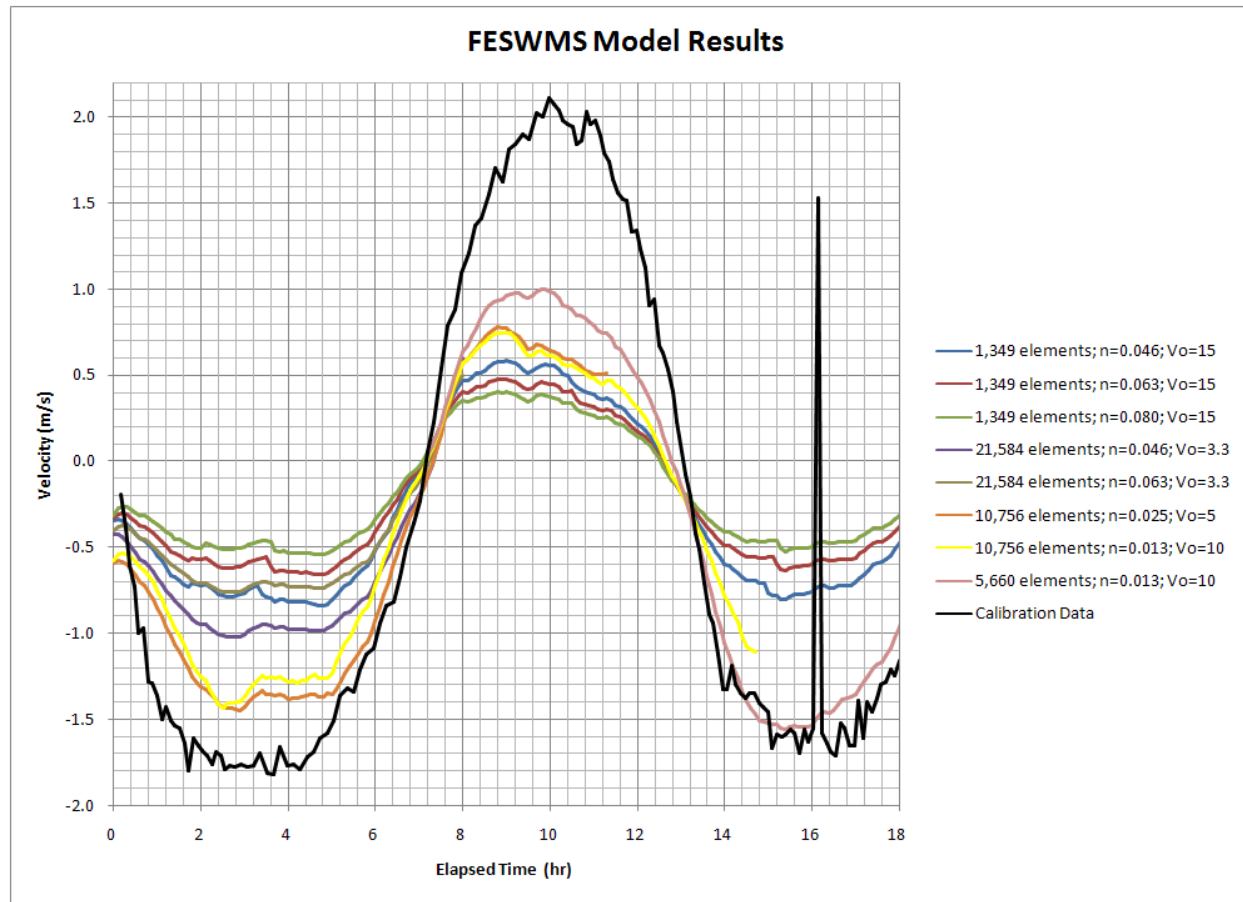


**Figure 21 FESWMS Model Results**

#### 4.5. Conclusion

Much of the time spent working in this study is spent in an attempt to achieve results from FESWMS that match the calibration data; however, these efforts are not successful. Choosing between stability and realistic eddy viscosities will not lead to successful model results. Wetting and drying of the elements may also be causing instabilities. Using FESWMS can be time consuming when considering that creating new models involves creating and editing the finite element mesh, performing a steady flow analysis to use as an initial condition for the unsteady run, performing the unsteady flow analysis, and changing parameters and repeating the process to achieve stability. Due to these reasons, FESWMS is not an effective tool to create a 2-D unsteady flow model of the East River.

## **5. TUFLOW Model**

After an unsuccessful attempt at modeling the East River with FESWMS, a second 2-D model, TUFLOW, is tried. TUFLOW is touted as being a robustly stable model that can easily handle unsteady flow. The model is also advertised as easy to use. Both of these reasons make TUFLOW an attractive alternative. TUFLOW is a 2-D finite difference model that also runs within SMS (for more information on TUFLOW see section 2.4.2.3). The process used with TUFLOW is similar to that used in FESWMS. A finite difference grid is created, boundary conditions are entered, and initial runs are made followed by a sensitivity analysis. Attempts to match the calibration data are successful with TUFLOW.

### **5.1. Model Setup**

The first step in creating a TUFLOW model is setting up the finite difference grid. A rectangle is drawn around the area to be modeled and a grid is created within this rectangle. The model user only needs to specify the size of the grid elements. The grid is composed of rectangles all of which are the same size. The grid is used to represent the geometry and calculate parameters such as velocity and water depth. Elevation data for the grid is taken from the DTM outlined in section 3.1. Setting up the grid is a relatively easy process when compared with creating a finite element mesh. Material properties are assigned to the grid to account for roughness parameters. For this model, a constant roughness value is used throughout the entire model domain; however, GIS data can be imported or different areas traced out within SMS to represent different materials. Once boundary conditions are assigned and the model properties are set up, the model is ready to run. Running the TUFLOW model within SMS is a very simple, straightforward task. Once the model is set up, export the TUFLOW files and run TUFLOW. A base Manning's roughness value is set to 0.025 for all runs unless stated otherwise (this value is chosen because it is the default value used in FESWMS and is initially used for comparisons).

### **5.2. Initial Runs**

A few issues are encountered during the first few runs, resulting in the model crashing. In an attempt to achieve stable runs, a few modifications to the initial model setup are made. In SMS, the boundary conditions assigned to the TUFLOW model are specified on arcs that span the model. These arcs that make up the boundary conditions, one at the southern end of the reach and one at the northern end, are modified to minimize potential issues on the boundary conditions locations

(these arcs originally spanned the width of the model, but are shortened to span the width of river at its highest elevation). TUFLOW uses a level water surface profile to start the model. In order to satisfy this criterion, the boundary condition data is edited such that the initial water surface is level across the entire reach. Four grid resolutions are used in the initial runs, 20-m, 10-m, 8-m, and 5-m (20-m grid resolution means the rectangles in the finite difference grid are roughly 20-m by 20-m). For the finer grid resolution models (5-m and 8-m), part of the grid is turned off due to instabilities in those areas (see Figure 22). The part of the grid that is turned off is near the upstream (north) boundary, and it is assumed that the readings taken, which are in the middle of the reach, are not significantly affected. These modifications resulted in stable initial model runs.

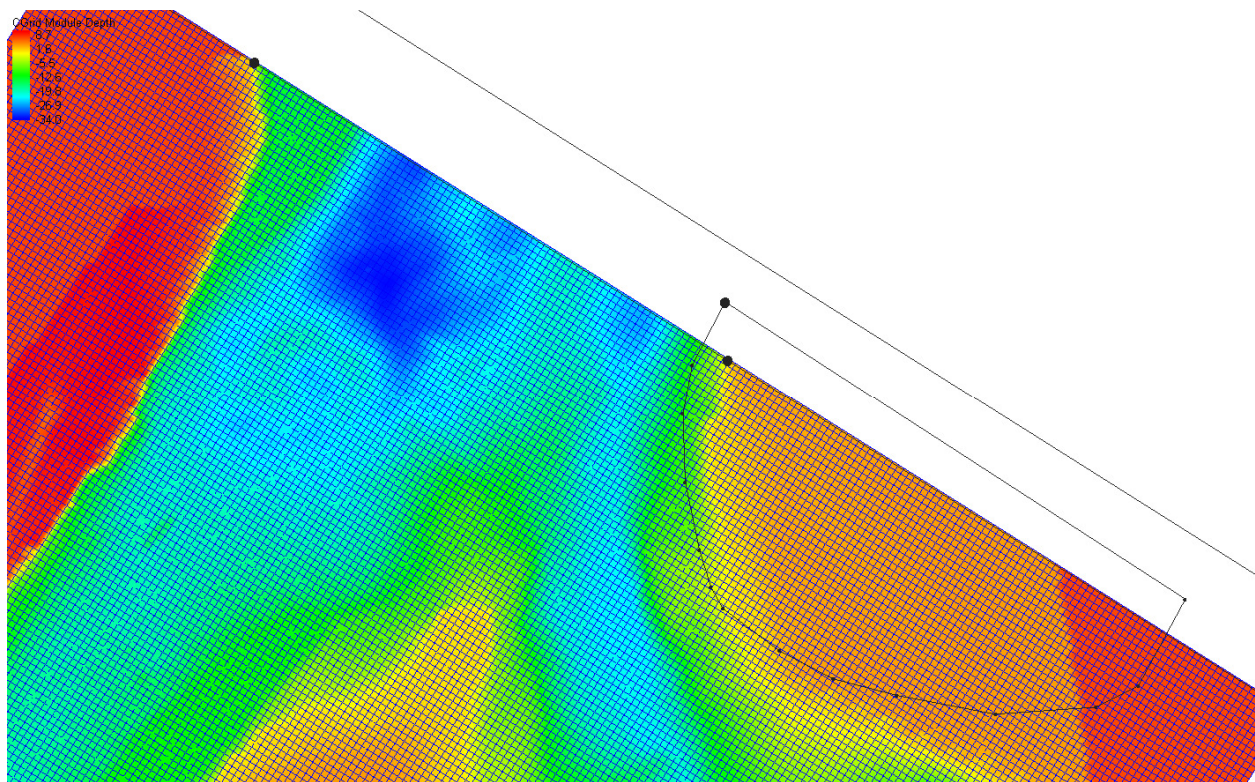


**Figure 22 TUFLOW 5-m Grid Showing the Part of Grid Turned Off (The Area Enclosed by the Rough Half Circle)**

### 5.3. Sensitivity Analysis

Once the initial modeling attempts are made, a sensitivity analysis is performed on various model parameters to what effect they have on the model. The resulting changes in model output (velocity,

water surface elevation, flow rate) are measured at the point where calibration data is provided (see Figure 4).

#### 5.3.1. Grid Resolution

Four grid resolutions are used in the model, 20-m, 10-m, 8-m, and 5-m. All of the settings except time step are the same for each of these initial models. The time step is set to roughly half of the grid resolution as suggested in the TUFLOW manual (2-sec for the 5-m grid, 5-sec for the 10-m grid). A time step of 5-sec is used for the 20-m grid to achieve stability. The 8-m grid uses a 1-sec time step due to previous attempts to achieve stability (the time step was set to 1-sec before finding the actual problem and was not changed back).

The results of these runs are compared with calibration data provided by Verdant Power (see section 3.3). The velocities reported by TUFLOW match the pattern of the calibration data, and match velocities flowing south rather well; however, northward velocities were significantly off (see Figure 23). For the 5-m and 20-m grids, the average error for velocity magnitudes greater than 1-m/s are 0.82-m/s and 0.76-m/s for north flows and 0.42-m/s and 0.19-m/s for south flows, respectively (see section 7.1.1 for details on error calculations), thus indicating that the coarser 20-m grid more closely mimicked real world conditions. The run times for the 5-m, 8-m, 10-m, and 20-m were 24.82-hr, 18.22-hr, 2.9-hr, and 0.7-hr, respectively for a 66-hr simulated duration.

As the grid resolution becomes finer the following happens: north flow velocities change little, south flow velocities increase significantly, water surface elevation changes little, and the data tends to oscillate more.

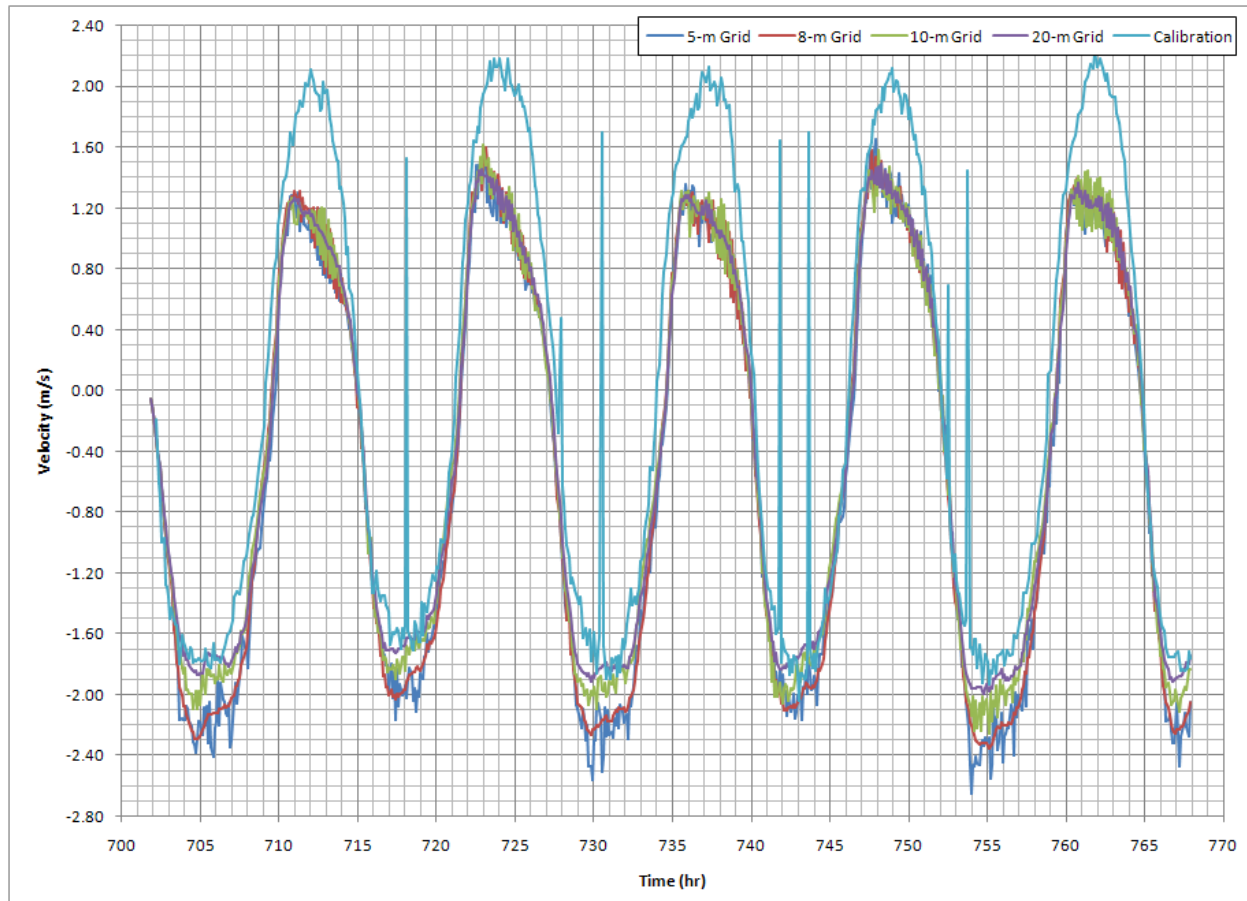


**Figure 23 TUFLOW Velocity vs. Time for Various Grid Resolutions**

### 5.3.2. Manning's $n$ Value Analysis

Manning's  $n$  values of 0.012 to 0.040 are used to compare their effects on model results using the 20-m grid. Varying Manning's  $n$  has a significant impact on model output. As Manning's  $n$  decreases, velocities increase, much more in the south flow direction than in the north direction (Figure 24). Water surface elevations decrease as  $n$  decreases. Also, the oscillations seen at the peaks tend to increase as  $n$  decreases. The unit flow rate magnitude is decreased as  $n$  increases.

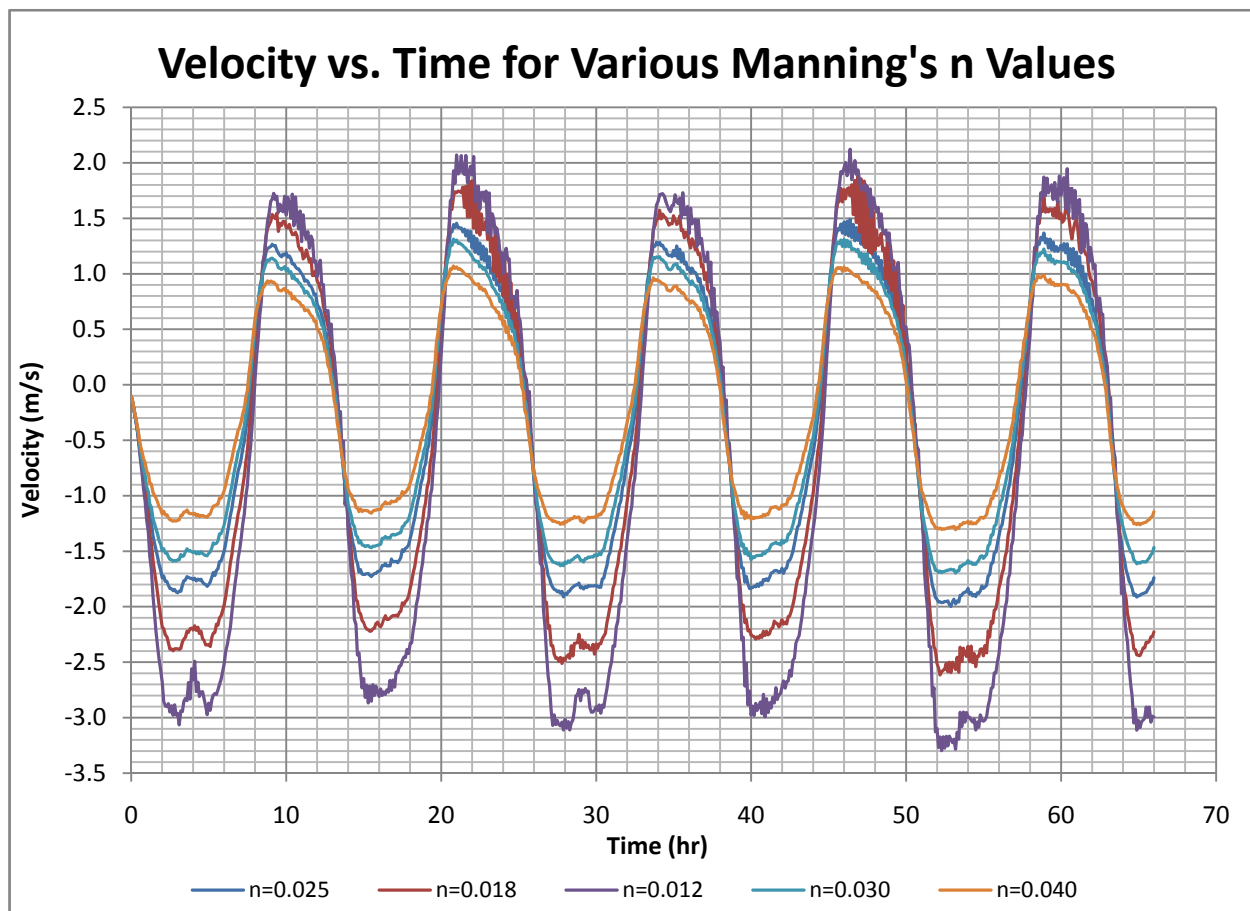


Figure 24 TUFLOW Velocity vs. Time for Various Manning's n Values

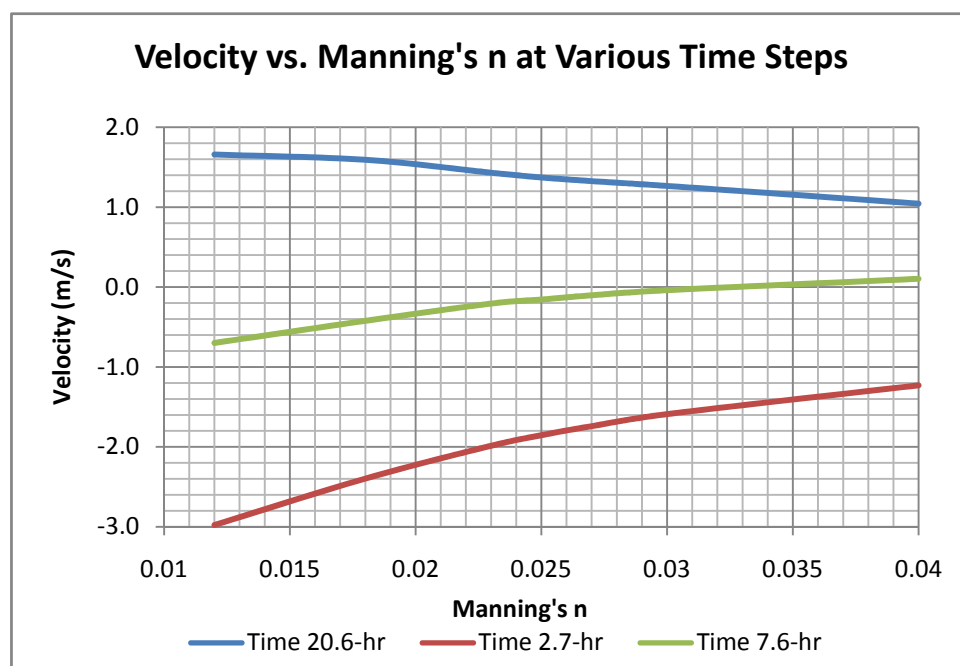


Figure 25 TUFLOW Velocity vs. Manning's n

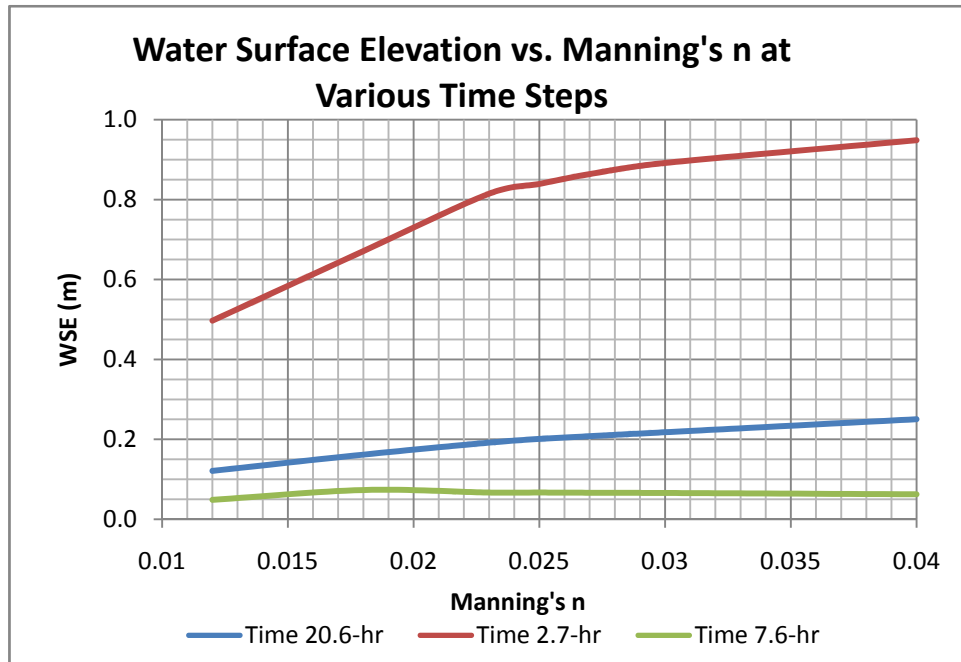


Figure 26 TUFLOW WSE vs. Manning's n

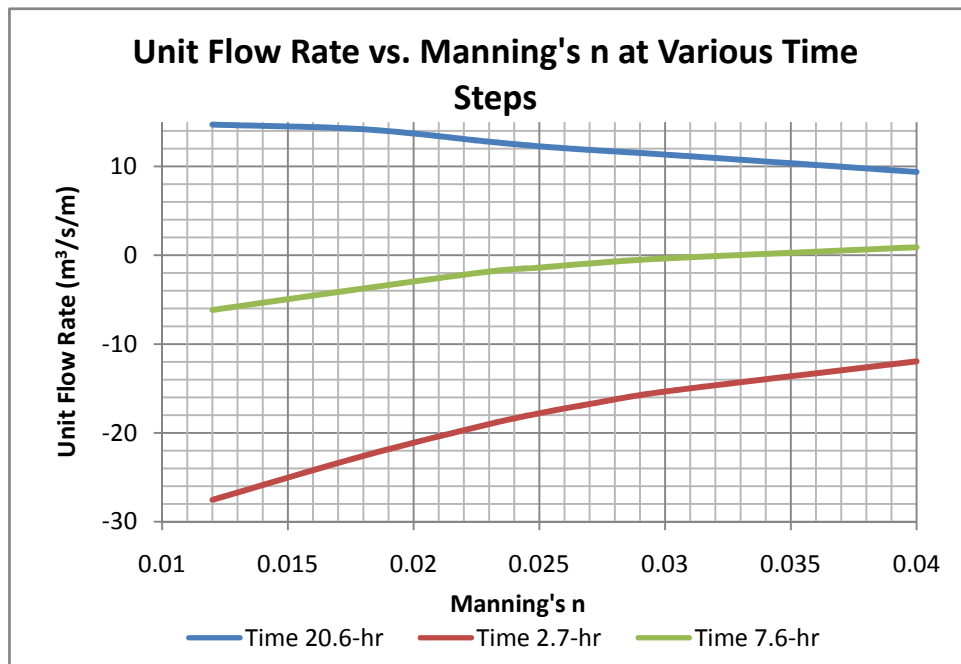


Figure 27 TUFLOW Flow vs. Manning's n

### 5.3.3. Eddy Viscosity Analysis

The effects of changing eddy viscosity parameters on the model are also analyzed. Both the Smagorinsky formulation and constant eddy viscosity methods are used. Coefficients of 0.1 to 1 are



use for the Smagorinsky formulation to compare their effect. Constant values of 0.1 to 10-m<sup>2</sup>/s are used for the latter method. There is absolutely no change in model output when these parameters are changed regardless of the method used.

#### 5.3.4. Boundary Condition Analysis

Varying Manning's n values, eddy viscosities and other values does not result in a model that successfully matches the calibration data. Perhaps there is a problem with the boundary condition data (see section 3.2 for details regarding the boundary condition data). Attempts are made to use predicted data that closely matches actual data; however, a certain amount of error is present. In order to determine if this error is significant, an analysis is done to see what effect changing the southern water surface elevation boundary condition will have on model results. Constants were added and subtracted from all points in the in the southern boundary condition. The model is set up as before, with the 20-m grid. A constant n value of 0.025 is used.

Adding constants to the southern boundary condition shifted the velocity versus time curve up and down (Figure 28). Adding these constants alone did not make the velocity data match the calibration data any better than previous attempts; however, when a constant is added to the southern boundary condition data and Manning's n is decreased, the model's predicted velocities and the calibration velocities begin to match much better (see section 7.2.269).

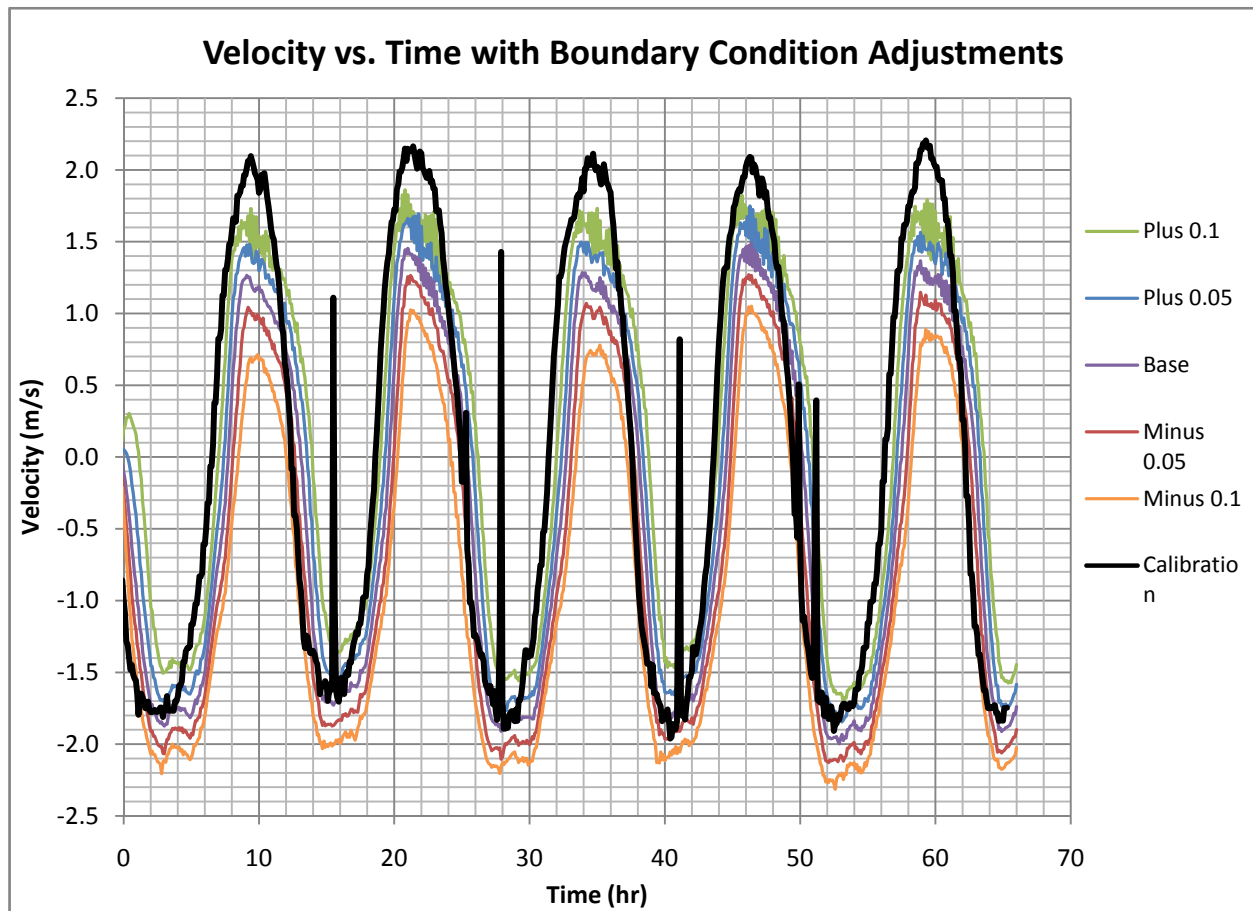


Figure 28 TUFLOW Velocity vs. Time for Various Boundary Conditions

### 5.3.5. Time Step Analysis

An analysis is also performed to see what effect changing model time step has on output. Time steps of 0.25-sec, 1-sec, 2-sec, and 5-sec are used. A Manning's  $n$  of 0.18, modified boundary conditions (0.1-m added to all southern water surface elevation ordinates), and the 20-m grid are used. A 66-hr period is modeled. Varying the time step had little impact on the magnitude of results. Velocity, water surface elevation, and unit flow rate remain relatively constant for various time steps (Figure 31, Figure 32, and Figure 33). Increasing the time step reduces model run time (from a 6.5-hr run time for a time step of 0.25-sec to 0.4-hr run time for a time step of 5-sec). Reducing the time step did help dampen the oscillations in model output (Figure 29, Figure 30, Figure 35, and Figure 36). Equation (18) is used as a measure of oscillation and is only an indication of oscillation. Equation 18 does not yield the actual average value of the oscillations.

$$\text{Average Velocity Oscillation} = \sqrt{\frac{1}{n} \sum_{i=1}^n (V_i - V_{i+1})^2} \quad (18)$$

where  $V_i - V_{i+1}$  is the difference between velocities for two adjacent time steps ( $t_i$  and  $t_{i+1}$ ).

Note: the same equation is used to measure average water surface elevation oscillation by replacing velocity terms with water surface elevation terms.

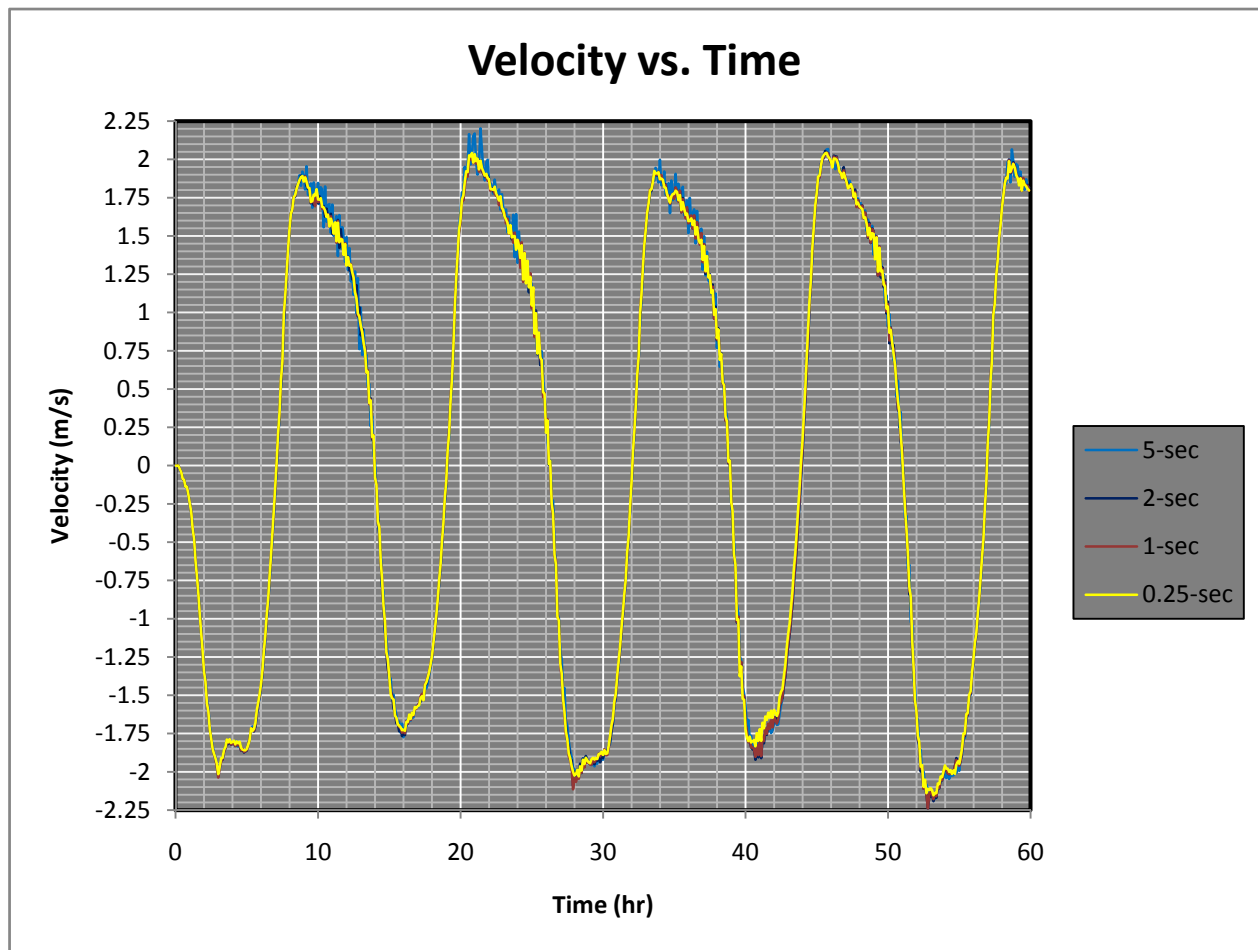


Figure 29 TUFLOW Time Step Analysis Velocity vs. Time

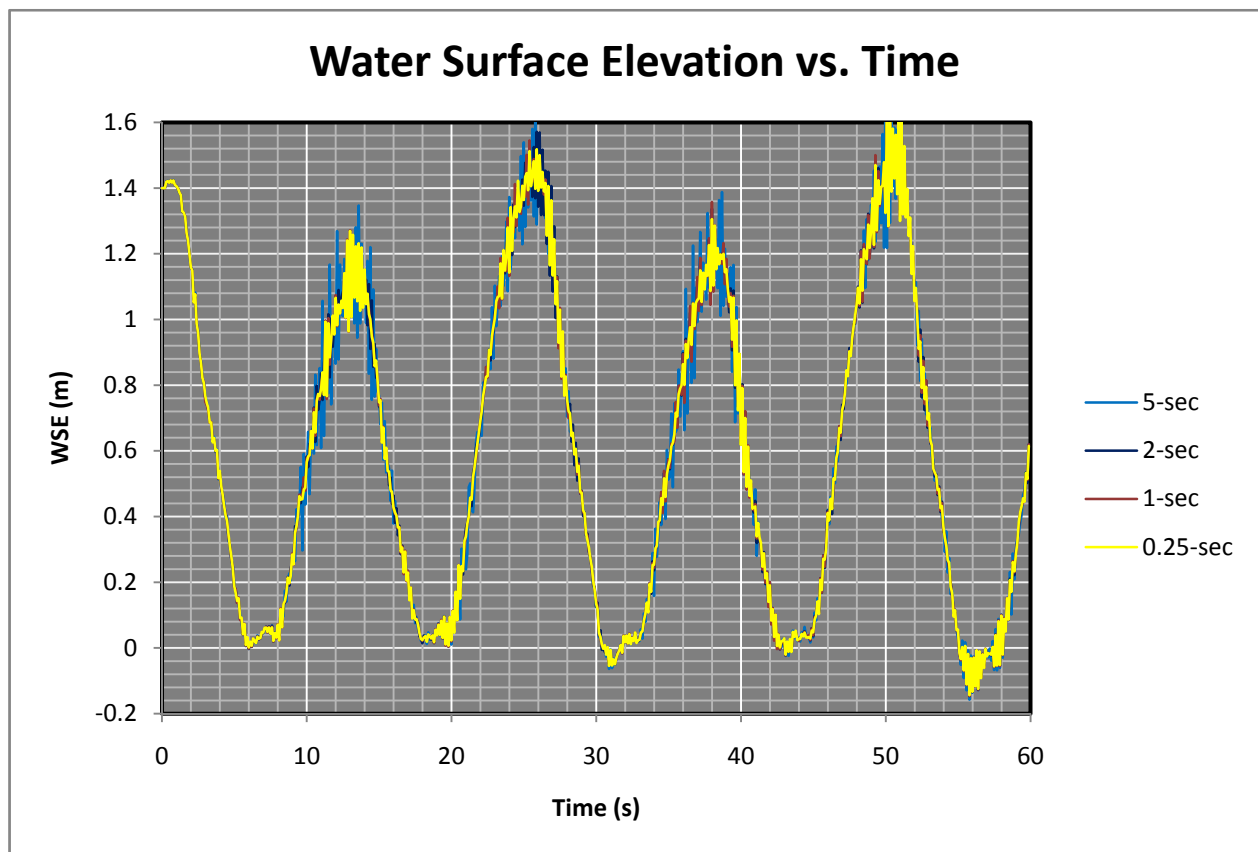


Figure 30 TUFLOW Time Step Analysis Water Surface Elevation vs. Time

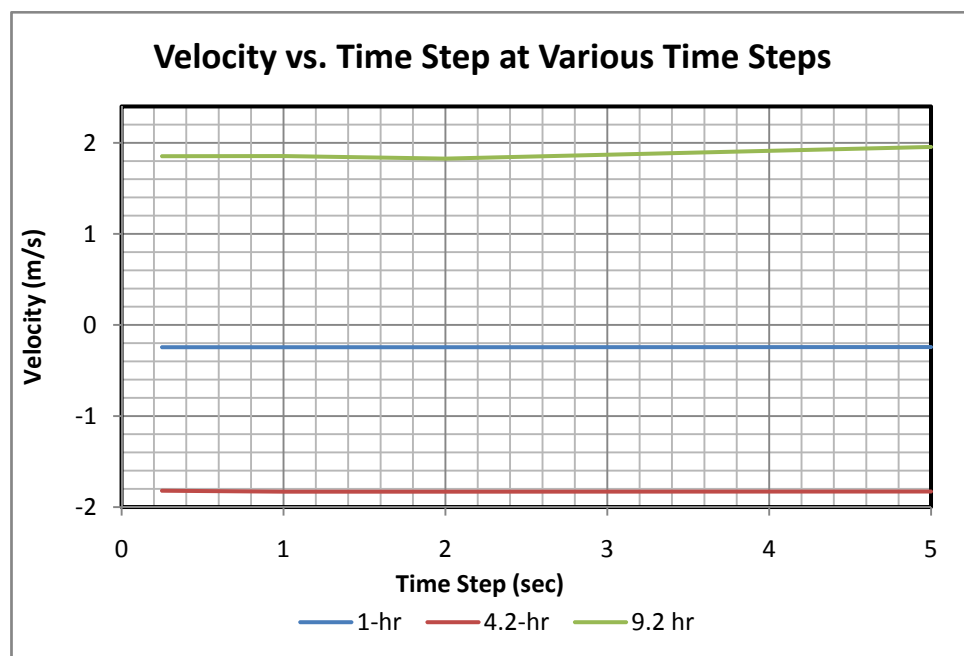


Figure 31 TUFLOW Time Step Analysis Velocity vs. Time Step

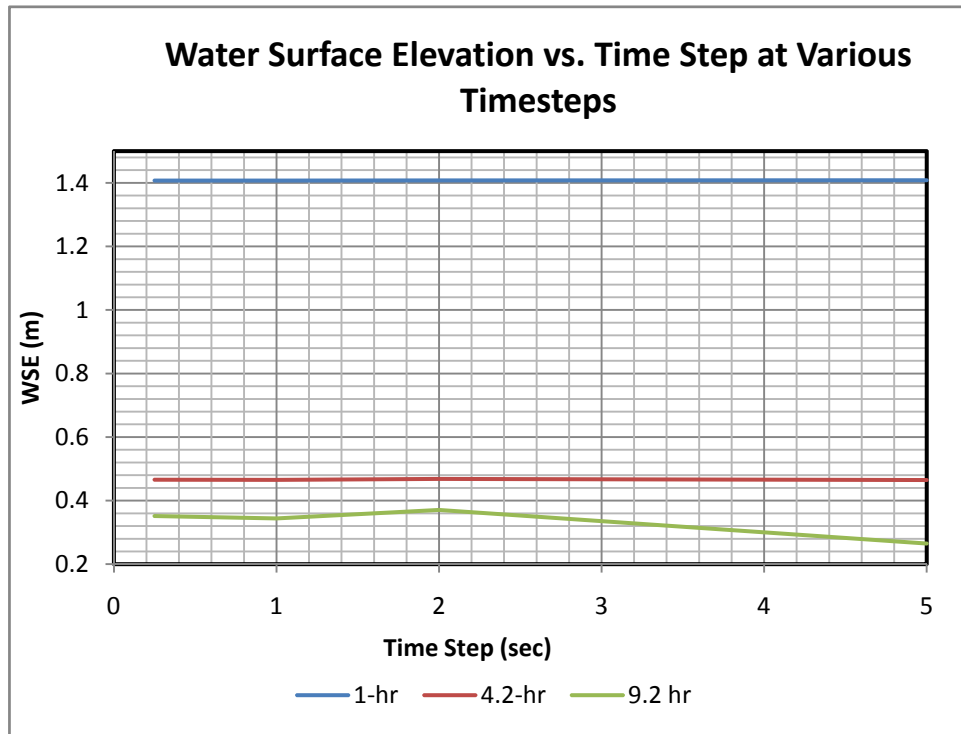


Figure 32 TUFLOW Time Step Analysis Water Surface Elevation vs. Time Step

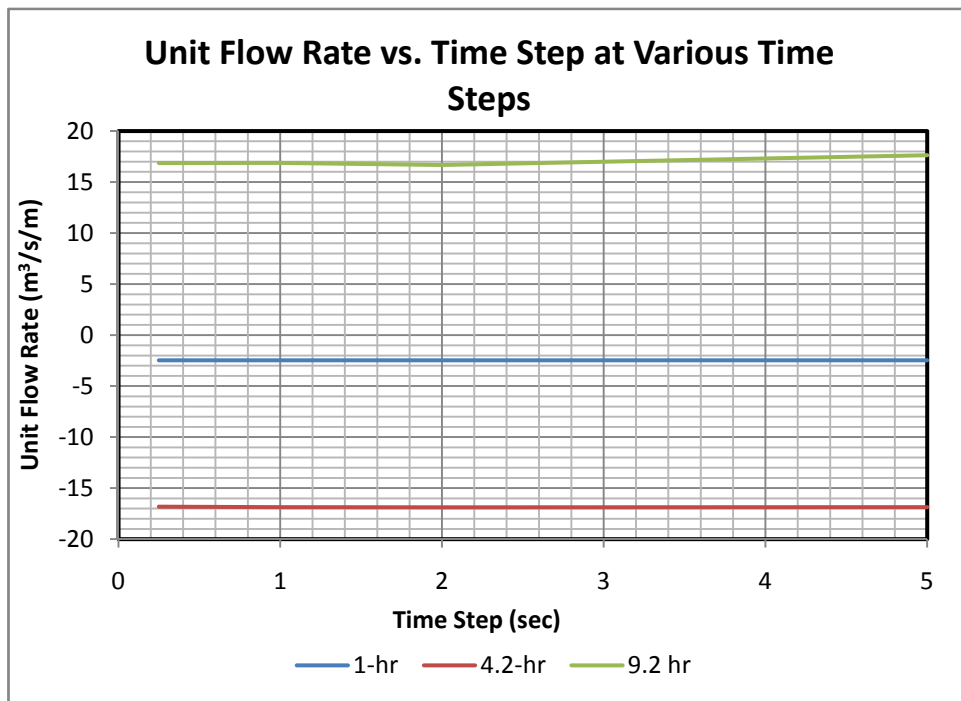


Figure 33 TUFLOW Time Step Analysis Unit Flow Rate vs. Time Step

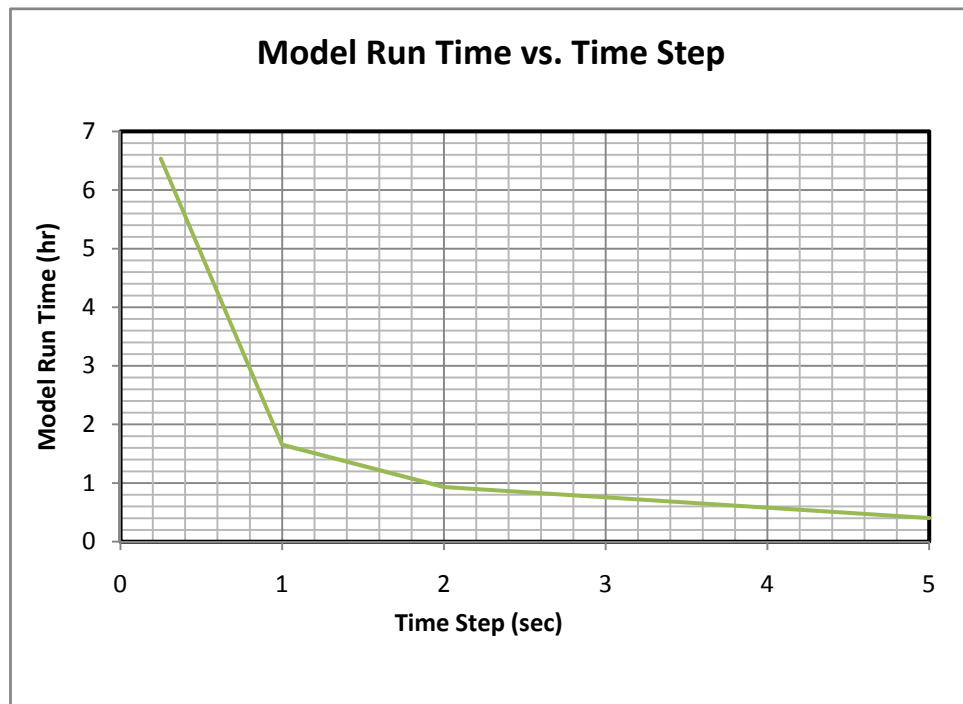


Figure 34 TUFLOW Time Step Analysis Model Run Time vs. Time Step

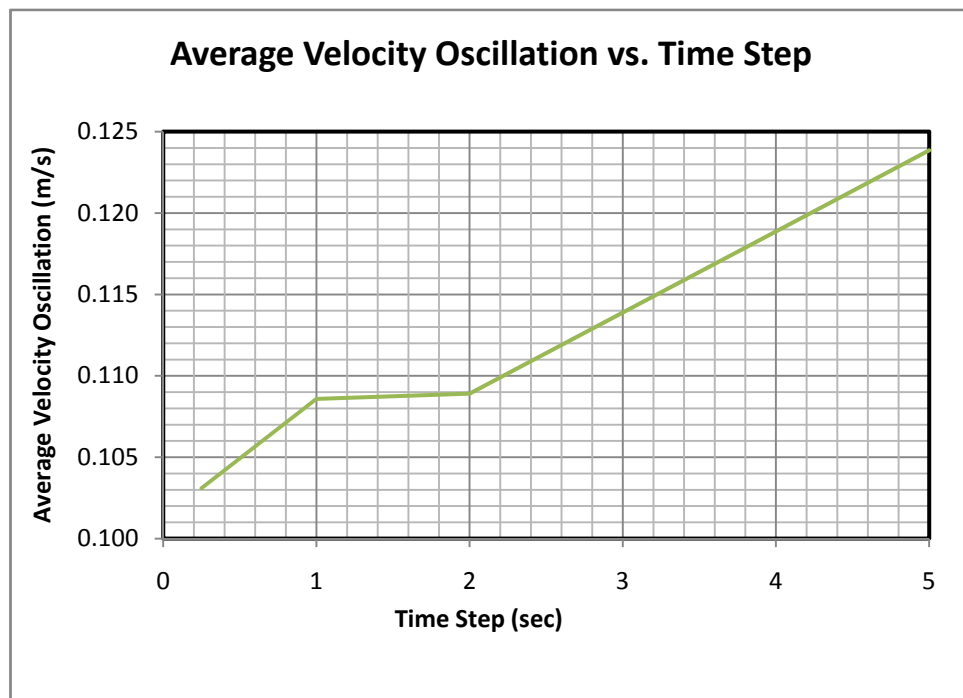
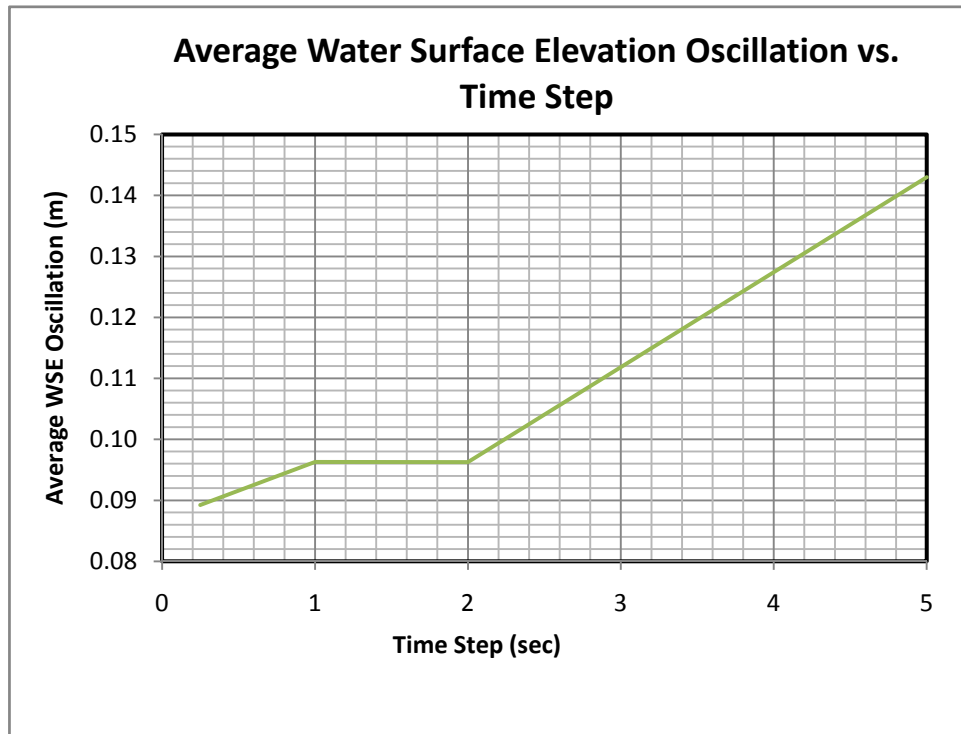


Figure 35 TUFLOW Time Step Analysis Velocity Oscillation vs. Time Step



**Figure 36 TUFLOW Time Step Analysis Water Surface Oscillation vs. Time Step**

#### 5.3.6. Sensitivity Analysis Conclusions

From the above sensitivity analysis the following conclusions are made. A course grid resolution of 20-m is preferred over a finer grid. As the grid becomes finer, the model output oscillates more and diverges from the calibration data. Decreasing the size of the grid elements also significantly increases model run time. Manning's  $n$  has a significant impact on model output. Decreasing  $n$  by half results in roughly doubling flow velocity peaks. Varying eddy viscosity parameters have absolutely no impact on model output. Adjusting the southern boundary condition also has a significant impact on model output. Adding a constant of 0.1-m to all water surface elevations in the southern boundary condition begins to align the model output and calibration data. By adjusting Manning's  $n$  and adjusting the southern boundary condition, the model can be calibrated. The time step should be set to a relatively low value to reduce the oscillations in the model output. By using the results from the sensitivity analysis, a successful model of the East River can be developed.

#### 5.4. Attempt to Match Calibration Data

From the above sensitivity analysis, a better attempt at matching the calibration data can be made. By adding a constant to the southern boundary condition, the entire velocity series can be adjusted up or down. By changing Manning's  $n$ , the velocity peak magnitudes can be increased or decreased. A model run is made by adding 0.1-m to the southern boundary condition and changing Manning's roughness value to 0.018. Doing so yields results much closer to the calibration data than any previous run (Figure 37). For the purpose of this study, this run is deemed a successful model of the East River. Further analysis of how well these results, and additional trial runs, match the calibration data is provided in section 7.2.2.

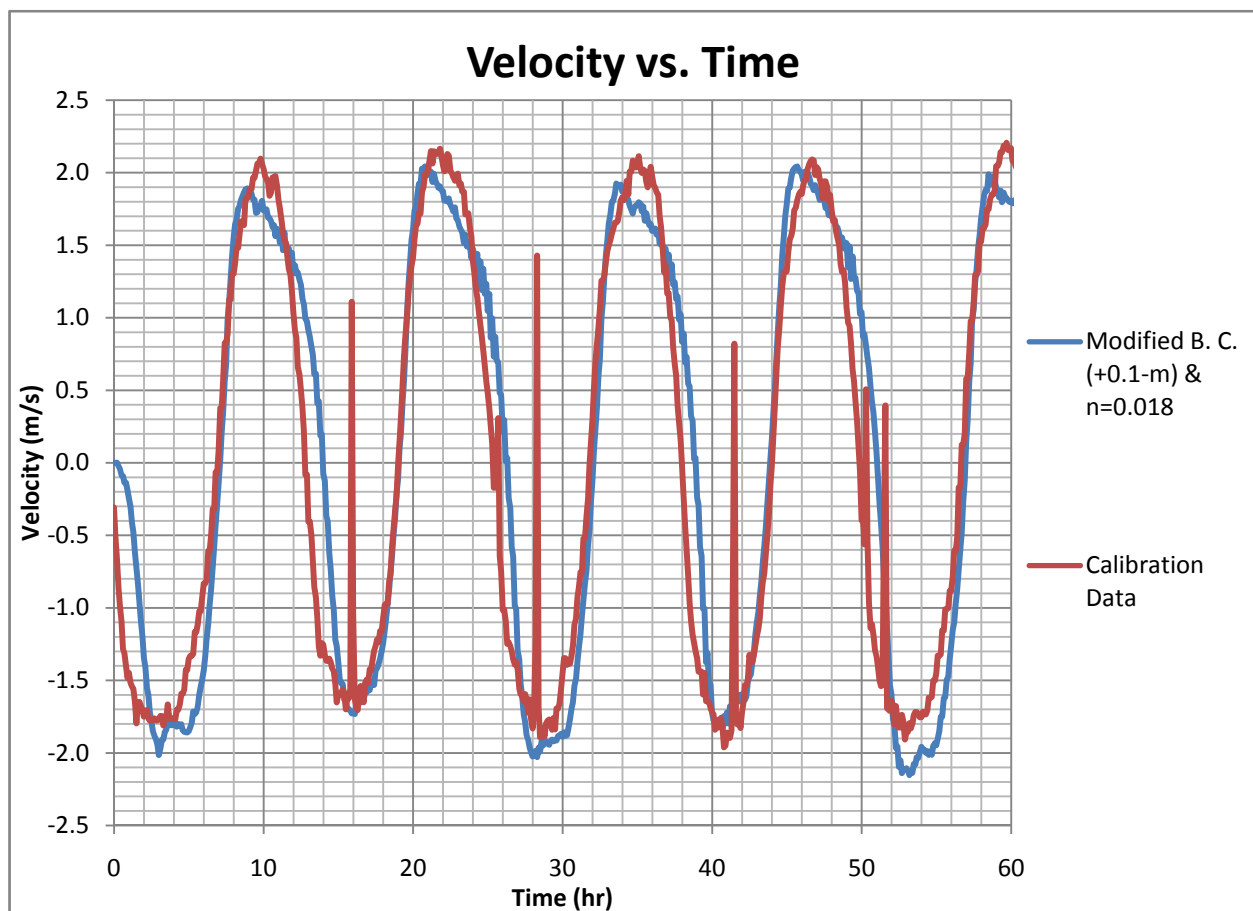


Figure 37 TUFLOW Success



## **5.5. Conclusion**

TUFLOW is able to create a model of the East River that matches the calibration data. Using the TUFLOW model is a relatively easy process as compared to using FESWMS. The model grid is automatically created and cannot be edited as is needed with the FESWMS finite element mesh. There is no need to artificially spin-up the model as in FESWMS. Very few stability issues are encountered while using TUFLOW. Using the initial runs and results from the sensitivity analysis, a successful model of the East River is created. This model uses the 20-m grid, a Manning's  $n$  of 0.018, and modified boundary conditions with 0.1-m added to all water surface elevation ordinates in the boundary condition data set. Additional runs are also made and checked against the calibration data; however, analysis of these results is described in section 7. Due to its ease of use and successful results, the TUFLOW model of the East River is used in this study as the 2-D model.

## **6. HEC-RAS Model**

The above models used are 2-D, which can predict flow patterns and velocities in a horizontal 2-D plane. One goal of this model is to see if a 1-D model, which only predicts velocities parallel to the stream thalweg, can produce adequate results. The advantage of a 1-D model is that free, user friendly alternatives exist. Data requirements are not as high as 2-D models, for example, and 1-D model usage is quite widespread. The 1-D model used in this study is HEC-RAS. HEC-RAS is a free 1-D model maintained and distributed by the United States Army Corps of Engineers. The model is a standalone program that does not require a pre- and post-processor such as SMS. For further information on HEC-RAS see section 2.4.2.4.

The process of creating a model in HEC-RAS is similar to the processes used in FESWMS and TUFLOW. Geometry data requirements are different; however, the program HEC-GeoRAS allows an easy conversion of the geometry data within ArcView. After the geometry data is loaded, boundary conditions and initial conditions are needed, and then the model can be run. No “initial runs” are made as in the 2-D models because the 1-D model is much simpler and does not require as much tweaking as a 2-D model. A sensitivity analysis is performed on HEC-RAS model parameters. This work results in a model that successfully matches the calibration data.

### **6.1. Creating Model Geometry**

HEC-RAS uses cross sections for its calculations. Velocities, flow rates, water surface elevations, etc. are calculated for each cross section along a river reach. In order to use the geometry data created in section 3.1, it needs to be converted into cross sections. The cross sections used in HEC-RAS are developed using HEC-GeoRAS within ArcView. HEC-GeoRAS is [a] set of ArcGIS tools specifically designed to process geospatial data for use with the Hydrologic Engineering Center’s River Analysis System (HEC-RAS) (from HEC-GeoRAS manual). The set of points that comprises the DTM is converted to a TIN to work with HEC-GeoRAS. At first, a DEM was created; however, because there were holes (areas without elevation data) in the DEM, HEC-GeoRAS would not run properly; therefore, a TIN is used.

Using HEC-GeoRAS is a simple matter of tracing elements in ArcView to create various stream features. Stream centerlines, bank lines, flow path centerlines, and cross section cut lines have to be digitized to create the necessary geometry. Other features can be created within HEC-GeoRAS;

however, they are not necessary for this model. Once the necessary features are traced, HEC-GeoRAS interpolates and exports a file that can be imported to HEC-RAS.

Some minor editing is necessary once the data is imported to HEC-RAS. HEC-RAS will only accept 500 points per cross section, so some points have to be removed. HEC-RAS provides a tool, Cross Section Point Filter, that quickly removes cross sections points within certain tolerances. Also, Manning's roughness values have to be assigned to each cross section.

## **6.2. Boundary Conditions & Initial Conditions**

The boundary conditions used in HEC-RAS are the same as used in the other models. An attempt is made to enter equal water surface elevations at both ends of the model so that zero flow can be assumed throughout the model at time zero. Initial flow conditions are set to zero at the upstream end of each reach.

## **6.3. Sensitivity Analysis**

For the below sensitivity analysis and subsequent runs, the geometry preprocessor, unsteady flow simulation, and post processor programs are run. The computation interval, hydrograph output interval and detailed output interval are all set to 6-min and Manning's  $n$  is set to 0.025 unless otherwise noted. For the analysis of Manning's  $n$  and time step, one reach is used and parameters for the east channel are obtained by setting the east channel as the left overbank (see section 6.3.3 for further details). All velocities reported are cross sectionally averaged velocities, and do not necessarily represent the velocity values at the exact point where the calibration data is recorded (the cross sectionally averaged velocity values are calibrated to the calibration data).

### **6.3.1. Manning's $n$**

An analysis is performed to see what affect varying Manning's roughness coefficient,  $n$ , has upon model output. Manning's  $n$  values of 0.018 to 0.032 are used. Results are reported at the cross section containing the calibration data mentioned above. As Manning's  $n$  decreases, both velocity and flow rate increase significantly. Velocity increases roughly from 1.1-m/s to 2.0-m/s for north flow peaks and from 1.6-m/s to 2.8-m/s for south flow peaks over the range of  $n$  values, roughly doubling the magnitude of the velocity peaks when  $n$  is halved. Decreasing  $n$  also causes water

surface elevations to decrease significantly when flow is in a south direction (about 30-cm), but has little effect on water surface for north flows.

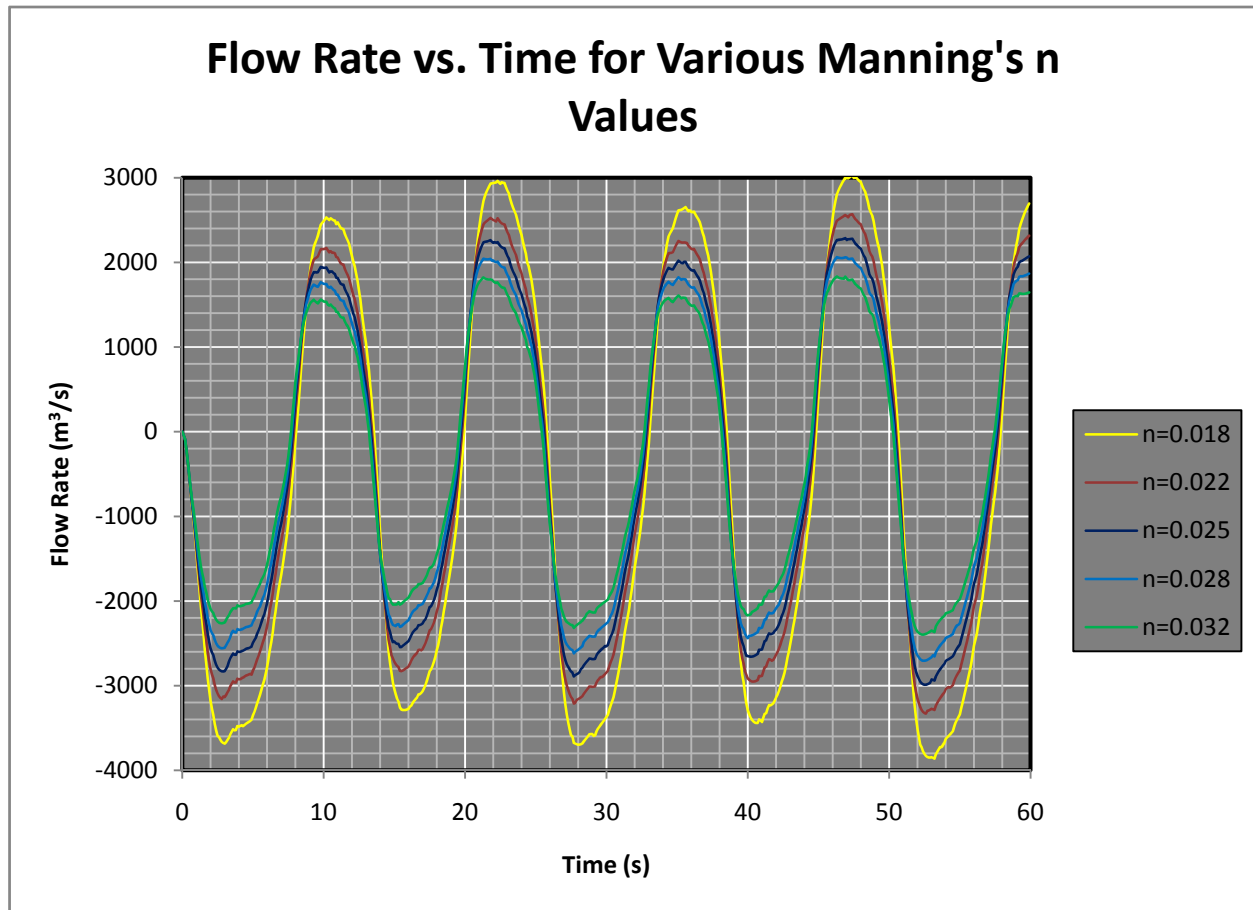


Figure 38 HEC-RAS Flow vs. Time for Various Manning's n Values

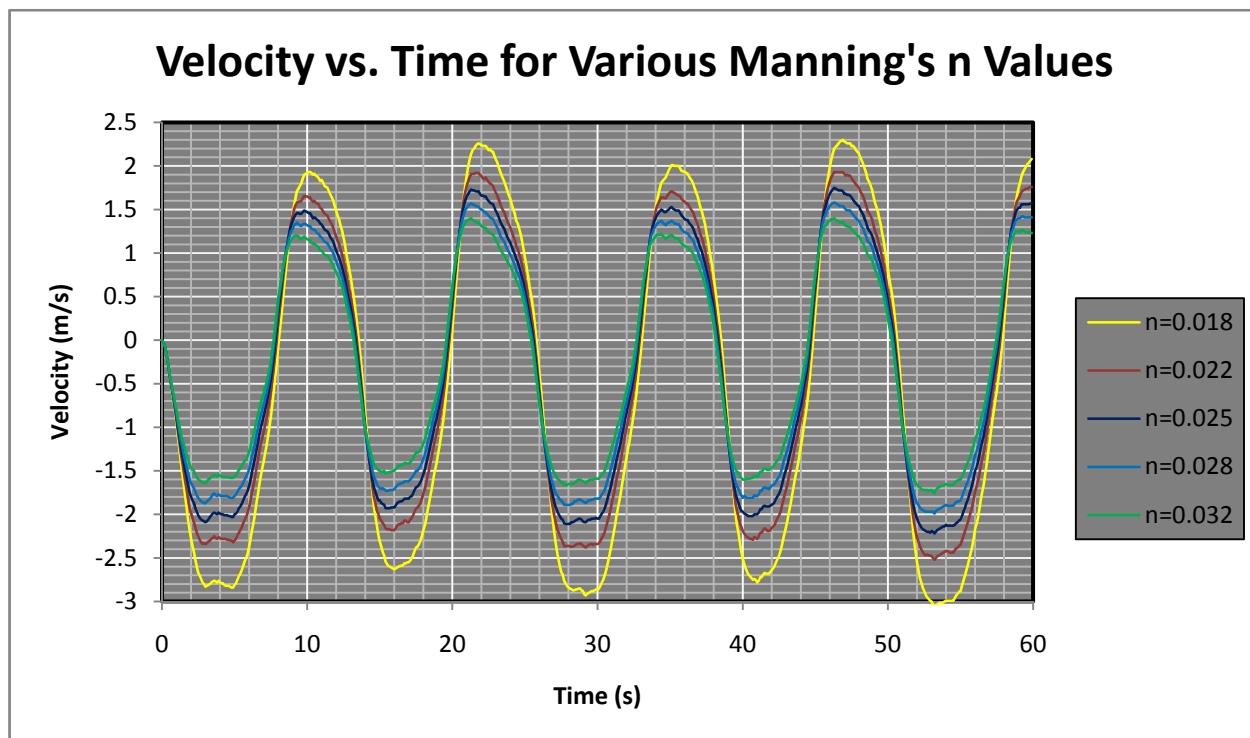


Figure 39 HEC-RAS Velocity vs. Time for Various Manning's n Values

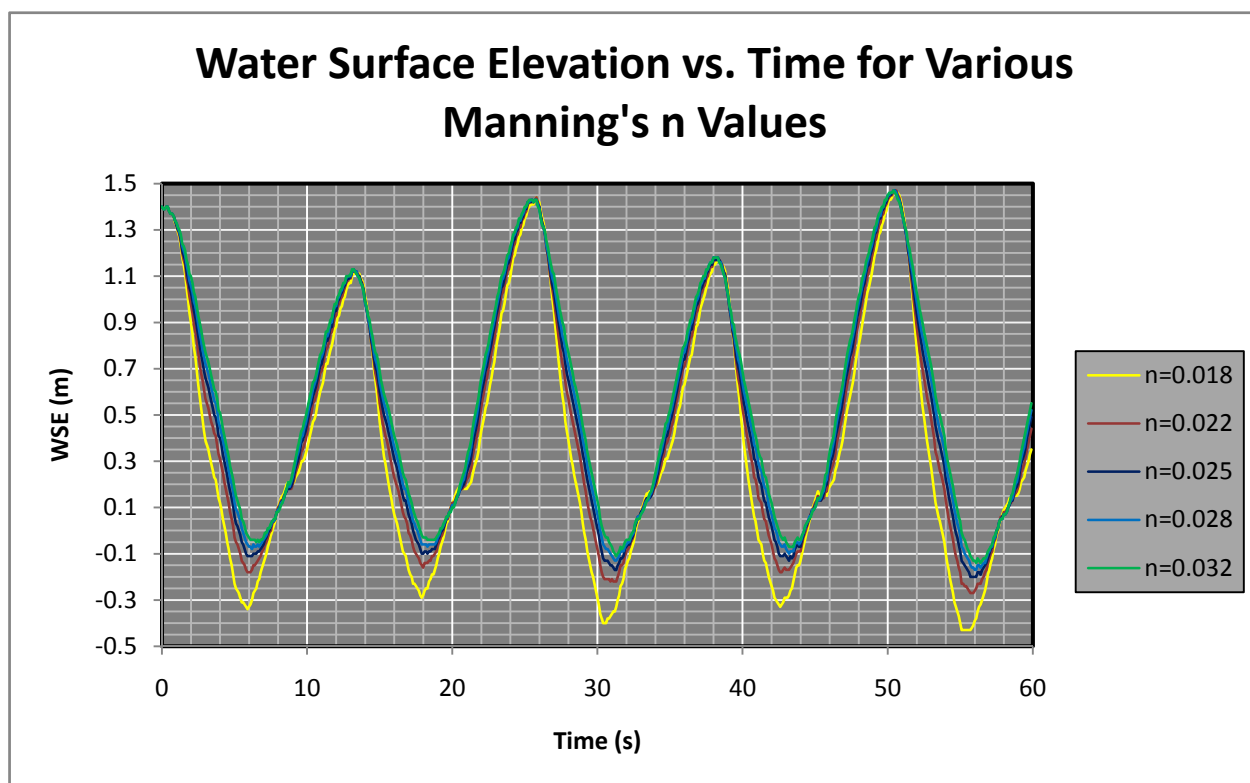


Figure 40 HEC-RAS WSE vs. Time for Various Manning's n Values

### 6.3.2. Computational Time Step

An analysis is also performed to see what affect changing the computational interval, or time step, has on model output. Time steps of 0.5, 3, 6, 12, and 30-min are used. Changing the times step had very minor changes on model output. Water surface elevations are affected little. Peak velocities and flow rates increase slightly as time step decreases, maximum changes of about 0.1-m/s and 50-m<sup>3</sup>/s occur for north flow peaks and very little changes for south flows.

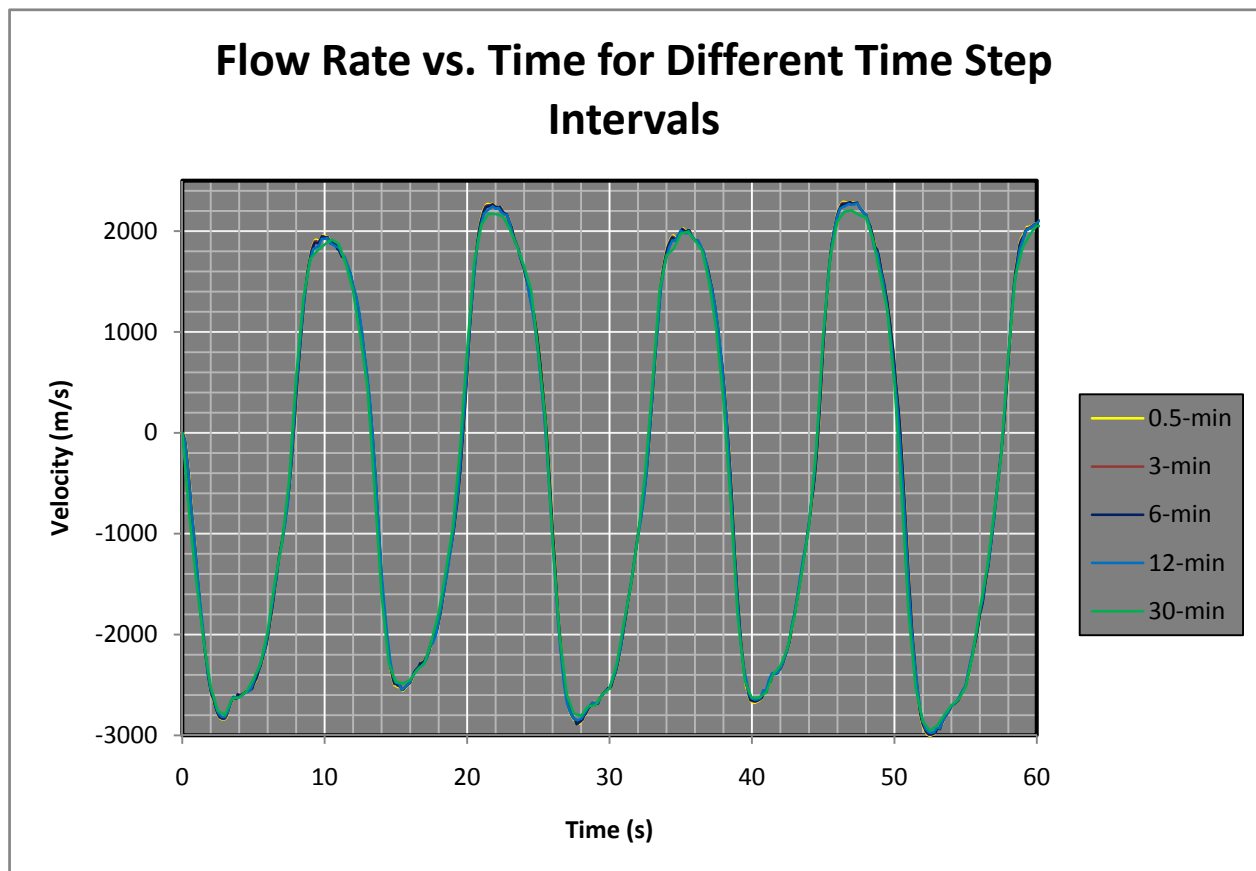


Figure 41 HEC-RAS Flow vs. Time for Various Time Steps

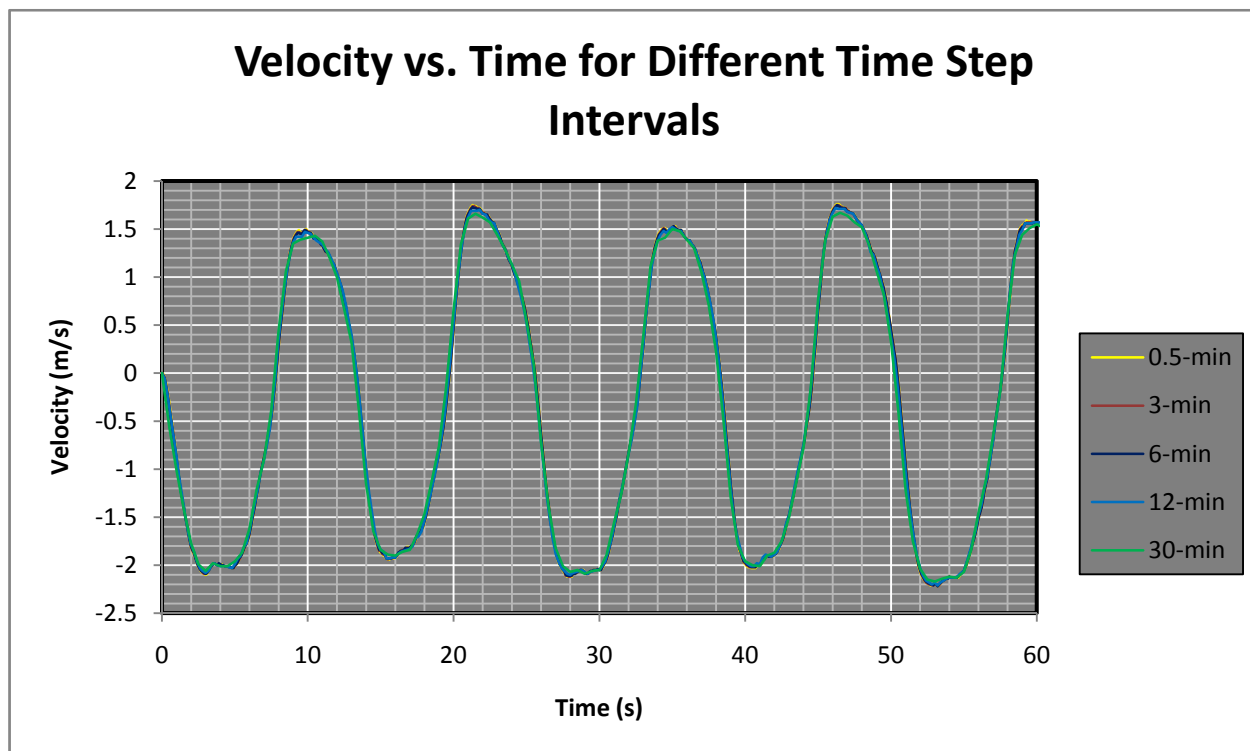


Figure 42 HEC-RAS Velocity vs. Time for Various Time Steps

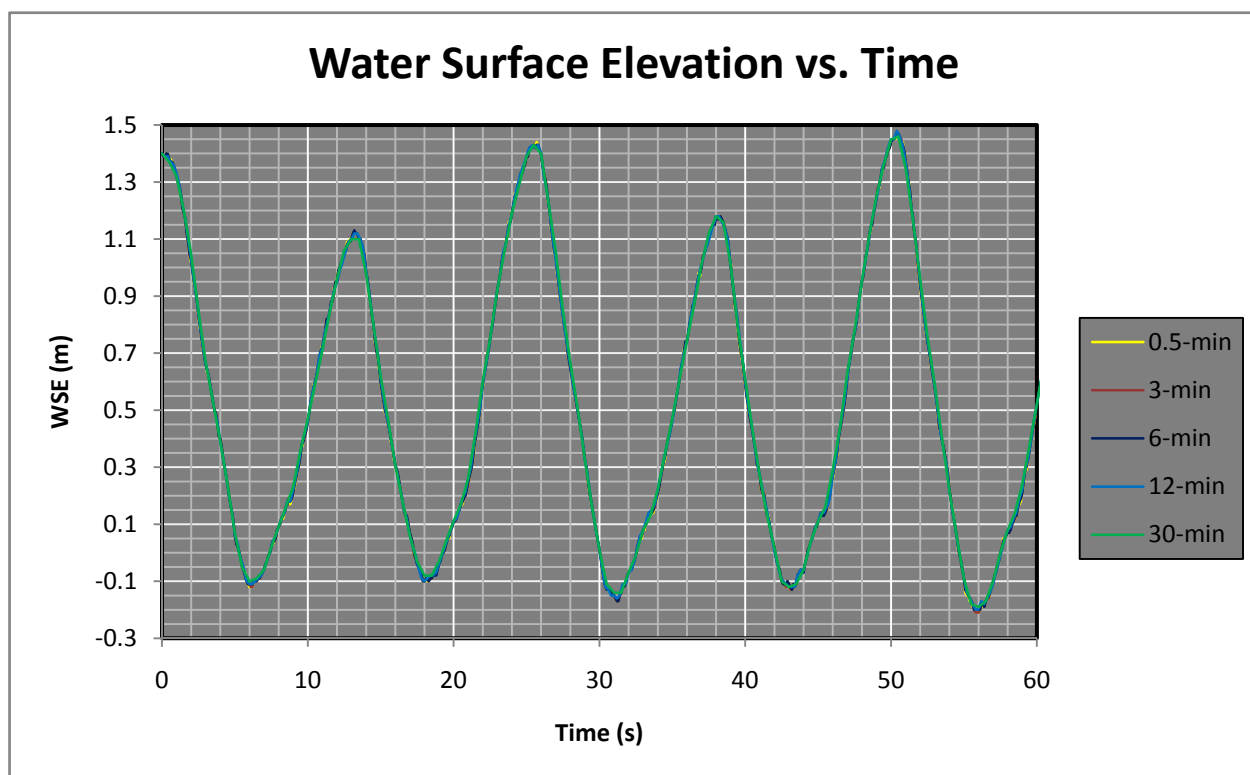


Figure 43 HEC-RAS WSE vs. Time for Various Time Steps

### 6.3.3. Channel Geometry Analysis

HEC-RAS computes parameters on a cross section to cross section basis. Cross sections are broken up into three sections: left overbank, main channel, and right overbank. HEC-RAS can distinguish between velocities and flow rates between these three areas, yielding results for each area (sometimes referred to as a quasi 2-D model). For the above analyses, one reach is used and the bank stations are set up such that the east channel of the East River lies entirely within the left overbank area of the cross sections while the west channel is made up of the main channel and right overbank (see Figure 47).

A separate analysis is performed to see what affect modeling the east and west channels as individual river reaches will have. Four separate reaches are used to create the “multiple channel” model in HEC-RAS. The multiple channel model is made up of a reaches immediately upstream and downstream of Roosevelt Island and a reach on either side (see Figure 48).

The multiple channel model produces peak flows and velocities that are greater than the single channel model. These peaks increase more in the south flow direction (about 300-cfs and 0.1-m/s) than the north (about 100-cfs and 0.05-m/s). Water surface elevations change little for high tides, and increase by about 5-cm for low tides for the multiple channel model. Since there is only one point with which to calibrate the model, the benefits of using a multiple channel cannot be fully evaluated.



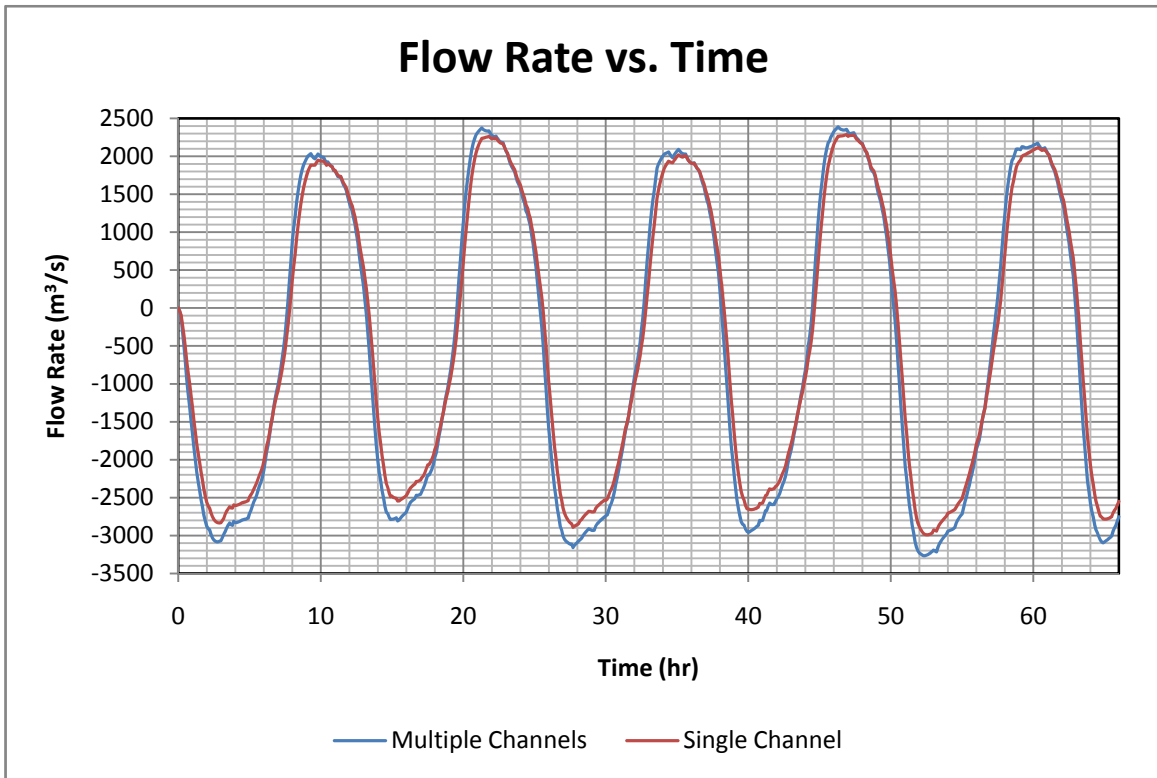


Figure 44 HEC-RAS Flow vs. Time for Single and Split (Multiple) Channels

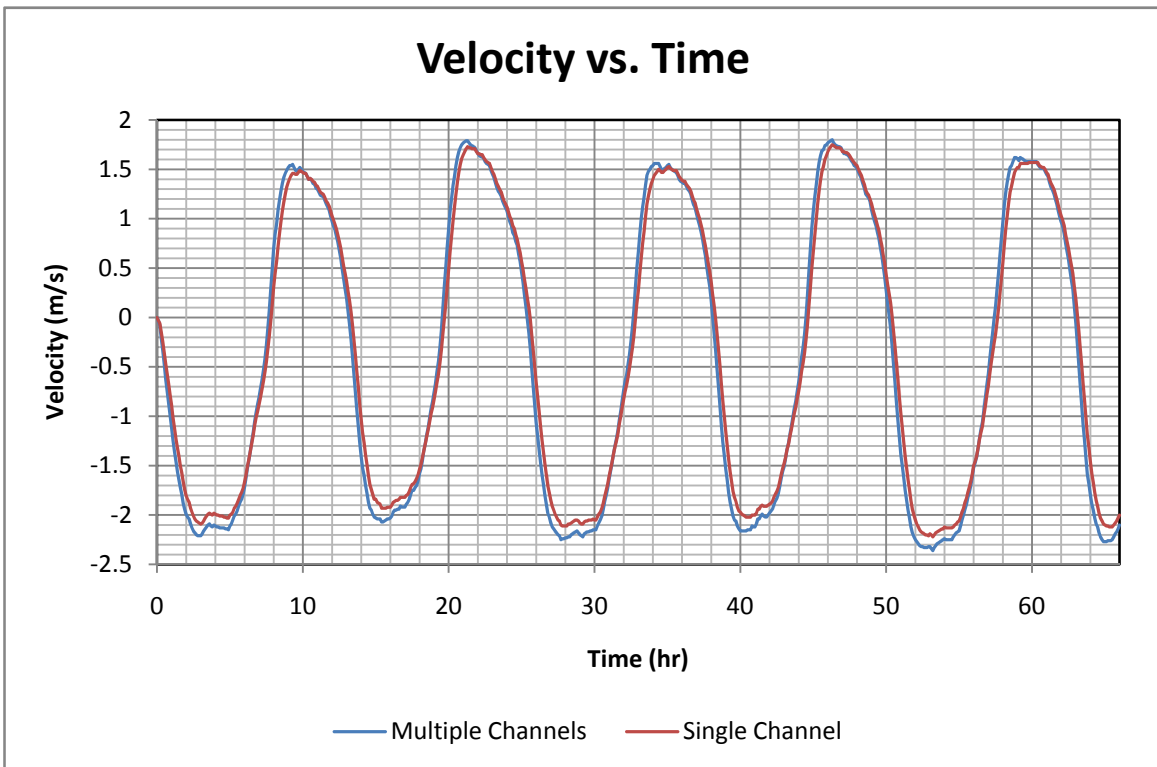
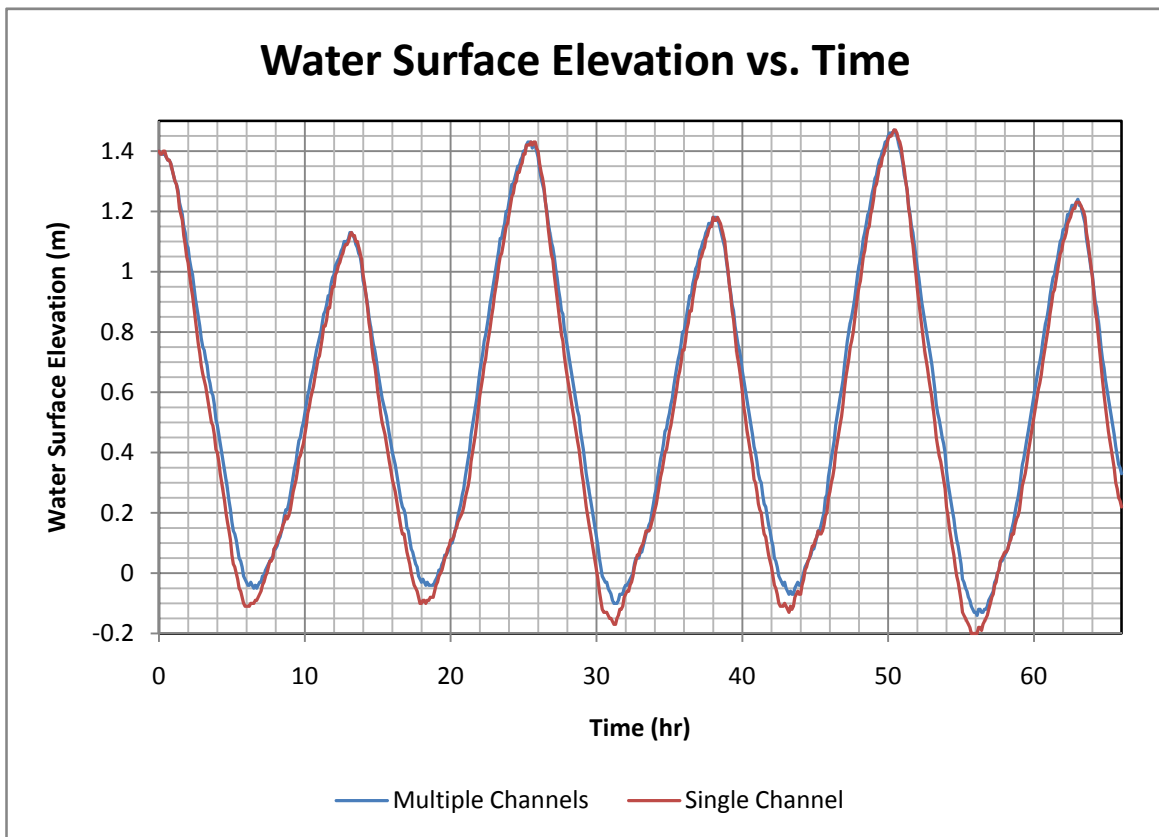


Figure 45 HEC-RAS Velocity vs. Time for Single and Split (Multiple) Channels



**Figure 46 HEC-RAS WSE vs. Time for Single and Split (Multiple) Channels**



Figure 47 HEC-RAS Single Channel Model





**Figure 48 HEC-RAS Split (Multiple) Channel Model**

#### 6.3.4. Sensitivity Analysis Conclusion

The results of the sensitivity analysis are as follows. Manning's  $n$  has a significant effect on model output. As  $n$  increases, velocities and flow rates decrease. Water surface elevations during south flows are increased as  $n$  increases. Changing time step has no significant impact on model output. The effects of using one reach and multiple reaches to model the river are also analyzed. The multiple channel model reported slightly higher velocities and flow rates. The multiple channel

model would likely outperform a single channel model if more calibration data were provided to compare velocities in the west channel; however, such data is not available and the benefits of the multiple channel model cannot be fully evaluated at this time. This analysis indicates that Manning's  $n$  can be used to calibrate the model, while changing other parameters has little impact.

#### **6.4. Results**

Attempts are made to match HEC-RAS model results to the calibration data. The model is set up with the computation interval, hydrograph output interval, and detailed output interval all set to 6-min. Various models are run in an attempt to match the calibration data. The initial results are unable to successfully match the calibration data; therefore, the boundary conditions are modified as in the TUFLOW model. Once 0.1-m is added to all points in the southern boundary condition, the model began to match the calibration data. An  $n$  value of 0.025 yields a model that successfully matches the calibration data. Both multiple and single channel geometries are used to see if either better match the calibration data; however, no significant advantage is seen for either (see Figure 49). For more information on comparison of model results and calibration data see section 7.2.3.

#### **6.5. Conclusion**

The HEC-RAS model is capable of matching the calibration data. The model is very easy to use and widely accepted in the United States. The model runs quickly when compared to 2-D models (less than 5-minutes compared to hours). Despite HEC-RAS's advantages, it is only a 1-D model. HEC-RAS only provides cross sectionally averaged velocities. These cross sectionally averaged velocities are used to match the calibration data; however, no work has been done to see how well the cross sectionally averaged velocities compare to the actual velocities where the calibration data is measured. HEC-RAS is capable of matching the calibration data, but may not be an adequate model for this study (further comparisons of HEC-RAS and TUFLOW model results are made in section 8).

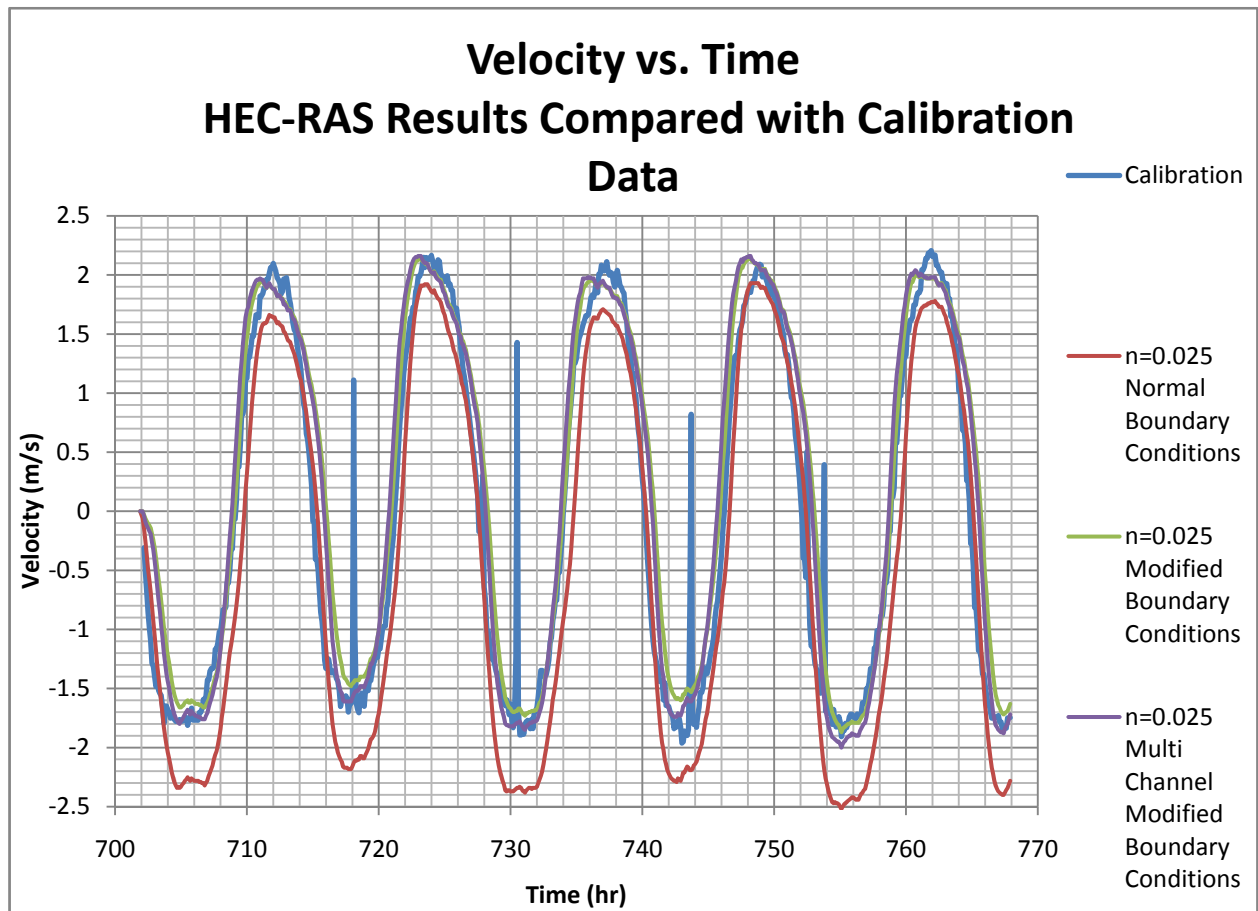


Figure 49 HEC-RAS Data Compared with Calibration Data

## 7. Comparison of Model Results in Relation to the Calibration Data

### 7.1. Introduction

In order to accomplish the goals of the modeling efforts, the results must mimic real world conditions. In order to make sure this happens, the model results are compared with the calibration data provided by Verdant Power (section 3.3). Only velocity vs. time data is provided for only one point on the entire river reach. More confidence could have been placed in the results had calibration data been provide in multiple locations throughout the reach.

This section compares the results from FESWMS, TUFLOW, and HEC-RAS with the calibration data using a numerical method. Equation 19, presented below, is the basis for a numerical comparison of model runs with calibration data. Before comparisons are made, it is necessary to smooth the oscillations in certain TUFLOW runs to obtain better comparisons. After the error of each model run is calculated, the results are compared for each model. Finally, the models that best fit the calibration data from each of the FESWMS, TUFLOW, and HEC-RAS model runs are selected and compared.

#### 7.1.1. Determining the Error in Model Runs

In order to compare model runs, a way of comparing results with calibration data is required. The following equation is used:

$$Error = \sqrt{\frac{1}{N} \sum_{i=1}^N (V_{model_i} - V_{Calibration_i})^2} \quad (19)$$

where:

N = Number of Samples in a Set

$V_{calibration}$  = Calibration Velocity

$V_{model}$  = Velocity Reported by Model

This equation yields the average difference or error between the calibration velocities and model output velocities. Squaring the difference preserves the error and prevents positive and negative errors from cancelling.

When dealing with underwater turbines, velocities below a certain magnitude will not produce significant power. Therefore, it is important for the model to match the peak velocities. Due to this, errors are also calculated that ignore velocities less than 1-m/s.

#### 7.1.2. Correcting TUFLOW Results

Before errors can be calculated, a way of smoothing the TUFLOW results is needed. Due to the oscillatory nature of these results (for example, see Figure 24), unsmoothed data from TUFLOW used in the above equation can produce artificially high errors. To solve this problem, a nine point moving average is used to smooth excessively oscillatory results. This technique is selected because it conserves many of the larger velocity variations that are not due to the oscillations in the TUFLOW results while still smoothing out the oscillations.



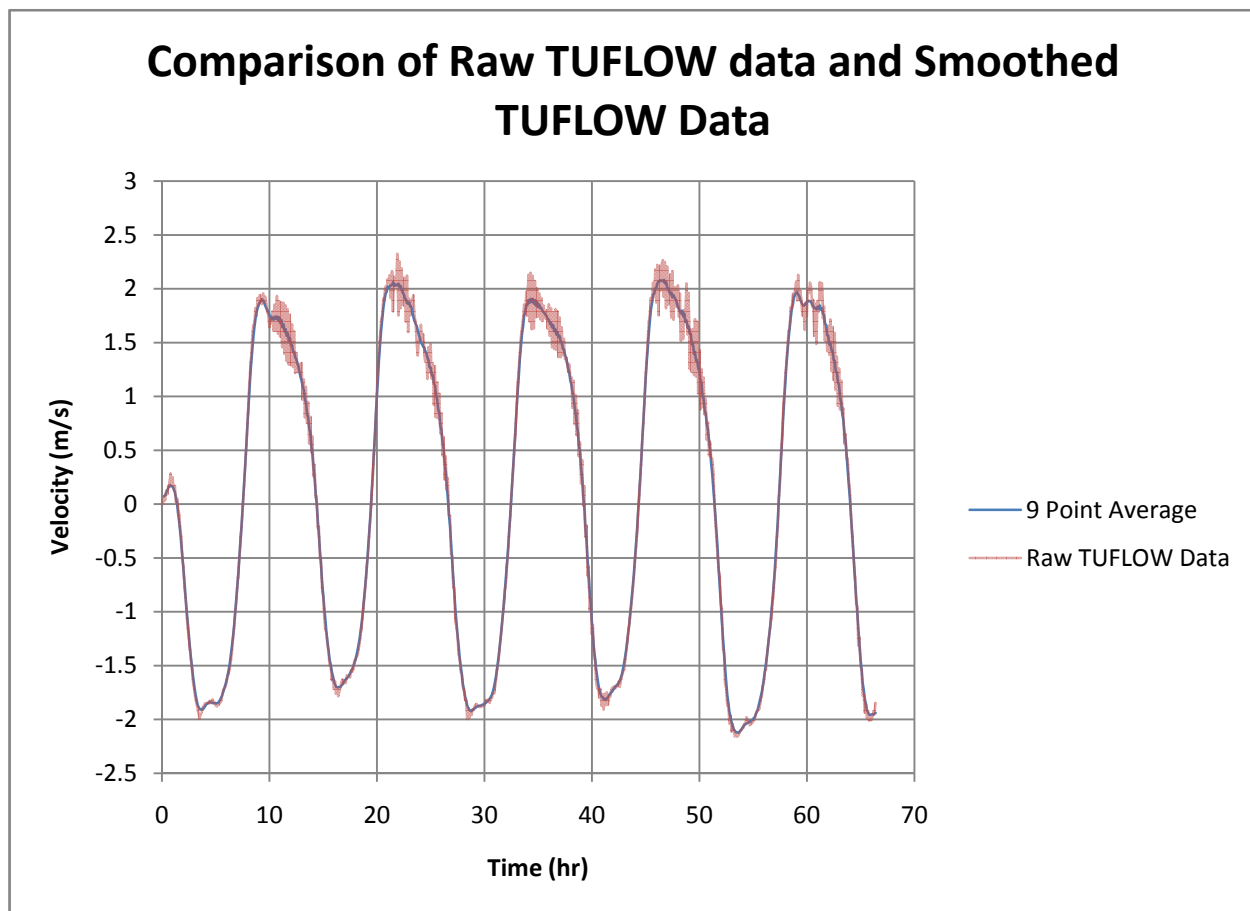


Figure 50 Smoothing of TUFLOW Data

## 7.2. Data Comparison

Once all the data is prepared, each data set (the output from a model run) is compared with the calibration data. Calibration data is provided at a single point as a table of time and velocity. The velocities are given in roughly 8.4-min increments. Since model output is given every 6-min, the calibration data is interpolated to match these 6-min intervals. Further details about the calibration data can be found in section 3.3.

### 7.2.1. FESWMS Results

The results from select FEWSMS Model Runs are presented below (see Figure 21 also).

**Table 2 Error from Select FESWMS Runs**

	n=0.046	n=0.063	n=0.080	n=0.046	n=0.063	n=0.025	n=0.013	n=0.013
Eddy Viscosity (m <sup>2</sup> /s)	15			3.3	3.3	5	10	10
Number of Elements	1349			21584		10756		5660
Run Reference	F1	F2	F3	F4	F5	F6	F7	F8
Error (m/s) for entire range of velocities	0.630	0.595	0.544	0.698	0.566	0.539	0.531	0.535
Error for velocities flowing to the north greater than or equal to 1-m/s	0.820	0.782	0.770	1.000	0.849	0.798	0.762	0.720
Error for velocities flowing to the south greater than or equal to 1-m/s	0.425	0.403	0.250	0.470	0.200	0.151	0.190	0.278

It can be seen from Figure 21 and Table 2 that none of the FESWMS model runs are close to the calibration data. Run F4 (see Table 2) appears to be relatively close; however, the numbers are deceiving because the model crashes after only completing 8-hr of data. The run that matched the calibration data best is F8; however, it matched the north flow peak velocities poorly, with an average error of 0.967-m/s.

#### 7.2.2. TUFLOW Results

The initial results from the TUFLOW model are more encouraging. The very first model ran with TUFLOW (T7 in Table 3) provided results that match the calibration data much better than any of the FESWMS results. The average error of run T7 is 0.531-m/s for the entire run, 0.762-m/s for north flow velocity peaks, and 0.190-m/s for south flow velocity peaks.

TUFLOW results begin to match very well when the boundary condition data is modified. The error for the original model run, T7, is 0.762-m/s. For model run T18, which has 0.1-m added to all ordinates in the boundary condition data, the error reduces to 0.481-m/s. Also, the errors for velocity peaks are 0.381-m/s for north flow and 0.370-m/s for south flow. This indicates that the model run with modified boundary conditions provides much better results, especially since higher velocities are more important when dealing with turbines.



### 7.2.3. HEC-RAS Results

The results from HEC-RAS match rather well with the calibration data, also. Run H5 (see Table 4) appears to match the calibration data best; however, there is a large amount of error for north flow velocity peaks (see Figure 49). Run H10 matches the calibration data best. Although run H10 has the least error, the difference in error between the single and multiple channel models is not enough to indicate that the multiple channel model is better. Further testing is needed to verify this.

Since HEC-RAS is a 1-D model, all reported velocities are cross sectionally averaged and are not necessarily the actual velocities at the exact point where calibration data is recorded; however, these cross sectionally averaged velocities are used for this comparison. This could explain the discrepancy between Manning's n values for the runs that best match the calibration data between TUFLOW (n=0.018) and HEC-RAS (n=0.025).

**Table 4 Error from Select HEC-RAS Runs**

	Single Channel									Split
	Unmodified BC					0.1				
	n=0.022	n=0.0235	n=0.025	n=0.0265	n=0.028	n=0.018	n=0.0235	n=0.025	n=0.0265	n=0.025
Run Reference	H1	H2	H3	H4	H5	H6	H7	H8	H9	H10
Error (m/s) for entire range of velocities	0.580	0.527	0.493	0.476	0.474	0.813	0.530	0.502	0.490	0.477
Error for velocities flowing to the north greater than or equal to 1-m/s	0.505	0.527	0.560	0.598	0.639	0.778	0.380	0.340	0.330	0.379
Error for velocities flowing to the south greater than or equal to 1-m/s	0.560	0.444	0.343	0.260	0.198	0.723	0.508	0.490	0.491	0.362

### 7.3. Conclusion

The above numbers can be somewhat deceiving and unclear. They indicate that the average error for the best FESWMS run is about 0.7-m/s, while the average error for the best TUFLOW and HEC-

RAS runs are about 0.48-m/s (a 37% difference). A quick look at Figure 51, however, clearly shows that both HEC-RAS and TUFLOW are capable of matching the calibration data for the East River, but FESWMS is not. FESWMS is capable of matching the direction of flow; however, velocity magnitudes are inadequate. Both HEC-RAS and TUFLOW can match flow directions and velocity magnitudes rather well. Therefore, only TUFLOW and HEC-RAS are viable alternatives to use to model the East River.

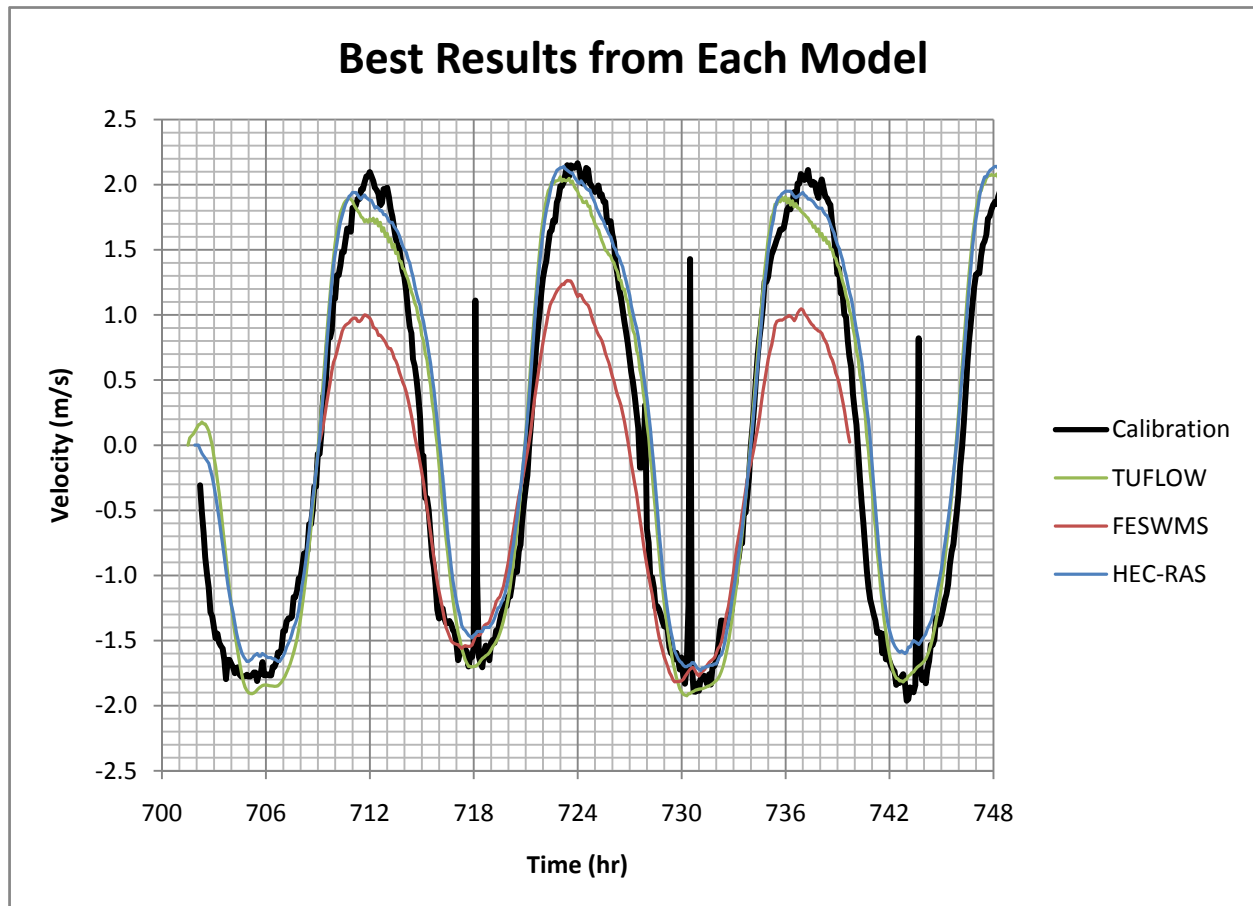


Figure 51 Best Results from Each Model

## **8. Comparison of 1-D and 2-D Model Results**

### **8.1. Introduction**

In the last section, FESWMS is eliminated as a viable alternative to model the East River. The results of the remaining models, the 1-D HEC-RAS and the 2-D TUFLOW, are compared in this section. The model parameters that resulted in the least error with the calibration data are used in any new models created in this section. The models used in this comparison correspond to the neap and spring tidal periods explained below.

#### **8.1.1. Tidal Definitions**

In order to compare the models over a large range of flows, an extremely low and high tidal range is used. A brief description of tides and tidal terminology is given here.

Tides are caused by the gravitational forces exerted by the moon along with the sun and the rotation of the earth. A neap tide is when the difference between high tide and low tide is less than average. A spring tide is when the difference between high tide and low tide is greater than average. When the sun, earth, and moon are in a straight line, spring tides occur. When the sun and moon are 90° apart relative to the earth, neap tides occur. Also, the moon revolves about the earth in an elliptical orbit. When the moon is closest to the earth (at perigee) tidal ranges increase. When the moon is farthest from the earth (at apogee) tidal ranges decrease.

From January 11, 2007 to January 14, 2007 the moon was at its most distant apogee, coinciding with neap tide, resulting in the slowest tidal currents of the year. From October 25, 2007 to October 28, 2007 the moon was at its closest perigee, coinciding with spring tide, resulting in the fastest tidal currents of the year.

#### **8.1.2. HEC-RAS Model**

HEC-RAS is an attractive model because it is widely used and accepted, it is relatively easy to use, and it is free. Although the 1-D HEC-RAS model is not nearly as sophisticated as TUFLOW, these

facts make it worthwhile to see if HEC-RAS is capable of modeling the East River for tidal energy purposes.

The geometry used in the HEC-RAS model is the multiple channel model. This model is represented by two different reaches around Roosevelt Island (for further information see section 6.3.3). This geometry was chosen because the water surface elevations are not required to be the same on both sides of the island, which may better match the 2-D model results (HEC-RAS is a 1-D model; therefore it only calculates one water surface elevation per cross section; if one reach is used that included both sides of the island, then the cross sections would span both the east and west channels, forcing the water surface elevation to be the same on either side of the island for a given cross section). Cross sections are roughly 30-m apart. A Manning's  $n$  of 0.025 is used because it best matched the calibration data. The southern boundary condition water surface elevation ordinates all have 0.1-m added.

#### 8.1.3. TUFLOW Model

The TUFLOW model is chosen for this study because of it is known as a very robust, stable, user friendly model; however, this model has not been widely used in the United States. The model is also relatively expensive when compared with the free HEC-RAS. The main advantage of TUFLOW is that the model results are 2-D and far more detailed than the 1-D results produced by HEC-RAS

The following parameters are used in TUFLOW: a 20-m grid, Manning's  $n$  of 0.018, time step of 1-sec, and modified boundary conditions with 0.1-m added to all water surface elevation ordinates on the southern boundary condition. All other parameters are left at their default values.

## 8.2. Results

The results of the two models described above are compared below. Data compared includes time series data at the calibration point, cross-section data for both the east and west channels, and data along the entire reach.

#### 8.2.1. Time Series Data at the Calibration Point

The first comparison between the two models is time series data of velocity and water surface elevation at the point where the models are calibrated.

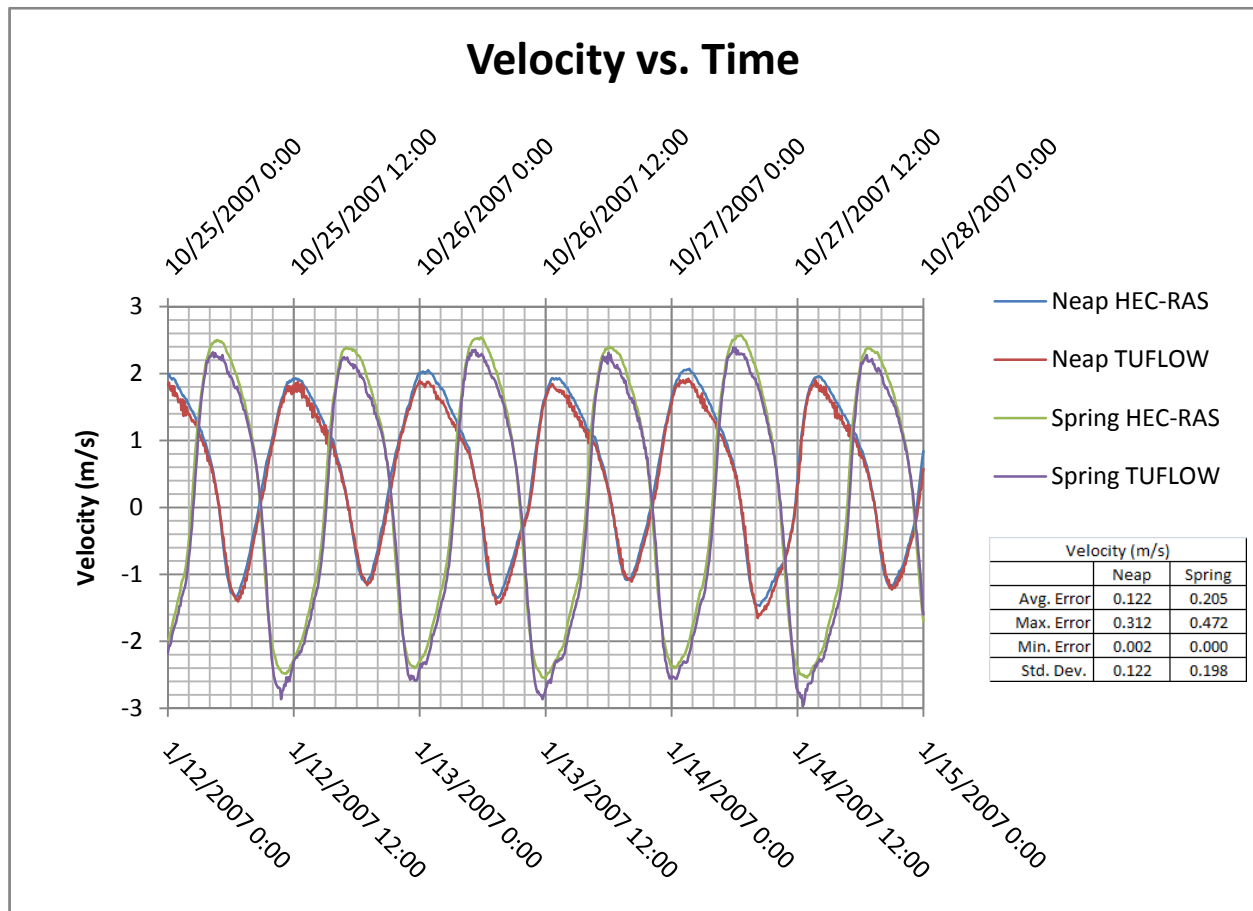


**Figure 52 1-D v. 2-D Velocity v. Time at Calibration Point**

The velocities reported by each model match well, with an average error between the two of 0.12-m/s for neap tides and 0.20-m/s for spring tides. TUFLOW reported slightly higher velocities for south flows, while HEC-RAS reported slightly higher velocities for north flows. It is expected that velocities at this point will match well between the two models since this is where the models are calibrated to. The water surface elevations matched very well. The neap tide has an average error between the two of 5.6-cm, and 7.5-cm for the spring tide. This is also expected since water surface elevations are used as boundary conditions.



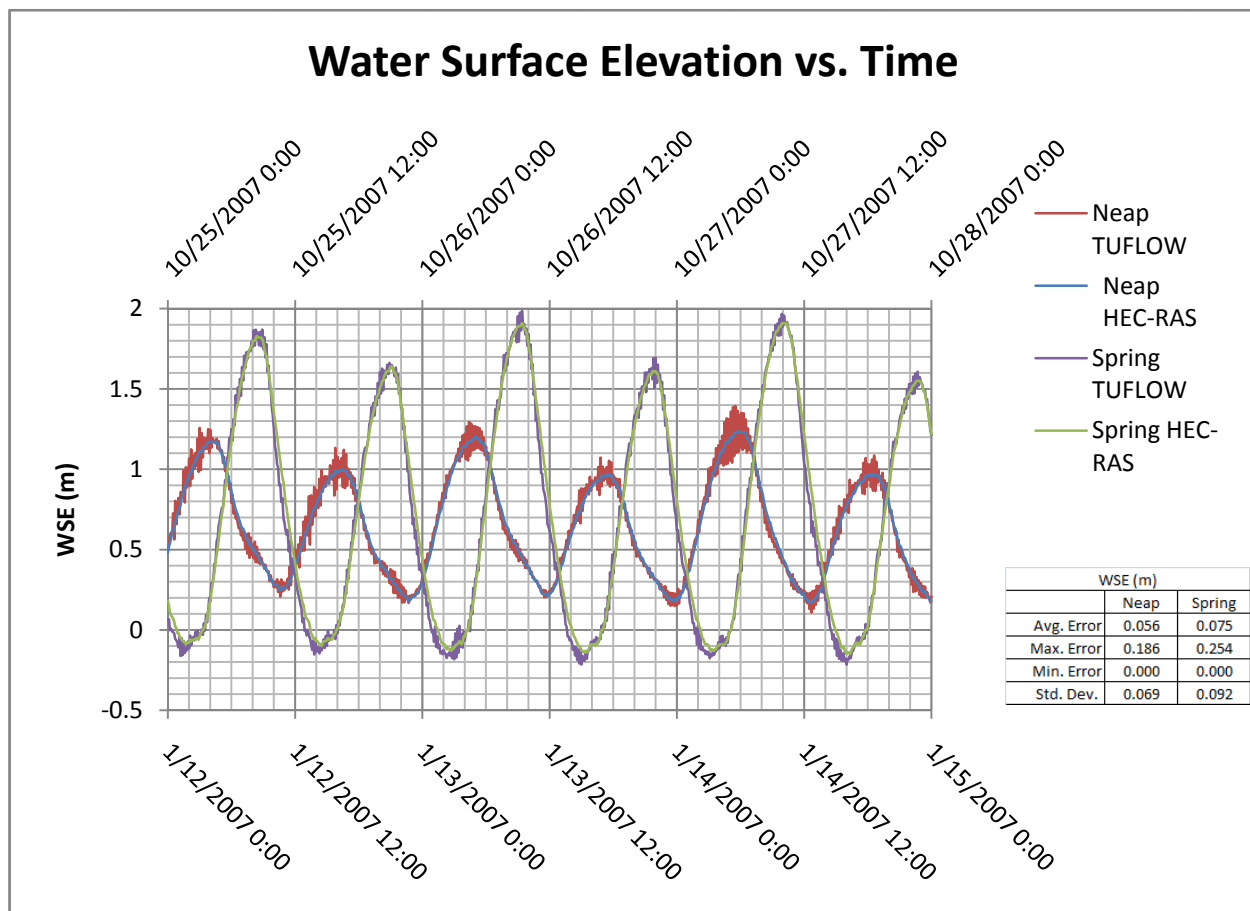


**Figure 53 1-D v. 2-D WSE v. Time at Calibration Point**

#### 8.2.2. Cross Sectional Comparison of Spring Peak Velocities

A cross sectional comparison of HEC-RAS and TUFLOW model results is also performed. The east channel cross section passes through the calibration point (Figure 54). The west channel cross section intersects Queensboro Bridge (Figure 55). The time used for these comparisons is October 27, 2007, 12:30, which corresponds to the highest velocity magnitudes reported.

Several advantages and disadvantages of each model are evident from the cross section plots below. The most obvious advantage is that the 2-D TUFLOW model reports a variable velocity across the cross section, while the 1-D HEC-RAS only gives an average velocity for the entire cross section. TUFLOW can also have a variable water surface as evident in Figure 54; however, the large change in water surface is questionable and may be an artifact of the wetting and drying scheme in TUFLOW. HEC-RAS reports a level water surface for the cross sections. The TUFLOW model is grid

based, and points used to obtain model geometry are evenly spaced (20-m in this case). Decreasing the size of grid elements can have a significant impact on model run times. Points on a HEC-RAS cross section can be spaced at any interval as long as there are less than 500 total points per cross section, and generally do not significantly impact model run time. For the given cross sections, HEC-RAS appears to better capture the geometry of East River, especially at the cross section near the Queensboro Bridge. TUFLOW cuts out a large section of the hump at 270-m along the west cross section.

#### 8.2.2.1. East Channel

The cross section in the east channel contains the calibration data point. It is difficult to compare the results of the two models since the TUFLOW results vary across the cross section, while the HEC-RAS results are constant. In order to better compare the two models, numerical integrations are carried out on the TUFLOW data to compute the flow rate and average velocity for the cross section. These numbers are reported directly by HEC-RAS. The flow rate calculated for TUFLOW is 4,661-m<sup>3</sup>/s and the reported flow rate for HEC-RAS is 3,571-m<sup>3</sup>/s, a percent difference of 26%. The average velocity calculated for TUFLOW is 3.2-m/s and the reported velocity for HEC-RAS is 2.5-m/s, a percent difference of 25%. This is likely due to the fact that Manning's *n* for the TUFLOW model is 0.018 and 0.025 for the HEC-RAS model (a percent difference of 33%, rather close to 25% and 26%). The water surface elevations are relatively close, 0.78-m for TUFLOW and 0.98-m for HEC-RAS, a percent difference of 23%.

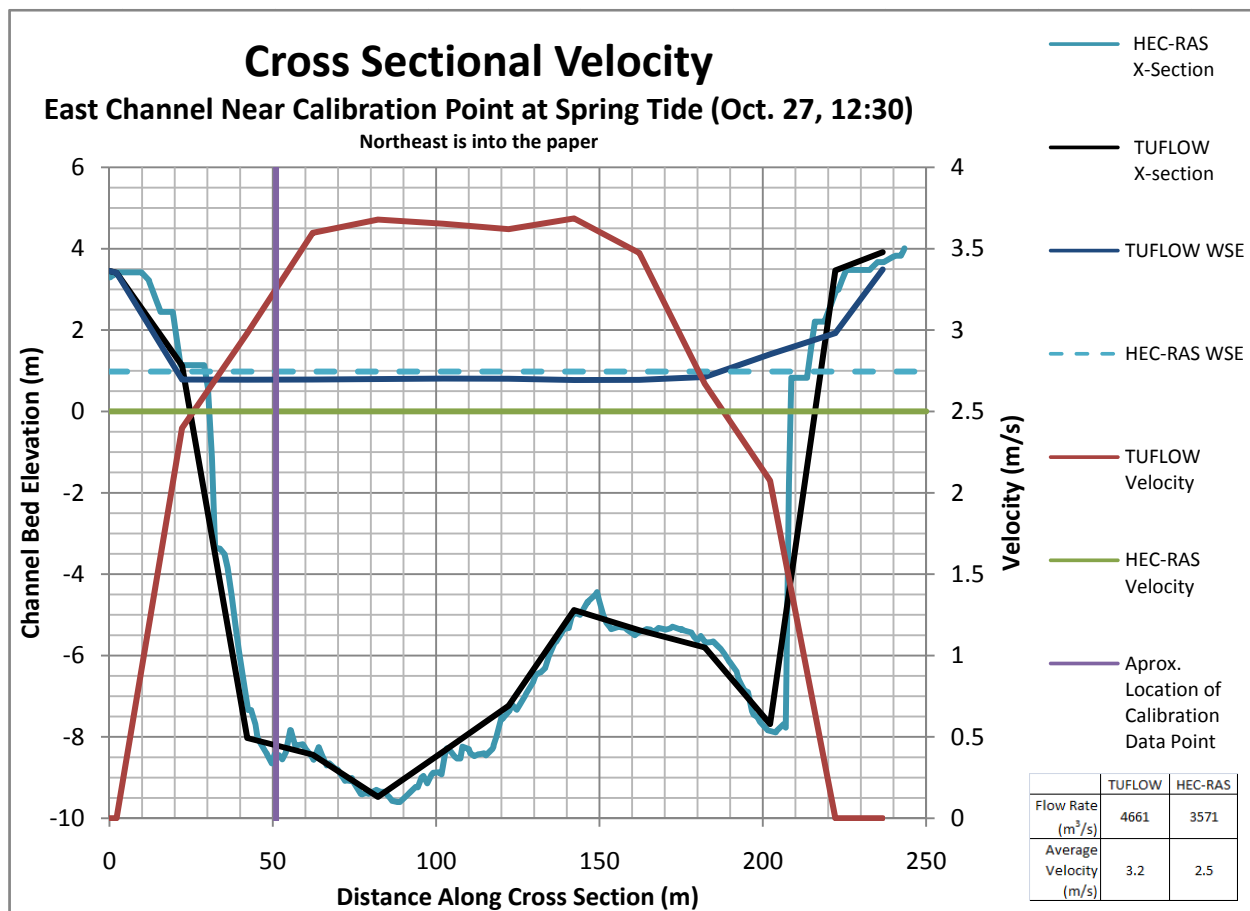


**Figure 54 1-D v. 2-D Cross Section at Calibration Point**

#### 8.2.2.2. West Channel

As stated above, the west channel cross section is near the Queensboro Bridge. Numerical integrations are carried out for this cross section as well. The flow rate in the west channel calculated for TUFLOW is 9,280-m<sup>3</sup>/s and the reported flow rate for HEC-RAS is 8,360-m<sup>3</sup>/s, a percent difference of 10%. The average velocity calculated for TUFLOW is 1.7-m/s and the reported velocity for HEC-RAS is 1.5-m/s, a percent difference of 12%. This could be partially due to the fact that Manning's n for the TUFLOW model is 0.018 and 0.025 for the HEC-RAS model (a 33% percent difference), but since no calibration points existed in the west channel, other factors likely cause the difference. The water surface elevations are very close, 1.0-m for TUFLOW and 1.1-m for HEC-RAS, a percent difference of 10%.

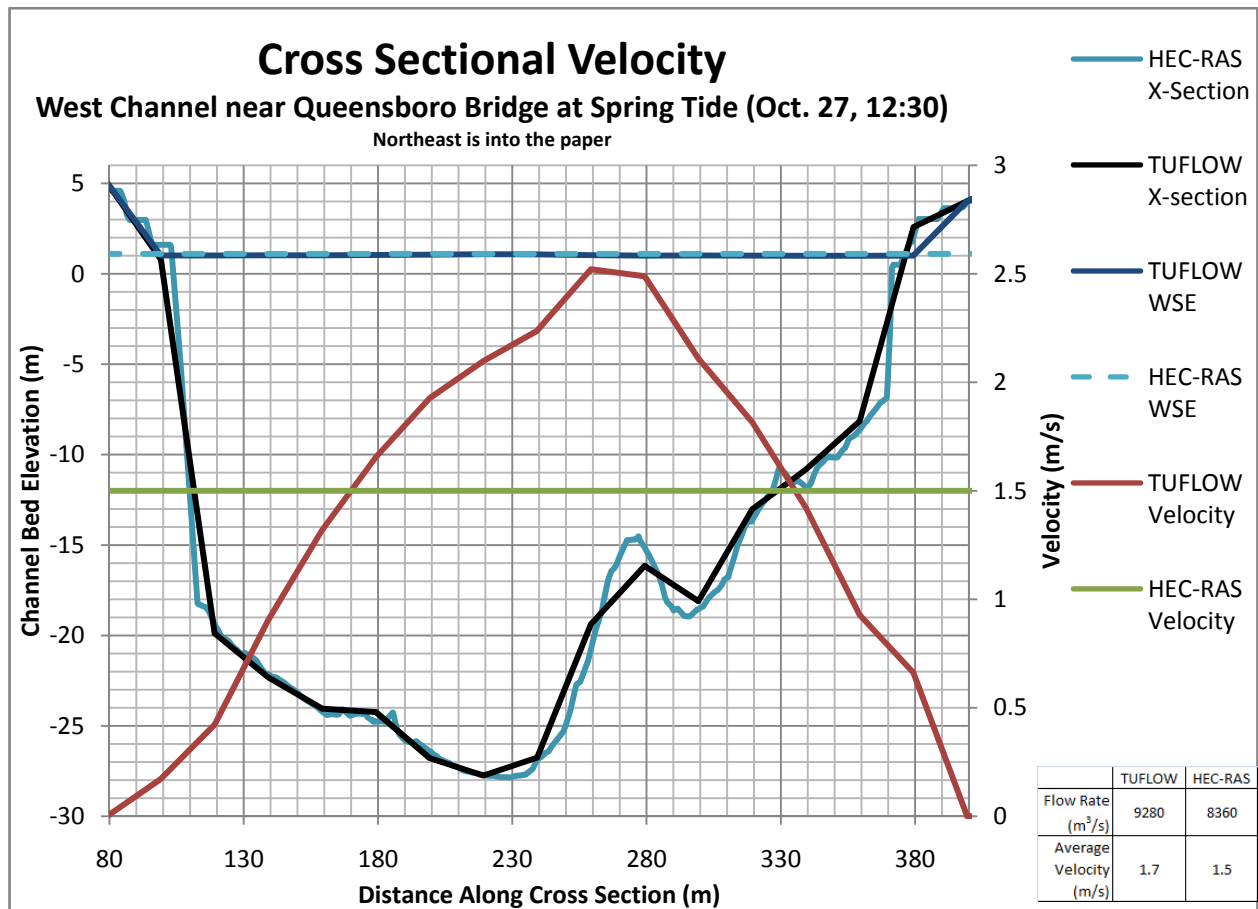


**Figure 55 1-D v. 2-D Cross Section in the West Channel near Queensboro Bridge**

### 8.3. Velocity Profile

The main advantage of a 2-D model over a 1-D model can be seen in the below plots of velocity. HEC-RAS simply indicates the cross-sectionally averaged velocity at each cross section (Figure 56) and assumes that flow is parallel to the river reach. TUFLOW gives depth averaged velocity for the river at the corner of each grid (20-m by 20-m is this case) and interpolates between grid points (Figure 57). TUFLOW also allows flows in the X and Y direction as opposed to simply parallel to the reach as in HEC-RAS (note the eddies forming in the top-right corner of Figure 57).

## Velocity Profile Plot of the East River

October 27 12:30 (Spring Tide)

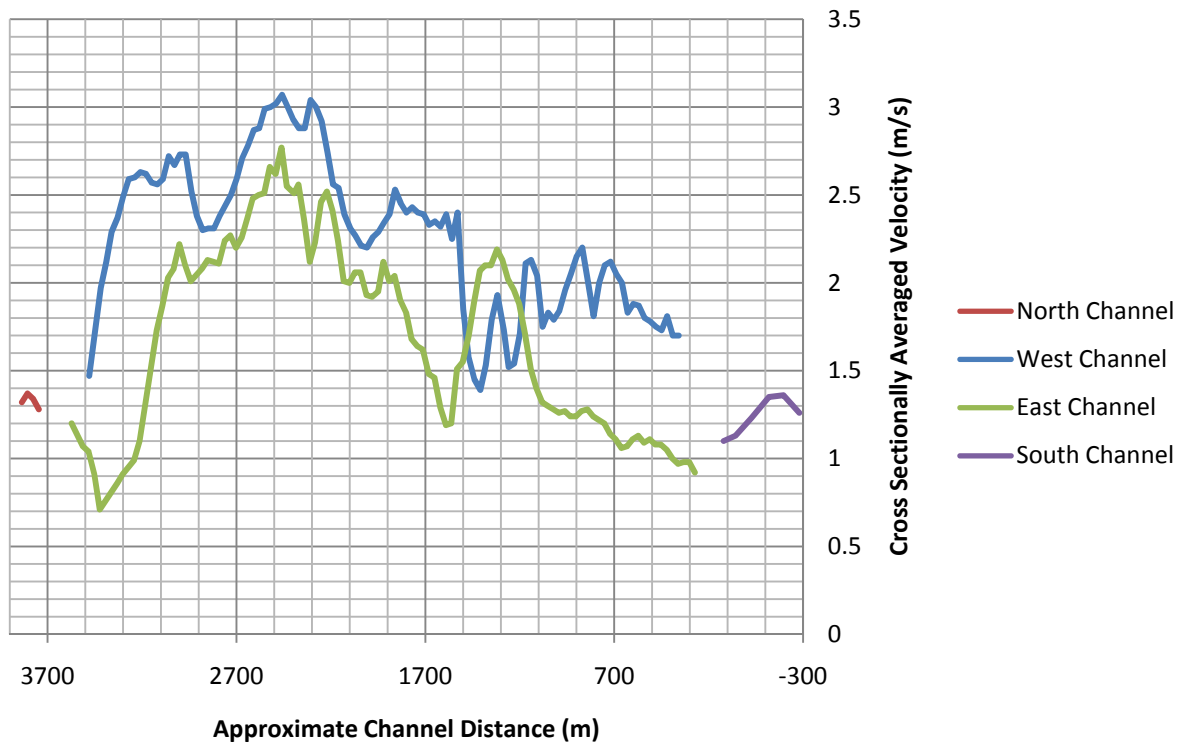


Figure 56 HEC-RAS Velocity Profile

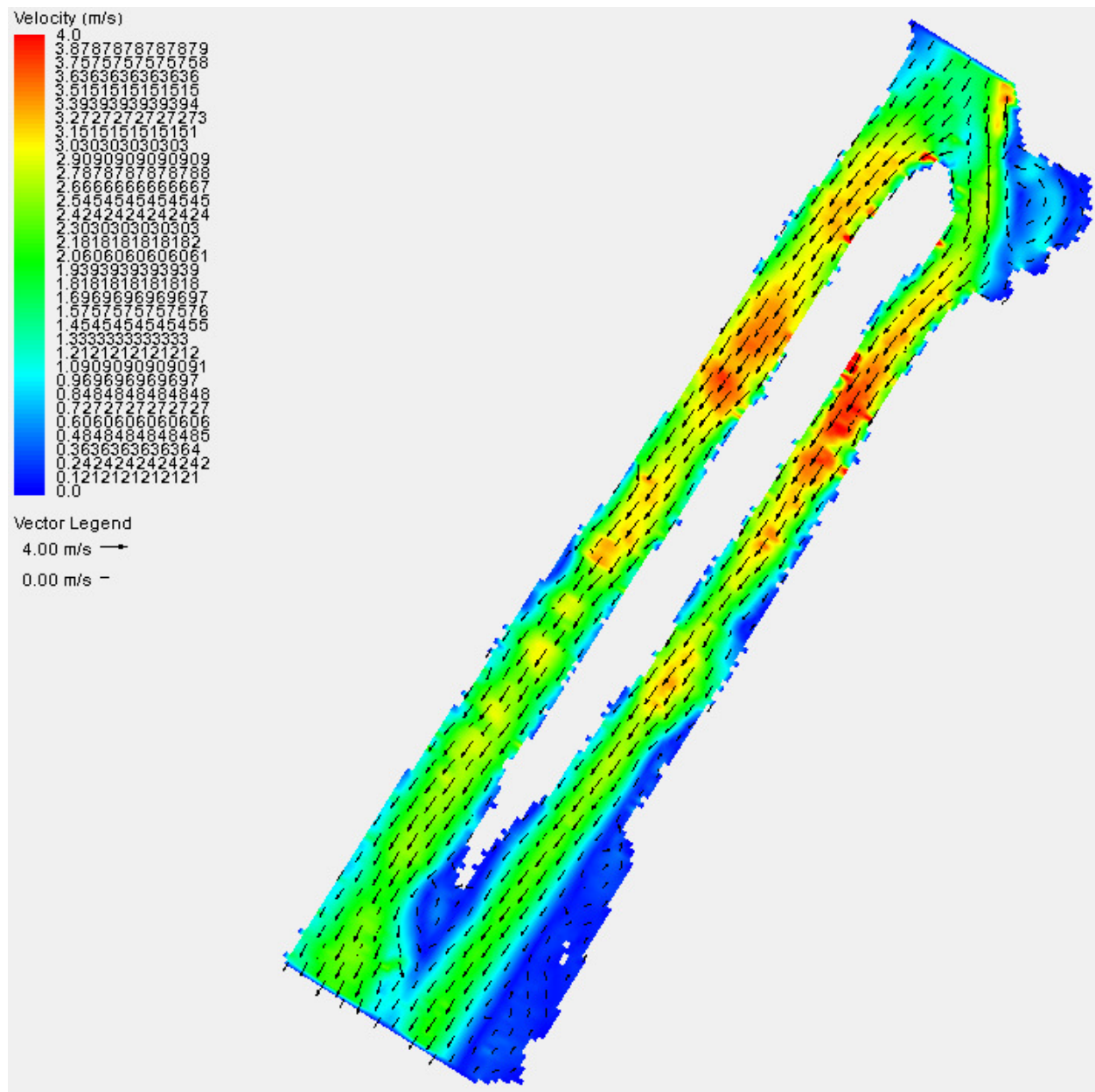


Figure 57 TUFLOW Velocity

#### 8.4. Conclusion

The model results from HEC-RAS and TUFLOW are compared in three ways. The first set of comparisons, time series data at a point, is relatively the same for each model. This does not really indicate anything since the point used is where the models are calibrated and; therefore, should yield the same results. TUFLOW begins to show significant advantages when comparisons are

made at cross sections. TUFLOW allows a variable velocity and water surface across a cross section while HEC-RAS yields constant values. Although it appears that HEC-RAS may better represent the geometry when looking at the above cross sections, HEC-RAS ignores the geometry between cross sections. The last comparison along the river reach overwhelmingly shows the advantage of TUFLOW. HEC-RAS can only produce velocities parallel to the river, while TUFLOW allows velocities to vary in both the x and y directions.

The purpose of this study is to create a model of the East River in New York in order to find sites that are well suited for underwater turbine installation. Velocity is the most important variable, and must fall within a certain range. Locations with very low velocities are not suitable because very little or no power will be generated by the turbines. Locations with extremely high velocities could pose a threat to turbines due to excessive shear stress. Water depth is another important variable. Water depths that are too deep may prove difficult for installation and maintenance. Water depths that are too shallow could pose threats to boats and ships. HEC-RAS can adequately indicate water depth; however, since it only yields a cross sectionally averaged velocity, it does not adequately indicate where to place a turbine within the cross section. TUFLOW yields depth averaged velocity throughout the modeled reach. This gives a much better indication of potential turbine sites. Power production estimates can be made with the TUFLOW results and vertical velocity profiles can be extrapolated from TUFLOW results for more accurate estimates. Since the goal of this work is related to underwater turbines and power production, the 2-D model is preferred.

## **9. Month Long Runs and Analysis**

### **9.1. Month Long Data Sets**

Two month long periods are modeled with TUFLOW in order to capture periods of maximum and minimum peak velocities (extreme neap and spring tides). The first period, January 11, 2007 to February 10, 2007, captures when the moon is the most distant from the earth, resulting in the slowest tidal currents of the year. The second time period, October 19, 2007 to November 18, 2007, captures when the moon is closest to the earth, resulting in the fastest tidal currents of the year. These periods are used to calculate power and energy output by underwater turbines. First a 3-day period of extreme neap and spring tides are compared to see how velocity and power are affected. A month long data set is then compared to see how power is affected over a longer period.

#### **9.1.1. Model Set Up**

The month long data runs are performed using TUFLOW. The following parameters are used: 20-m grid, Manning's  $n$  of 0.018, time step of 1-sec, and modified boundary conditions with 0.1-m added to all water surface elevation ordinates on the southern boundary condition. All other parameters are left at their default values.

### **9.2. Results**

#### **9.2.1. Neap vs. Spring Tides**

Since velocity is a function of pressure gradient, or slope in open channel flow, a greater difference in upstream and downstream water surface elevations will produce a faster velocity. Since this study is concerned with underwater turbines and energy output, a faster velocity results in more power. An analysis is performed to see what affect these extreme tidal ranges have on velocity and power.



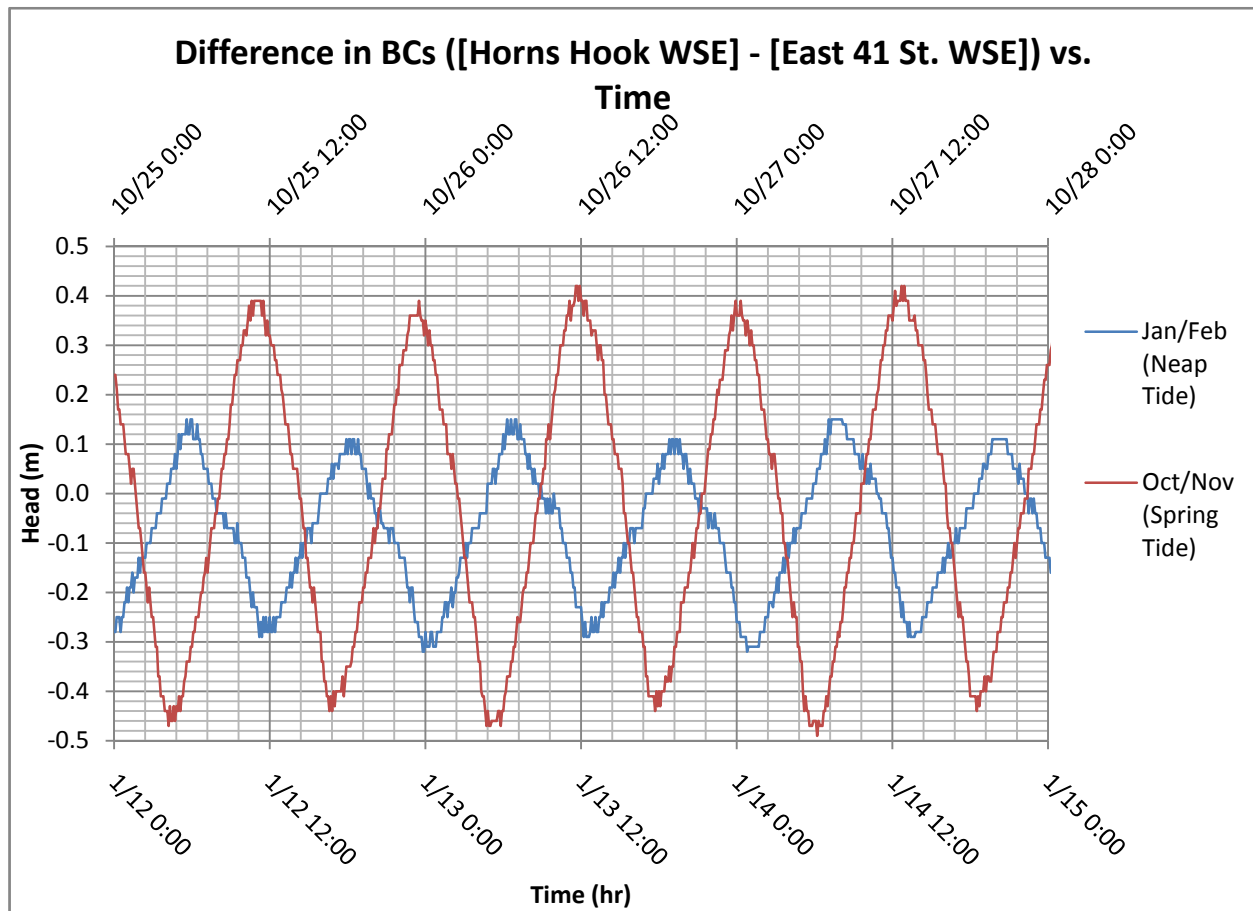


Figure 58 Head vs. Time

A three day time period is chosen to compare the most extreme neap and spring tides. The neap tide time period is January 12 through 15. The spring tide time period is October 25 through 28. Velocities are read from the point where calibration data is provided.

Figure 58 shows the difference in the north and south ends' water surface elevations and figures Figure 59 and Figure 60 show the resulting velocity and power for the neap and spring tidal ranges. Power is calculated using equation 2 with a coefficient  $c$  of 0.35 and a cross sectional area corresponding to a single 5-m turbine used by Verdant Power (see Figure 5). Power output is set to zero when velocities are less than 1-m/s. It can be seen that velocities are significantly greater during spring tide (neap tide north flow velocity peaks are about 1.8-m/s, 2.2-m/s for spring tides, a 22% increase, south flow velocity peaks increase from about 1.3-m/s to 2.7-m/s, a 108% increase). Since power is a function of velocity cubed, a more drastic increase occurs (the peak power output during neap tide is 24-kW, the peak power during spring tide is 90-kW, a 275%

increase). The energy output for the neap and spring tide periods is 459-kW·hr and 1690-kW·hr, respectively.

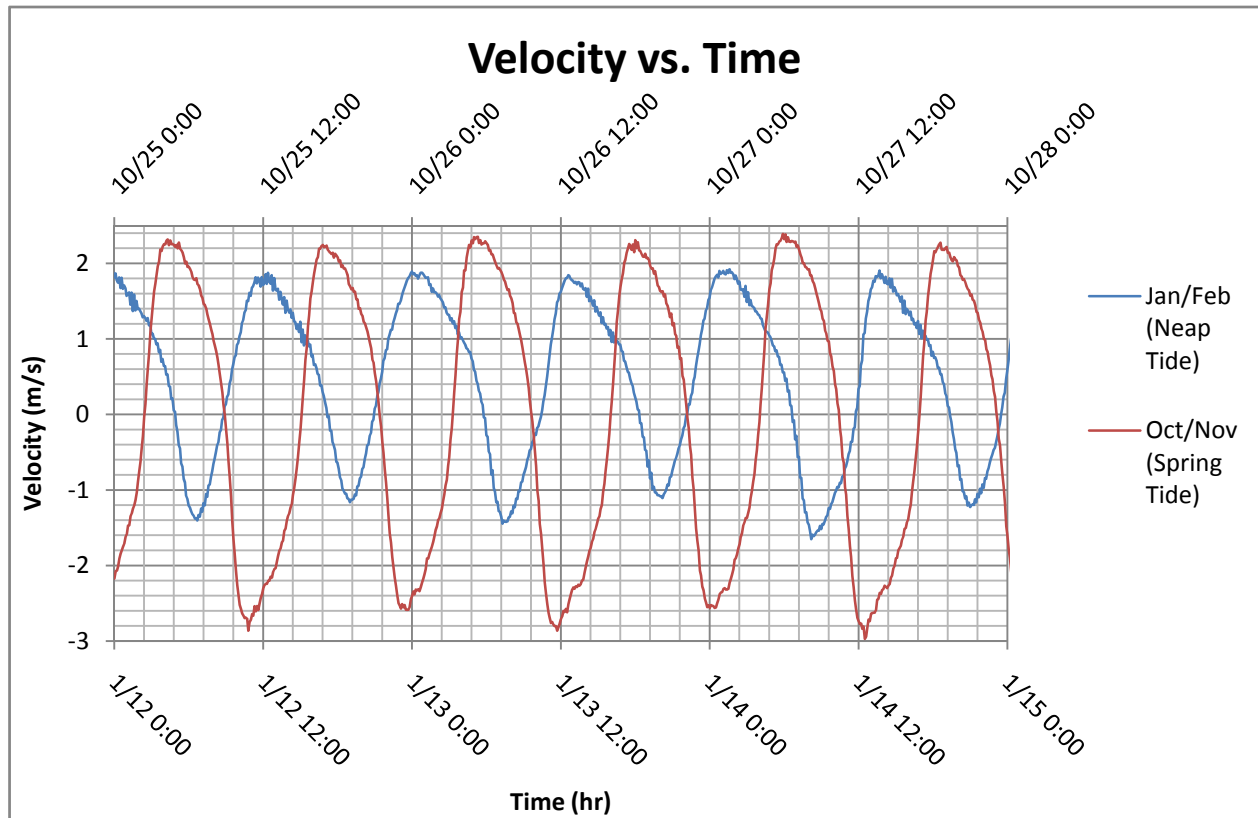
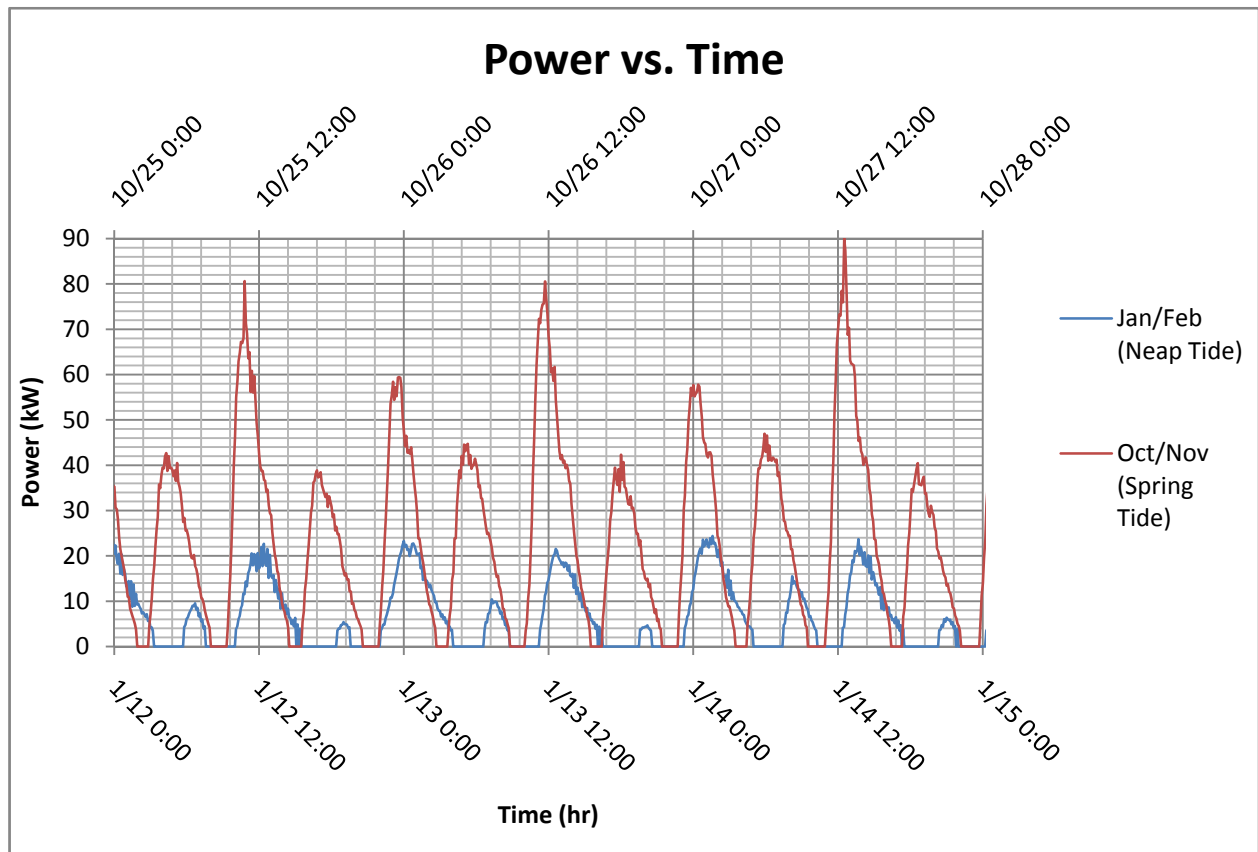
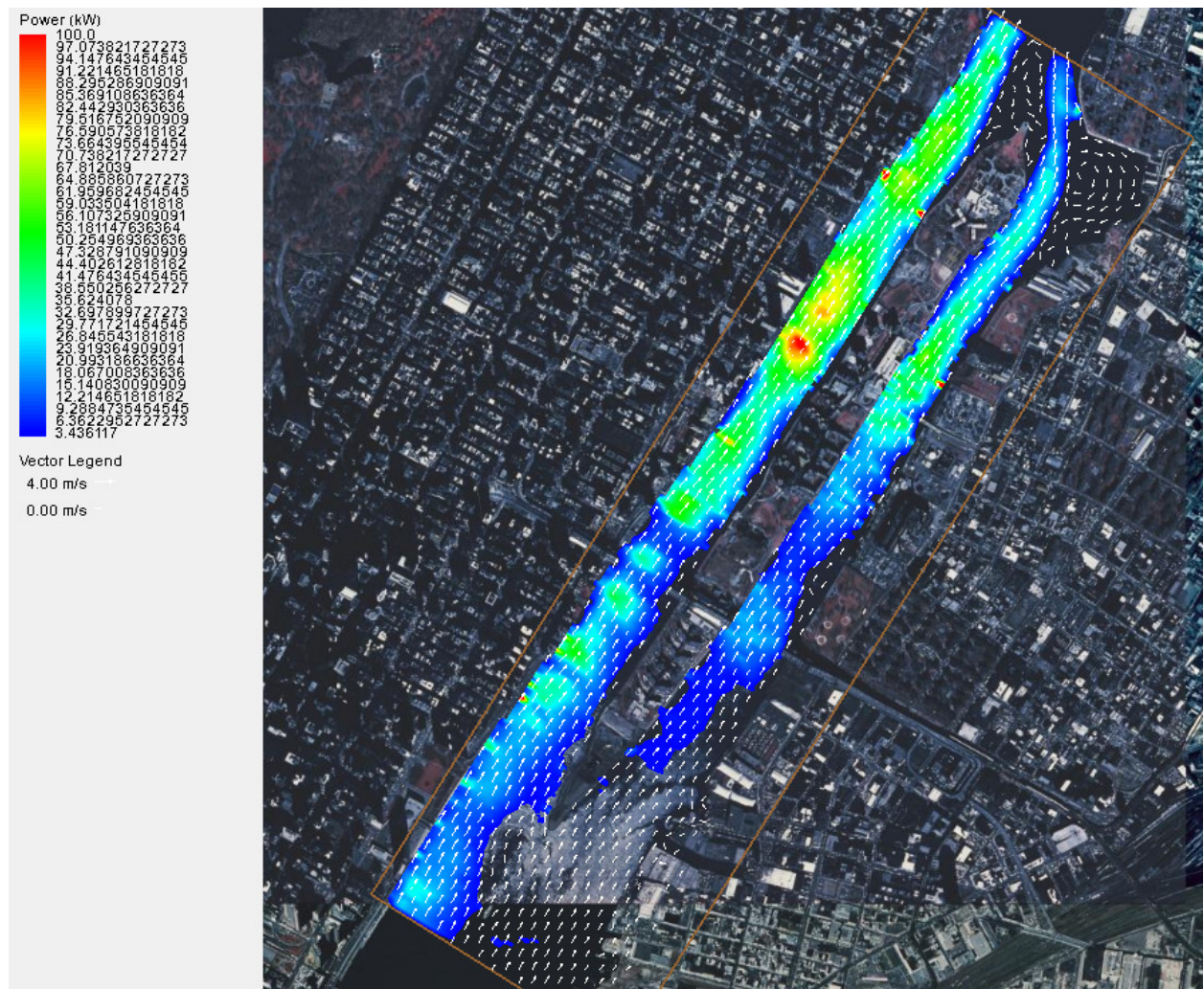


Figure 59 Velocity vs. Time for Spring and Neap Tides



**Figure 60 Power vs. Time for Spring and Neap Tides**

Figures Figure 61 and Figure 62 show the peak power output for a single turbine during the neap and spring tides, respectively. The color contour plots of power are calculated based on the same parameters mentioned above (a 5-m diameter turbine, a coefficient of 0.35, and using depth averaged velocity). Areas of the river flowing at less than 1-m/s are not colored in since it is assumed that power is not generated at such low velocities. It is interesting to note that power peaks during north flows for neap tides, and during south flows for spring tides.



**Figure 61 Peak Power Output from a 5-m Diameter Turbine During the Extreme Neap Tide**



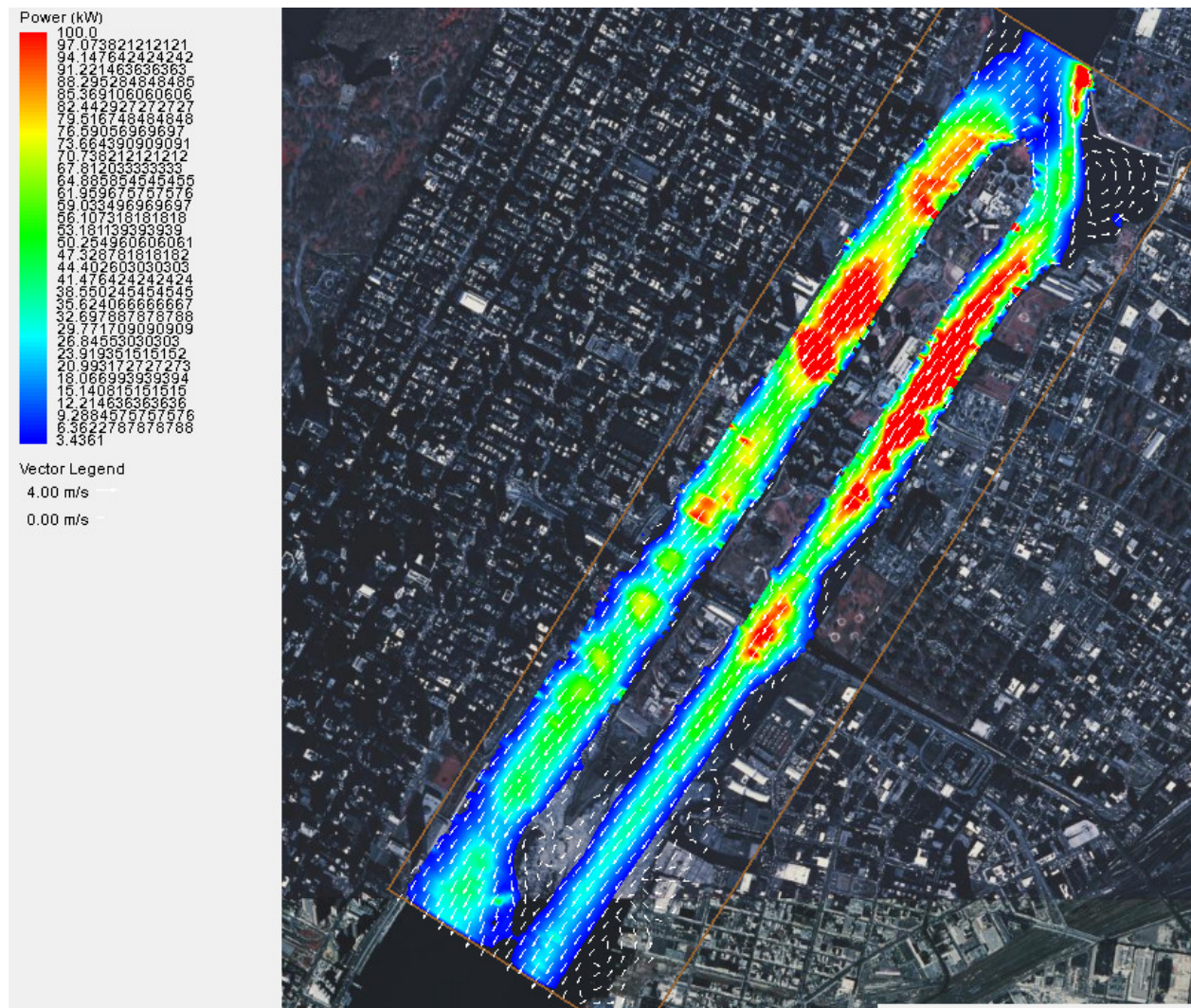


**Figure 62 Peak Power Output from a 5-m Diameter Turbine During the Extreme Spring Tide**

From Figure 63 it can be seen that peak velocities occur when the difference in upstream and downstream water surface elevations (head) are greatest. Negative (south flow) velocities are greater than positive (north flow) velocities for the same head, for example, when the head is -0.4-m, the velocity is about 2.3-m/s, when the head is 0.4-m, the velocity is about -2.8-m/s. This may indicate that there is less resistance to flow when the flow is south; however, during neap tide, flow velocities are greater in the north direction.

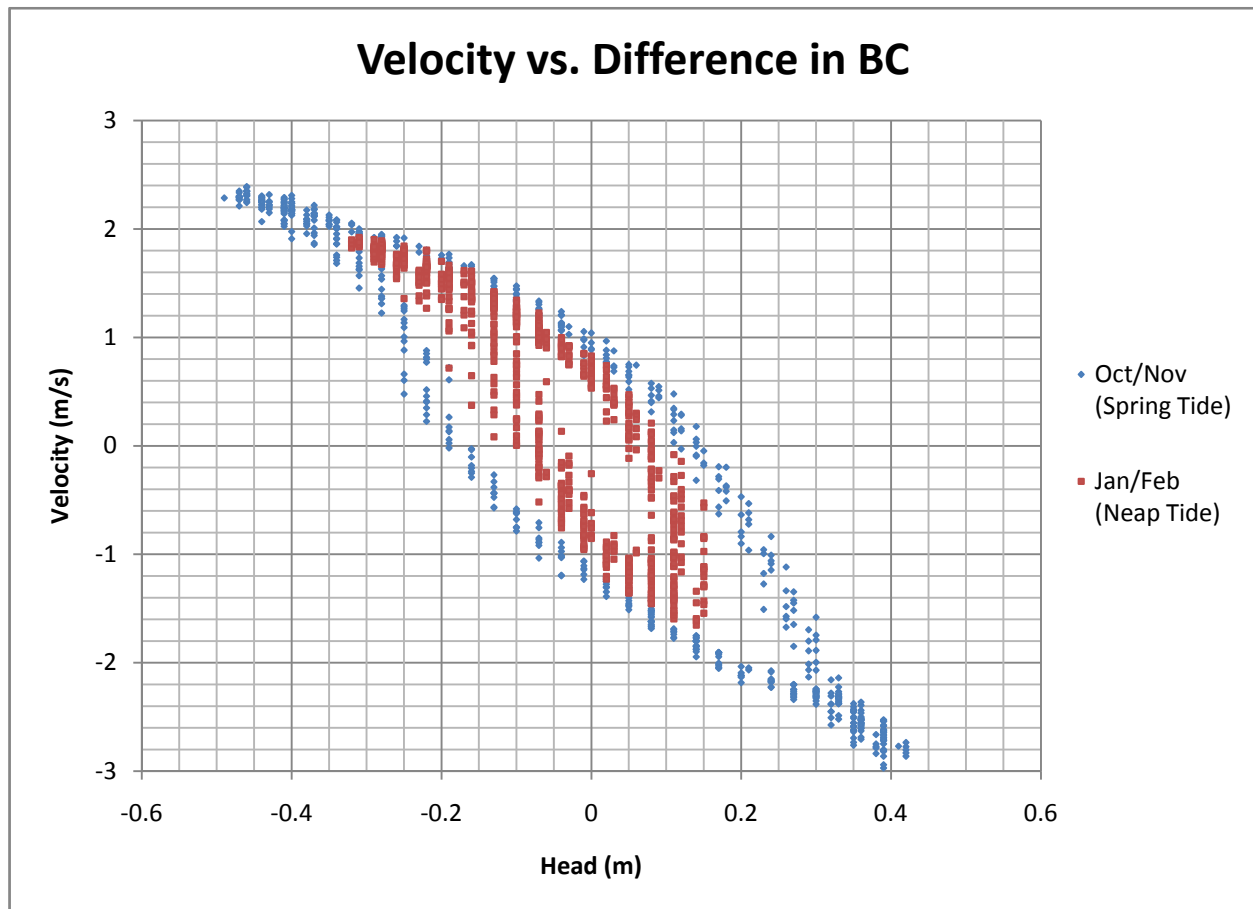


**Figure 63 Velocity vs. Head**

### 9.2.2. Month Long Data

From the above analysis, it is clear that spring tides generate higher velocities which produce more power and energy. A longer time period following the extreme spring and neap tides is analyzed to see how power generation and energy output is affected. 25-day periods are analyzed, one beginning January 12 and another beginning October 25 are used.

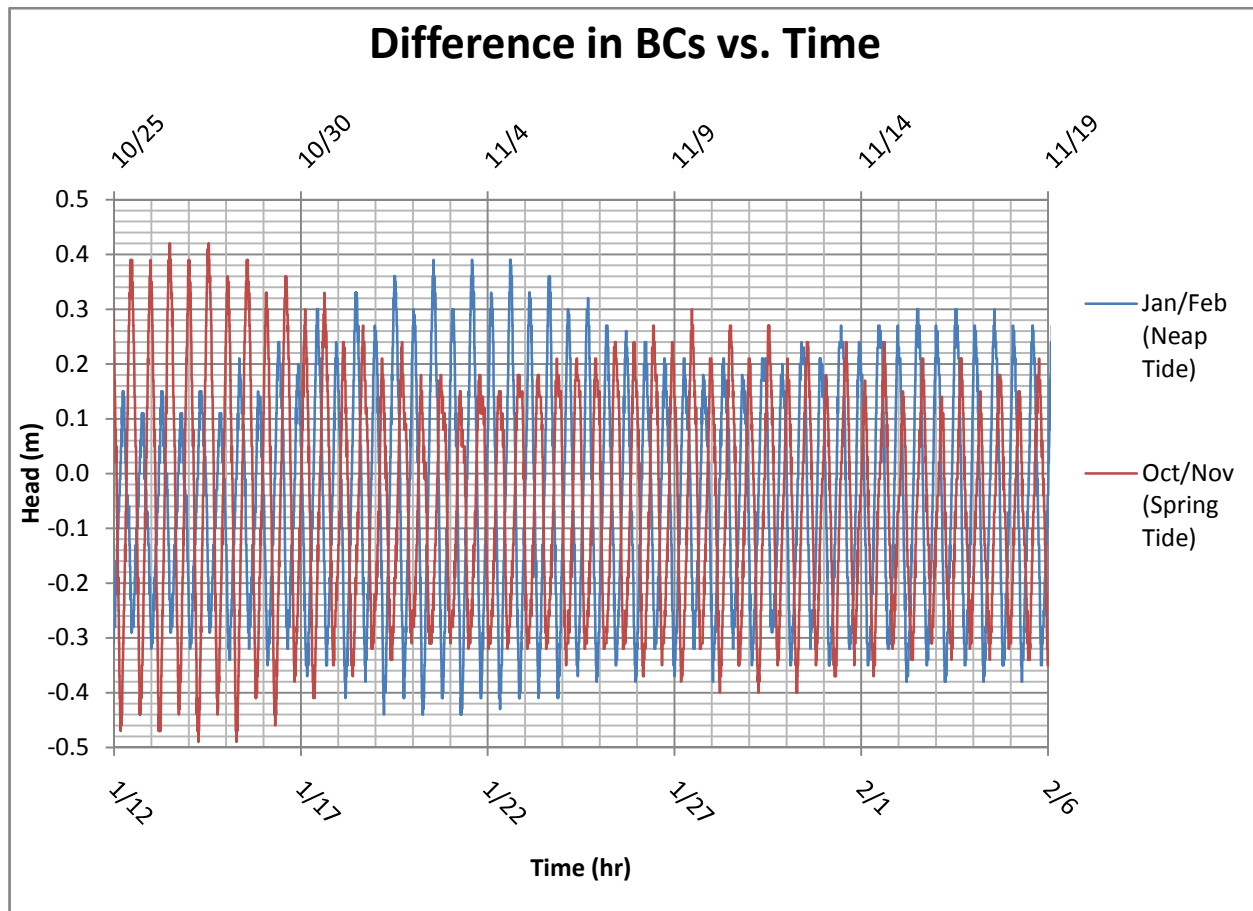


**Figure 64 Head vs. Time**

Figure 64 shows the head driving the flow for the 25-day periods and Figure 65 shows the resulting power curves. The total energy derived for the 25-day periods are 8,000-kW.hr for the January through February data and 8,090-kW.hr for the October through November data. This shows that, while short term variations can be very large, over a longer period, such as a month, tidal variations have very little impact on total energy output of turbines.

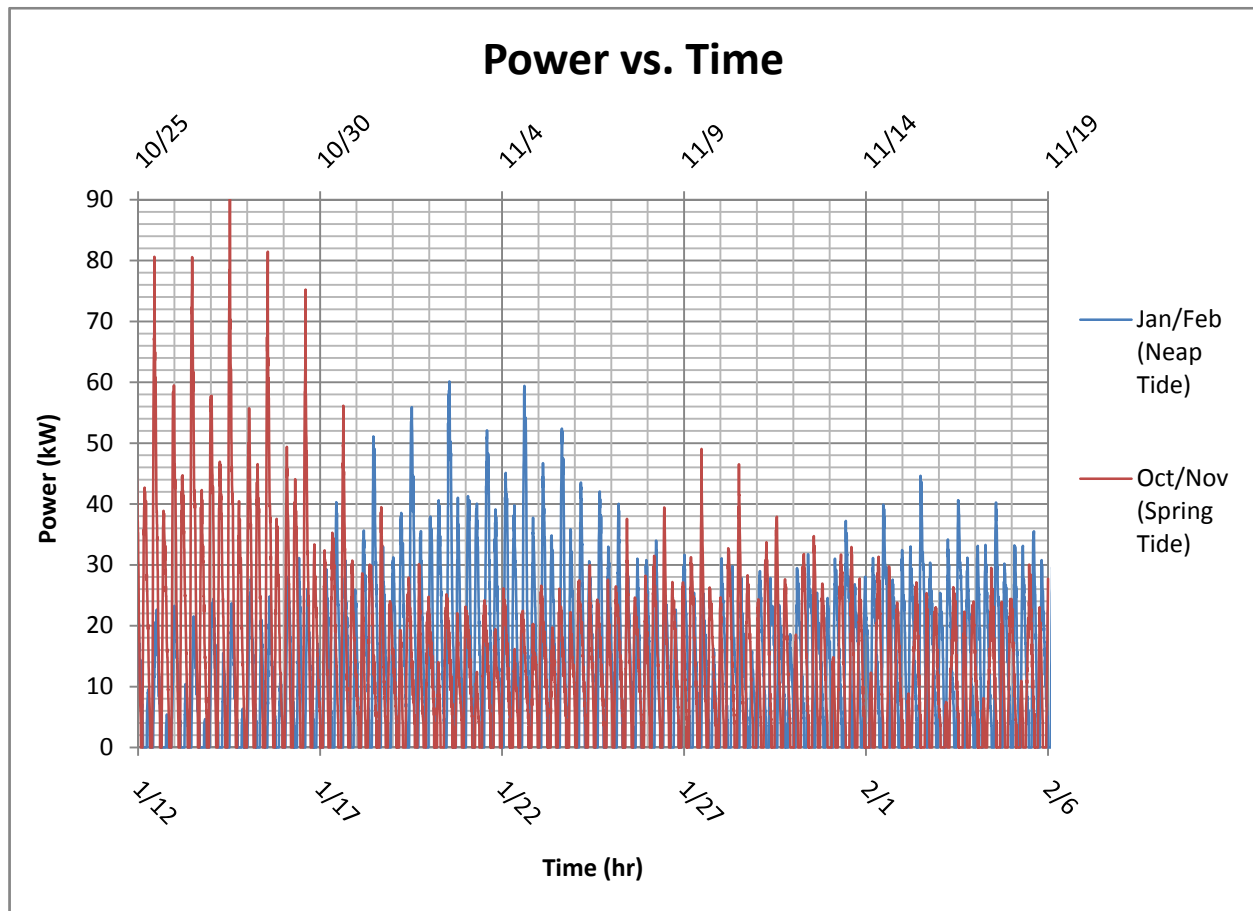


Figure 65 Power vs. Time

### 9.3. Conclusion

This study shows that power generated by underwater turbines can fluctuate widely. Since there are 2 or 3 velocity peaks every day, power generation will also peak 2 or 3 times a day. During an extreme neap tide, about 500-kW·hr of energy is generated over a 3 day period. During maximum spring tides, about 1,700-kW·hr of energy is generated over a 3 day period. Though the short term variation in energy generation is quite large, over a longer term, such as a month, the variation is quite small.

This chapter also shows that TUFLOW is a very useful tool for predicting power and energy output, and that TUFLOW can simulate long periods, such as a month. Coupling the TUFLOW results with GIS software could lead to extremely useful tools for finding potential sites for underwater turbines.



For example, sites that do not meet the proper criteria could be easily eliminated, such as sites that are outside certain depth and/or velocity ranges or sites where endangered species exist.

## **10. Modeling Methodology**

The main goal of this work is to use publically available data to model the East River in order to assess power generation potential. Publically available data reduces the costs and time of such analyses. For initial estimates, publically available data can give adequate estimates of flows in a water body. If sufficient power potential is found, then more accurate surveys can be performed if needed. The results of this work can then be used as a methodology for modeling other water bodies. The basic steps involved are outlined below.

### **10.1. Data**

The first step in developing a hydraulic model is to obtain the necessary data. This is described in detail in section 3. Bathymetry data is required for any hydraulic model to represent the surface upon which the water flows. In this study, topographic land data is merged with the bathymetry in an attempt to better represent the East River; however, topographic data may not always be necessary. Both of these sets of data are obtained from publically available sources on the internet (see section 3.1.1). Topographic data exists for the entire United States; however, bathymetry data can be more difficult to find, especially for rivers and streams. The other two sets of data, boundary conditions and calibration data, are not obtained from publically available data. In a rush to produce successful model results, public sources for these are overlooked. Boundary condition data is produced by a commercial software program; however, free alternatives exist. The USGS maintains stream gages across the US, which usually record stage and/or flow rate. NOAA keeps records of tidal gages in coastal waters. Data from these gages can be accessed via the internet and can provide adequate boundary condition data. The last piece of data required, calibration data, is obtained from Verdant Power. No public alternatives for calibration data are pursued in this study.

### **10.2. Data Manipulation**

Once the necessary data is obtained, it must be in a format that the hydraulic model can utilize. In this study, ArcView is used to convert data into formats that the SMS and HEC-GeoRAS can understand. The steps performed in ArcView may not always be necessary. For example, if the bathymetry data alone is used, SMS can read the file without the use of ArcView. ArcView is necessary to merge the bathymetry and topographic data, and to use with HEC-GeoRAS. For more details on these data conversion processes see sections 3.1 and 6.1.

### **10.3. The Hydraulic Model**

After the data is obtained and formatted such that the hydraulic model interface can read the data, the model can be set up. The steps involved at this point are specific to the chosen hydraulic model, but generally involve setting up the geometric data, including roughness parameters, boundary conditions, and various model parameters. The amount of detail involved can vary greatly depending on the model used. For example, HEC-RAS requires the least amount of work to setup and run while FESWSM is the most complex (see sections 4, 5, and 6 for further detail). Once the model is set up, run the model and check the results. If the results do not match the calibration data, change model parameters in order to make the results better match the calibration data. Once the model is properly calibrated, further runs and analysis can be performed.

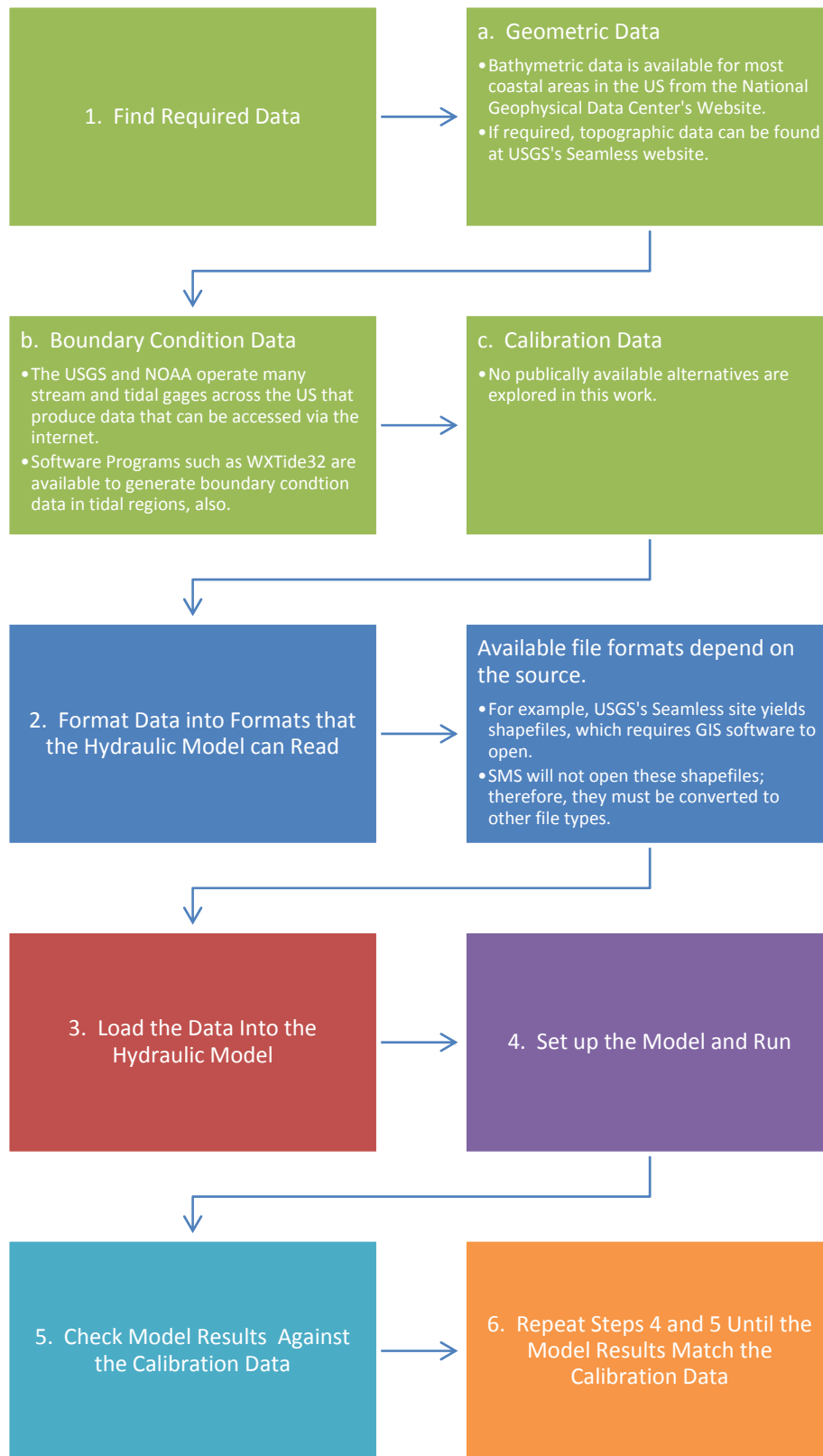


**Figure 66 Modeling Methodology Flow Chart**

## **11. Conclusions**

### **11.1. General Comments**

Tidal energy has real potential as an alternative energy source. As stated in the introduction it is more reliable and predictable than other forms of renewable energy. In many areas, available land is scarce and expensive, thus tidal energy has yet another advantage since turbines will be installed offshore. With tidal energy, there are no unsightly windmills and no pollution is generated by underwater turbines.

The main goal of this work is to develop a methodology for creating a hydraulic model of the East River in order to assess power potential using publically available data. This methodology can then be applied to other sites. The hydraulic models used in this study provide details about flow patterns at the site, the most important of which is velocity, since power generated by an underwater turbine is a function of velocity cubed. From the data provided from the models, estimates of potential suitable sites for underwater turbines can be identified and power and energy production estimates can be made. This type of modeling also has the potential to be used in the future to predict any adverse impacts to nearby structures and ecology as a result of turbine installation and to be used to find ways to minimize such effects.

### **11.2. Model Development and Data**

The main data used in this modeling effort are the geometry data, boundary condition data, and calibration data. The geometry data used in the models is a combination of on-shore topography data and bathymetry data. The merging of these two data sources proves to be difficult task. There are holes in the digital terrain model where the water is too shallow to collect bathymetry data. These holes are filled in by interpolating between the topography and bathymetry. This fact, along with the vertical datum conversion, could be a source of error in the models; however, with only one point to calibrate the model to, this is hard to determine. The geometry data is all publically available.

The boundary condition data is generated by the commercial software program Tides and Currents; however, publically available alternatives exist. The fact that 0.1-m have to be added to all water

surface elevation ordinates in the southern boundary condition for an accurate model run indicates that there may be some error in the boundary condition data. This may also indicate errors in the geometry data as well.

The calibration data is provided by Verdant Power. This data is simply a set of velocity vs. time ordinates for a single point in the East River. No publically available alternatives are explored.

### **11.3. Hydraulic Models**

Three hydraulic models are used in this study. FESWMS and TUFLOW are 2-D models that are used within the SMS interface. The third model, HEC-RAS, is a 1-D model that includes its own interface. The FESWMS model is found to be incapable of representing the flows in the East River due to stability issues. The eddy viscosity had to be set to an artificially high value to achieve stability in the FESWMS model, which did not allow velocity magnitudes to reach actual values. Both TUFLOW and HEC-RAS are capable of recreating the flow situations in the East River. TUFLOW is chosen as the best alternative due to it being 2-D. This allows better estimates of potential turbine sites and power generation. Estimates of power and energy generation from an underwater turbine are made from the TUFLOW results of the smallest and largest tidal variations of the year.

### **11.4. Month Long Runs and Power Analysis**

Both spring and neap tide periods are modeled in TUFLOW in order to analyze power and energy potential. The power produced during an extreme spring tide is 2.75 times greater than power produced during extreme neap tide. The overall energy output during the extreme spring tide is about 3 times greater than during the extreme neap tide. Although the difference in power generation between neap and spring times varies greatly over a short duration, energy output varies little between the two extremes when a longer period of 25-day is analyzed.

### **11.5. Recommendations for Future Work**

This study successfully created a model of the East River showing flow velocities and accompanying data from the model. These velocities are then converted to power by use of equation  $P = \frac{1}{2} c \rho A V^3$  (2. Energy estimates are made for a single turbine for spring and neap tides. Future work might incorporate GIS software in order to automatically create a map of potential sites that

meet a certain set of criteria, such as a certain range of water depths, a site that has a certain range of velocities, or even a site that could produce a certain amount of energy in a given time. This could then be expanded to encompass arrays of turbines rather than just one. Also, modeling could be applied to ascertain the impact to nearby structures and ecology and find ways to minimize such impacts.

#### **11.6. Conclusion**

This study shows that underwater turbines are an attractive source of energy because of their predictability and sustainability. This study also shows that a 2-D hydraulic model, such as TUFLOW, can provide a great tool for analyzing power potential in a water body. Using results from a 2-D model, planners can quickly choose sites that have potential for tidal power generation. As more and more data, such as bathymetry and topography, becomes readily available on the internet, setting up these models will become quicker and more economical. This study provides a methodology for assessing power potential for tidal sites. This study calculated that the energy produced by a single 5-m diameter turbine in the East River can produce roughly 8,000-kW·hr per month. This is roughly the amount of energy used in 5 small houses per month. With the installation of multiple turbines in arrays, and ever expanding technology, the amount of energy produced by tidal currents could become a significant portion of the world's energy generation.

## Appendix A: Bibliography

- (2003). "Underwater turbine heralds sea change in tidal current generators." *Professional Engineering*, 16(11), 10-10.
- (2005). *TUFLOW (and ESTRY) User Manual*, WBM Oceanics Australia.
- (2007a). "ESRI GIS and Mapping Software." <<http://www.esri.com/software/arcgis/arcview/about/features.html>> (December 28, 2007).
- (2007b). "TUFLOW Flood and Tide Simulation Software." <[http://www.tuflow.com/Description\\_Background.htm](http://www.tuflow.com/Description_Background.htm)> (December 12, 2007).
- Ackerman, C. T. (2005). *HEC-GeoRAS, An Extension for Support of HEC-RAS using ArcGIS, User's Manual*, 4 Ed., US Army Corps of Engineers, Davis, CA.
- Bahaj, A. S., and Myers, L. (2004). "Analytical estimates of the energy yield potential from the Alderney Race (Channel Islands) using marine current energy converters." *Renewable Energy*, 29(12), 1931-1945.
- Blumberg, A. F., and Pritchard, D. W. (1997). "Estimates of the transport through the East River, New York." *Journal of Geophysical Research-Oceans*, 102(C3), 5685-5703.
- Blunden, L. S., and Bahaj, A. S. (2006). "Initial evaluation of tidal stream energy resources at Portland Bill, UK." *Renewable Energy*, 31(2), 121-132.
- Brooks, D. A. (2006). "The tidal-stream energy resource in Passamaquoddy-Cobscook Bays: A fresh look at an old story." *Renewable Energy*, 31(14), 2284-2295.
- Brunner, G. W. (2002). *HEC-RAS, River Analysis System Hydraulic Reference Manual*, US Army Corps of Engineers, Davis, CA.
- Brunner, G. W. (2006). *HEC-RAS, River Analysis System User's Manual*, US Army Corps of Engineers, Davis, CA.
- Bryans, A. G., Fox, B., Crossley, P. A., and O'Malley, M. (2005). "Impact of tidal generation on power system operation in Ireland." *Ieee Transactions on Power Systems*, 20(4), 2034-2040.
- Caplow, T., Schlosser, P., Ho, D. T., and Enriquez, R. C. (2004). "Effect of tides on solute flushing from a strait: Imaging flow and transport in the East River with SF6." *Environmental Science & Technology*, 38(17), 4562-4571.



- Chang, I., Gallo, V., Myers, S., Hynes, C., Kass, S. L., Rizzo, C., Kelly, W. H., Paget, D., Sinding, K., O'Conner, K., Wang, P., Sanagavarapu, S., Kelly, E. B., Locke, A. M., and others, a. (2007). "East River Waterfront Esplanade and Piers Final Environmental Impact Statement."
- Chung, T. J. (2002). *Computational Fluid Dynamics*, Cambridge University Press, Cambridge, New York.
- Crowder, D. W., and Diplas, P. (2000). "Using two-dimensional hydrodynamic models at scales of ecological importance." *Journal of Hydrology*, 230(3-4), 172-191.
- Finnemore, E. J., and Franzini, J. B. (2001). *Fluid Mechanics with Engineering Applications*, 10 Ed., McGraw-Hill, New York.
- Fraenkel, P. L. (2002). "Power from marine currents." *Proceedings of the Institution of Mechanical Engineers Part a-Journal of Power and Energy*, 216(A1), 1-14.
- Fraenkel, P. L. (2006). "Tidal current energy technologies." *Ibis*, 148, 145-151.
- Froehlich, D. C. (2003). "User's Manual for FESWMS FST2DH." Federal Highway Administration.
- Garrett, C., and Cummins, P. (2004). "Generating power from tidal currents." *Journal of Waterway Port Coastal and Ocean Engineering-Asce*, 130(3), 114-118.
- Garrett, C., and Cummins, P. (2005). "The power potential of tidal currents in channels." *Proceedings of the Royal Society a-Mathematical Physical and Engineering Sciences*, 461(2060), 2563-2572.
- Gorban, A. N., Gorlov, A. M., and Silantyev, V. M. (2001). "Limits of the turbine efficiency for free fluid flow." *Journal of Energy Resources Technology-Transactions of the Asme*, 123(4), 311-317.
- Huxley, C. D. (2004). "TUFLOW Testing and Validation," Griffith University.
- Lhomme, J., Bouvier, C., Mignot, E., and Paquier, A. (2006). "One-dimensional GIS-based model compared with a two-dimensional model in urban floods simulation." *Water Science and Technology*, 54(6-7), 83-91.
- Mays, L. W. (2001). *Water Resources Engineering*, John Wiley & Sons, Inc., New York, NY.
- Myers, L., and Bahaj, A. S. (2005). "Simulated electrical power potential harnessed by marine current turbine arrays in the Alderney Race." *Renewable Energy*, 30(11), 1713-1731.

- Pasternack, G. B., Gilbert, A. T., Wheaton, J. M., and Buckland, E. M. (2006). "Error Propagation for Velocity and Shear Stress Prediction using 2D Models for Environmental Management." *Journal of Hydrology*, 328(1-2), 227-241.
- Ports, M. A., Turner, T. G., and Froehlich, D. C. (Year). "Practical comparison of one-dimensional and two-dimensional hydraulic analyses for bridge scour." Publ by ASCE, New York, NY, USA, San Francisco, CA, USA, 1732-1737.
- Sabersky, R. H., Acosta, A. J., Hauptmann, E. G., and Gates, E. M. (1999). *Fluid Flow a First Course in Fluid Mechanics*, 4 Ed., Prentice-Hall, Inc., Upper Saddle River, NJ.
- Stamou, A. I., Christodoulou, G. C., Bensasson, L. A., and Lazaridis, I. E. (1995). "A comparison of models for coastal circulation." *Water Science and Technology*, 32(7), 55-62.
- Swanson, R. L., Parker, C. A., Meyer, M. C., and Champ, M. A. (1982). "Is the East River, New York, a River or Long Island an Island." United States.
- Syme, W. J. (1991). "Dynamically Linked Two-Dimensional / One-Dimensional Hydrodynamic Modelling Program for Rivers, Estuaries and Coastal Waters," The University of Queensland.
- Syme, W. J., and Apelt, C. J. (1990). "Linked Two-Dimensional / One-Dimensional Flow Modelling Using the Shallow Water Equations." In: *Conference on Hydraulics in Civil Engineering*, Sydney, Australia.
- Takenouchi, K., Okuma, K., Furukawa, A., and Setoguchi, T. (2006). "On applicability of reciprocating flow turbines developed for wave power to tidal power conversion." *Renewable Energy*, 31(2), 209-223.
- Tarbet, K., and Hardy, T. B. (1996). "Evaluation of One-Dimensional and Two-Dimensional Hydraulic Modeling in a Natural River and Implications in Instream Flow Assessment Methods." In: *2<sup>nd</sup> International Symposium on Habitat Hydraulics*.
- Tennekes, H., and Lumley, J. L. (1972). *A First Course in Turbulence*, MIT Press, Cambridge, Mass.
- Waddle, T., Steffler, P., Ghanem, A., Katopodis, C., and Locke, A. (2000). "Comparison of One and Two-Dimensional Open Channel Flow Models for a Small Habitat Stream." *Rivers*, 7(3), 205-220.
- Walton, Bardley, and Grindeland. (1997). "1-D or 2-D Models for River Hydraulic Studies?" In: *Managing water; coping with scarcity and abundance; proceedings of theme A; the 27th Congress of the International Association for Hydraulic Research*.
- Warner, J. C., Brunner, G. W., Wolfe, B. C., and Piper, S. S. (2002). *HEC-RAS, River Analysis System Applications Guide*, US Army Corps of Engineers, Davis, CA.

## Appendix B: Step by Step TUFLOW Model Creation

### Steps in creating a TUFLOW model

1. Add geometry data
2. Change the default map coverage type to TUFLOW grid extent
  - a. Create a 2-D frame grid around the area to be modeled
  - b. Convert the map to a 2-D grid (right click coverage, click convert)
    - i. Set the appropriate cell size
    - ii. Click Z under the Depth Options section and set the Extrapolation Value to a reasonable number (this sets the elevations of areas not in the DTM to whatever value is entered, it should be higher than the water surface, but not so high as to create extreme slopes and problems due to interpolation)
3. Once the new grid is created, change the options (right click on grid, click options)
  - a. Set materials options to Specify using area property coverage(s)
    - i. Set the default material (this is the value used if there is not a materials coverage over a particular region of the grid; roughness values will be specified later)
  - b. Set Cell Codes to Specify using BC coverage(s) and default code to Water cell
4. Create a new coverage (right click map data, new coverage)
  - a. set type to Area Property
  - b. Depending upon what type of data available, different steps will need to be followed
    - i. Convert GIS data to this coverage or
    - ii. Digitize areas of different types
      1. I simply created a polygon around my whole model and set that to the default material, this coverage may not be necessary if a default material is set in step 3.
5. Create a new coverage
  - a. Set type to TUFLOW BC
  - b. Create feature arcs across reaches where boundary conditions are located
  - c. Double click on feature arcs
    - i. Set type to whatever type of BC used
    - ii. Click on Boundary Conditions
      1. Name Components (different name for each BC location) and make sure the type is correct
        - a. Name Events (must be a common name at all BC locations)
        - b. Click on the box right of event name and set BC
  - d. Draw feature arcs such that they connect to the boundary conditions arcs and enclose all of the grid beyond the area to be model (basically, create a polygon around the “ends” of the model outside the boundary conditions).
    - i. Click on Feature Objects, Create Polygons
    - ii. Double click on the polygons

1. Set Type to Cell Codes
  2. Set Code to Inactive – not in mesh
6. Right click on the table of contents, click new, click TUFLOW Simulation
  - a. Right click on Components, click New 2-D Geometry Component
    - i. Drag the grid, boundary condition coverage, and material coverage to the new 2-D geometry component
  - b. Right Click on Material Sets, click New Material Set
    - i. Right click on the new material set and click properties
    - ii. Set Manning's roughness values
  - c. Drag the new 2-D geometry component to the simulation
  - d. Right click on the simulation and click Model Control
    - i. Set the properties in each tab
      1. Rule of Thumb: the time step should be about  $\frac{1}{2}$  of the grid size (a 20-m grid would have 10-s time step)
      2. Set the water level to the level of initial boundary conditions
      3. Set boundary condition event
  - e. Right click on simulation, click Export TUFLOW files
  - f. Right click on simulation, click Launch TUFLOW